

AN INVESTIGATION INTO THE MODELING OF A  
RIGID FLUID CONDUIT USING T<sup>3</sup> ELECTRICAL  
ANALOGY AND S-T METHOD

By

DAVID JON HEER

Bachelor of Science

Oklahoma State University

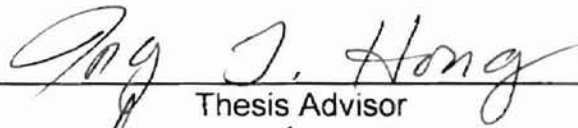
Stillwater, Oklahoma

1992

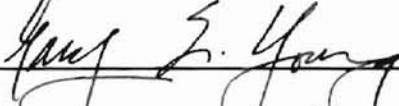
Submitted to the Faculty of the  
Graduate College of the  
Oklahoma State University  
in partial fulfillment of  
the requirements for  
the Degree of  
MASTER OF SCIENCE  
May, 1998

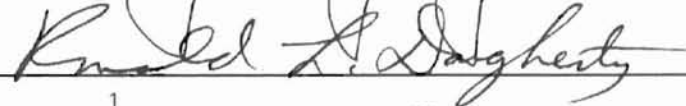
AN INVESTIGATION INTO THE MODELING OF A  
RIGID FLUID CONDUIT USING T<sup>3</sup> ELECTRICAL  
ANALOGY AND S-T METHOD

Thesis Approved:

  
\_\_\_\_\_

Thesis Advisor

  
\_\_\_\_\_

  
\_\_\_\_\_

  
\_\_\_\_\_

Dean of the Graduate College

## ACKNOWLEDGEMENT

I wish to extend my sincere thanks to my principle advisor, Dr. I.T. Hong, who patiently provided expert guidance and helpful suggestions throughout the course of my thesis effort. To my committee members, Professors R.L. Dougherty and G.E. Young, thank-you for your time and suggestions. I also wish to thank Dr. R.K. Tessmann for editorial assistance and encouragement. Particular appreciation is given to the laboratory at FES, Inc., Stillwater, Oklahoma, for providing excellent facilities and equipment during the experimental efforts. Lastly, I would like to thank my parents, family and friends for firm support throughout all of my educational endeavors.

## TABLE OF CONTENTS

Chapter	Page
I. INTRODUCTION .....	1
Problem Statement .....	1
Purpose of Study .....	3
Experimental Verification .....	4
II. LITERATURE REVIEW .....	5
Frequency Domain Models .....	5
Time Domain Models .....	11
III. THEORY OF EXACT FIRST ORDER MODEL.....	13
Mathematical Formulation of Problem.....	14
Solution Outline .....	17
Impedance Formulation .....	19
Rational Approximate Engineering Model .....	21
Simulation Results .....	25
IV. DEVELOPMENT OF ELECTRICAL ANALOGY FOR LINE DYNAMICS .....	30
T <sup>3</sup> Network .....	30
Resistance to Flow Calculation Methods .....	33
Hagen-Poiseuille Law .....	33
Moody Chart Method.....	35
S-T Method .....	37
Comparison of Hagen-Poiseuille Law and S-T Method .....	38
Application of S-T Method to T <sup>3</sup> Network .....	39
Multiple Lump Dynamic Simulation Results.....	46
A Note on Lumping by Length.....	47
Dynamic Simulation of 4 Lump Models Comparing S-T and H-P Methods.....	53
V. TRANSIENT RESPONSE COMPARISON OF RATIONAL APPROXIMATE MODEL AND T <sup>3</sup> MODEL.....	58
Rational Approximate Model of Water Hammer Problem.....	60

Chapter	Page
T <sup>3</sup> Model of Water Hammer Problem.....	65
<b>VI. EXPERIMENT.....</b>	<b>68</b>
Introduction.....	68
<b>PART 1: Steady State Testing to Verify S-T Method .....</b>	<b>69</b>
Experimental Apparatus.....	69
Computer Data Acquisition.....	72
Calibration and Identification .....	73
Procedure for Steady State Testing .....	76
Steady State Test Data.....	76
<b>PART 2: Dynamic Testing .....</b>	<b>78</b>
Experimental Apparatus.....	78
Procedure and Results for Dynamic Testing .....	78
<b>PART 3: Amplitude Decay Testing .....</b>	<b>81</b>
Experimental Apparatus.....	81
Procedure for Amplitude Decay Testing .....	81
Modeling Approach .....	81
Comparison of Data and Author's Model.....	83
<b>VII. CONCLUSIONS AND RECOMMENDATIONS.....</b>	<b>88</b>
Scope of Model.....	88
Conclusions .....	88
Recommendations .....	90
Literature Cited.....	92
Appendix A Listing of MATLAB M-Files for One, Two, and Three Terms of Rational Approximate Engineering Models.....	94
Appendix B Listing of MATLAB M-Files for One, Two, and Four Lump T <sup>3</sup> Models.....	98
Appendix C Listing of MATLAB M-Files Comparing S-T and H-P Methods for a Four Lump Model .....	109
Appendix D Listing of MATLAB M-Files for Solution of Water Hammer Problem.....	115

## LIST OF TABLES

Table	Page
3.1 Simulation Parameters for Rational Approximate Model.....	26
4.1 Describing Equations for Electrical Analogy of a Line.....	31
4.2 Parameters Used for q vs. $\Delta P$ Model Comparison.....	39
4.3 Multiple Lump Simulation Parameters .....	46
4.4 Steady State Calculations for Volumetric Flow Rate.....	53
5.1 Effective Area of Valve vs. Time .....	59
5.2 Simulation Parameters for Solution of Water Hammer Problem Using Rational Approximate Model.....	64
6.1 Primary Components of the Experimental Apparatus .....	73
6.2 Physical Parameters for Test Line.....	76
6.3 Water Hammer Experiment Percent Error for Peak Pressure Predictions .....	80
6.4 Simulation Parameters .....	83
6.5 Amplitude Decay Experiment Flow Rate Error Analysis.....	84

## LIST OF FIGURES

Figure	Page
2.1 Structure of the Models .....	6
2.2 Nomenclature for Line .....	7
3.1 Coordinate System.....	16
3.2 Diagram of Fluid Conduit for Fundamental Mode Transfer Equations.....	19
3.3 Diagram of a Fluid Conduit with Averaged Quantities at Each End .....	19
3.4 Variation of the Approximate Mode Parameter $F_{cn}$ With Axial Damping Number [20] .....	23
3.5 Variation of the Approximate Mode Parameter $\zeta_{cn}$ With Axial Damping Number [20] .....	23
3.6 Variation of the Approximate Mode Parameter $F_{sn}$ With Axial Damping Number [20] .....	24
3.7 Variation of the Approximate Mode Parameter $\zeta_{sn}$ With Axial Damping Number [20] .....	24
3.8 $n=0$ Amplitude Response vs. Angular Frequency .....	27
3.9 $n=0$ Amplitude Response vs. Frequency Number.....	27
3.10 $n=1$ Amplitude Response vs. Angular Frequency .....	28
3.11 $n=1$ Amplitude Response vs. Frequency Number.....	28
3.12 $n=2$ Amplitude Response vs. Angular Frequency .....	29
3.13 $n=2$ Amplitude Response vs. Frequency Number.....	29
4.1 Schematic of $T^3$ Lump.....	31
4.2 Modified Moody Chart [22] .....	36
4.3 Comparison Plot of $q$ vs. $\Delta P$ Models .....	40
4.4 Flow Chart Demonstrating Solution of Differential Equations.....	42
4.5 Schematic of $n$ -Lump $T^3$ Model .....	43

Figure	Page
4.6 Schematic for 2 Lump $T^3$ Model .....	43
4.7 Reduced Form of 2 Lump Network.....	44
4.8 1 Lump Pressure Response Graph ( $P_1, P_2, P_3$ ).....	48
4.9 1 Lump Flow Response Graph ( $q_2$ and $q_3$ ) .....	48
4.10 2 Lump Pressure Response Graph ( $P_1$ to $P_6$ ).....	49
4.11 2 Lump Flow Response Graph ( $q_2, q_3, q_5,$ and $q_6$ ).....	49
4.12 4 Lump Pressure Response Graph ( $P_1, P_2,$ and $P_3$ ) .....	50
4.13 4 Lump Pressure Response Graph ( $P_4, P_5,$ and $P_6$ ) .....	50
4.14 4 Lump Pressure Response Graph ( $P_7, P_8,$ and $P_9$ ) .....	51
4.15 4 Lump Pressure Response Graph ( $P_{10}, P_{11},$ and $P_{12}$ ) .....	51
4.16 4 Lump Flow Response Graph ( $q_2, q_3, q_5, q_6, q_8, q_9, q_{11},$ and $q_{12}$ ) .....	52
4.17 4 Lump Flow Response Graph ( $q_2$ and $q_{12}$ ).....	52
4.18 Comparison of H-P and S-T Pressure Response Step Input: 300 psig, Laminar Flow Region .....	55
4.19 Comparison of H-P and S-T Flow Response Step Input: 300 psig, Laminar Flow Region .....	55
4.20 Comparison of S-T and H-P Pressure Response, $P_5$ Step Input: 1500 psig, Transition Flow Region .....	56
4.21 Comparison of S-T and H-P Flow Response Step Input: 1500 psig, Transition Flow Region .....	56
4.22 Comparison of S-T and H-P Pressure Response, $P_5$ Step Input: 4500 psig, Turbulent Flow Region .....	57
4.23 Comparison of S-T and H-P Flow Response Step Input: 4500 psig, Turbulent Flow Regime .....	57
5.1 Illustration of Water Hammer Problem.....	58
5.2 Graph of Valve Area Data and Curve Fit Equation .....	60
5.3 Water Hammer Effect, One Term Rational Approximate Model, Comparison of Fanning Factor, S-T Method, and H-P Law .....	65
5.4 Schematic of Water Hammer Problem with Line Represented by 1 Lump $T^3$ Network.....	66



Figure	Page
5.5 Theoretical Responses for Water Hammer Problem .....	67
6.1 Schematic Diagram of Steady State Setup.....	70
6.2 Photograph of Experimental Setup.....	70
6.3 Photograph of Data Acquisition Terminal Card and Amplifiers.....	71
6.4 Photograph of Attachment of Outlet Pressure Transducer .....	72
6.5 Plot of Calibration Data and Best Fit Line for Inlet Pressure Transducer .....	74
6.6 Plot of Calibration Data and Best Fit Line for Outlet Pressure Transducer .....	74
6.7 Plot of Viscosity Data and Walther Equation .....	75
6.8 Comparison Plot of Steady State Data and Models .....	77
6.9 Physical Representation of Water Hammer Experiment.....	79
6.10 Comparison of Theoretical Curves and Experimental Data .....	79
6.11 Schematic Diagram of System for Amplitude Decay Testing .....	82
6.12 Inlet Data and Model Input Curve: 3 gpm .....	85
6.13 Outlet Data and Predicted Pressure: 3 gpm .....	85
6.14 Inlet Data and Model Input Curve: 2.25 gpm .....	86
6.15 Outlet Data and Predicted Pressure: 2.25 gpm .....	86
6.16 Inlet Data and Model Input Curve: 3.75 gpm .....	87
6.17 Outlet Data and Predicted Pressure: 3.75 gpm .....	87

## NOMENCLATURE

Roman Symbols	Definition	Units
$A_L$	inside cross-sectional area of line	$\text{in}^2$
$A_v$	valve flow area	$\text{in}^2$
$C$	fluid capacitance	$\text{in}^3/\text{psi}$
$c_o$	speed of sound in fluid	$\text{in}/\text{sec}$
$C_d$	discharge coefficient	dimensionless
$\nabla$	"del" operator	dimensionless
$d_i$	conduit inside diameter	$\text{in}$
$d_o$	conduit outside diameter	$\text{in}$
$E$	material elastic modulus	$\text{psi}$
$F$	frequency number	dimensionless
$f_D$	Darcy friction factor	dimensionless
$f_f$	Fanning friction factor	dimensionless
H-P	Hagen-Poiseuille law	terminology
$i$	current	amps
$L$	fluid inductance	$\text{lb}_f\text{sec}^2/\text{in}^5$
$\ell$	segment length	$\text{in}$
$L_c$	conduit length	$\text{in}$
$N_R$	Reynold's number	dimensionless
$P$	pressure	$\text{psi}$
$q$	volumetric flow rate	$\text{in}^3/\text{sec}$
$R$	fluid resistance	consistent units
$r$	conduit radius	$\text{in}$
R.A.	rational approximate	terminology
$s$	Laplace operator	dimensionless
$S$	dimensionless number	dimensionless
S-T	S-T method	terminology
$T$	dimensionless number	dimensionless
$t$	time	$\text{sec}$
$v$	fluid velocity	$\text{in}/\text{sec}$
$V$	voltage	volts
$V_{\text{line}}$	fluid volume in line	$\text{in}^3$
$W_t$	wall thickness	$\text{in}$
$x$	state variable representation	consistent units
$z$	impedance	consistent units

Greek Symbols	Definition	Units
$\beta$	.....bulk modulus.....	psi
$\Delta P$	.....differential pressure .....	psid
$\Gamma$	.....wave propagation operator .....	consistent units
$\mu$	.....shear or absolute viscosity .....	lb <sub>f</sub> sec/in <sup>2</sup>
$\nu$	.....kinematic viscosity.....	in <sup>2</sup> /sec
$\omega_n$	.....angular frequency .....	rad/sec
$\rho$	.....fluid density.....	lb <sub>f</sub> sec <sup>2</sup> /in <sup>4</sup>
$\zeta$	.....damping factor .....	dimensionless

CHAPTER I  
INTRODUCTION  
Problem Statement

In many types of fluid systems, transmission line dynamics play an important role in overall system performance. The variety of fluid systems where line dynamics are significant is diverse. Efforts to model line dynamics have been carried out in many engineering disciplines. Some of the applications include water distribution systems in hydroelectric power complexes, blood flow networks in biological systems, chemical process control, and hydraulic systems in industrial and mobile machinery.

Designers for hydraulic systems must couple a vast array of components together and mate them with a control strategy to achieve a desired outcome. The fundamental components of a hydraulic system include prime movers, actuators, energy storing devices, control devices, logic elements, and flow generators. Driven by market place competition, the response times and overall performance of the individual components are constantly improving. Thus, the fluid transmission lines used to link the individual components together in a hydraulic system play an increasingly important role in successful system performance. It is therefore necessary to accurately represent the dynamic effects of the hydraulic fluid transmission line in computer simulations.

The modeling techniques presented in the literature in the area of line dynamics can be categorized as frequency domain solutions or time domain solutions. There are approximately seven distinct linear, distributed models for uniform, rigid fluid transmission lines. These models are derived from the fundamental equations of fluid dynamics composed of the Navier-Stokes relations, the momentum equation, and an equation of state. While varying greatly in their complexity, assumptions, and range of application, they are of great utility in performing a system frequency analysis. However, they are often limited in obtaining transient response information. Also, the resistance terms used for the treatment of friction often assume laminar flow. In today's real hydraulic systems, laminar flow conditions from a qualitative standpoint may rarely occur. Dynamic flow rate changes and hydraulic pump flow pulsations often suggest turbulent behavior.

For the hydraulic system designer, time domain solutions are the most desirable. A time domain solution for a particular component in a hydraulic system is conducive to coupling with time domain solutions of other components for large scale system simulation. In particular, time domain solutions for the fluid transmission line often consist of the method of characteristics for the wave equation solution, and the use of the electrical analogy. The electrical analogy for a line model has typically been depicted as a "pi" or "tee" representation. This thesis will detail a new representation called "T<sup>3</sup>" which will also incorporate for the first time a resistance to flow modeling technique known as the S-T method. The resulting model is not restricted to laminar flow conditions as is the case if

the Hagen-Poiseuille law were employed. Nor is it dependent upon successive iteration techniques for calculating friction factors using manual charts. To the best knowledge of the writer, the use of the  $T^3$  representation and the S-T method is a unique contribution to the difficult problem of fluid transmission line modeling.

### Purpose of Study

The purpose of this thesis is to develop a successful modeling technique for a rigid fluid transmission line used in real hydraulic systems. Historically, this has been accomplished in varying degrees using models derived from fundamental fluid dynamics equations. This study will develop an electrical circuit analogy called  $T^3$ . The model will utilize terms for the resistive, capacitive, and inductive effects of the line and incorporate them in a distributed parameter approach. The resistance terms implemented can account for laminar, transition, or turbulent conditions set forth by the Reynold's Number. Many of the models investigated in the literature survey are restricted to fully developed laminar flow. For comparison purposes, the  $T^3$  model will be compared to the well established rational approximate model developed by Gerlach [2]. The rational approximate model will serve as a standard of reference. If the accuracy of the electrical circuit analogy approach can be demonstrated against the rational approximate model and experimental data, then hydraulic system modelers will have a new modeling tool in their arsenal that at last does not require cumbersome look-up charts or the restriction of laminar flow. The resulting model is capable of

predicting the time histories of pressure and flow rate at various nodes along a fluid transmission line.

### Experimental Verification

In support of the theoretical approach, an experimental apparatus was constructed. A variable displacement piston pump was used to provide an input signal to a rigid steel fluid conduit. The purpose of this testing was to verify the accuracy of the S-T Method for predicting pressure loss characteristics in laminar, transition, and turbulent conditions. Pressure transducers and a high speed data acquisition system were used to monitor the input and output pressure signals of the fluid conduit. For dynamic testing, test data collected during a water hammer experiment [2] will be used to assess the accuracy of the model. Finally, pressure amplitude decay testing was executed for comparison to the author's  $T^3$  model predictions.

CHAPTER II  
LITERATURE REVIEW  
Frequency Domain Models

From an extensive survey of over three hundred research papers covering engineering, medical, and biological applications, Stecki and Davis [1] identified seven distinct linear, distributed parameter models which have been used in the study of rigid, uniform fluid transmission lines. As noted by Stecki and Davis, the research efforts across the various fields were often paralleled, which caused some researchers to claim priority of their solution when prior solutions already existed. Regardless of the lack of cross referencing, Stecki and Davis gleaned seven distinct models rooted in the fundamental equations of fluid dynamics. Figure 2.1 illustrates the structure of the models [1]. The fundamental equations include the Navier-Stokes relations, the continuity equations, the state equation, and the energy equation. Auxiliary equations express the coefficients used in the fundamental equations as functions of pressure and temperature. To completely describe the fluid transmission line, boundary and initial conditions are applied to the set of equations. The difficulty of obtaining an analytical solution to the fundamental relations necessitates the use of simplifying assumptions to eliminate terms considered negligible in order to reduce the equations to a set of linear relations so that an analytical solution may be obtained. Referring to Figure



2.1, the more sophisticated models are those which have had the least number of terms removed.

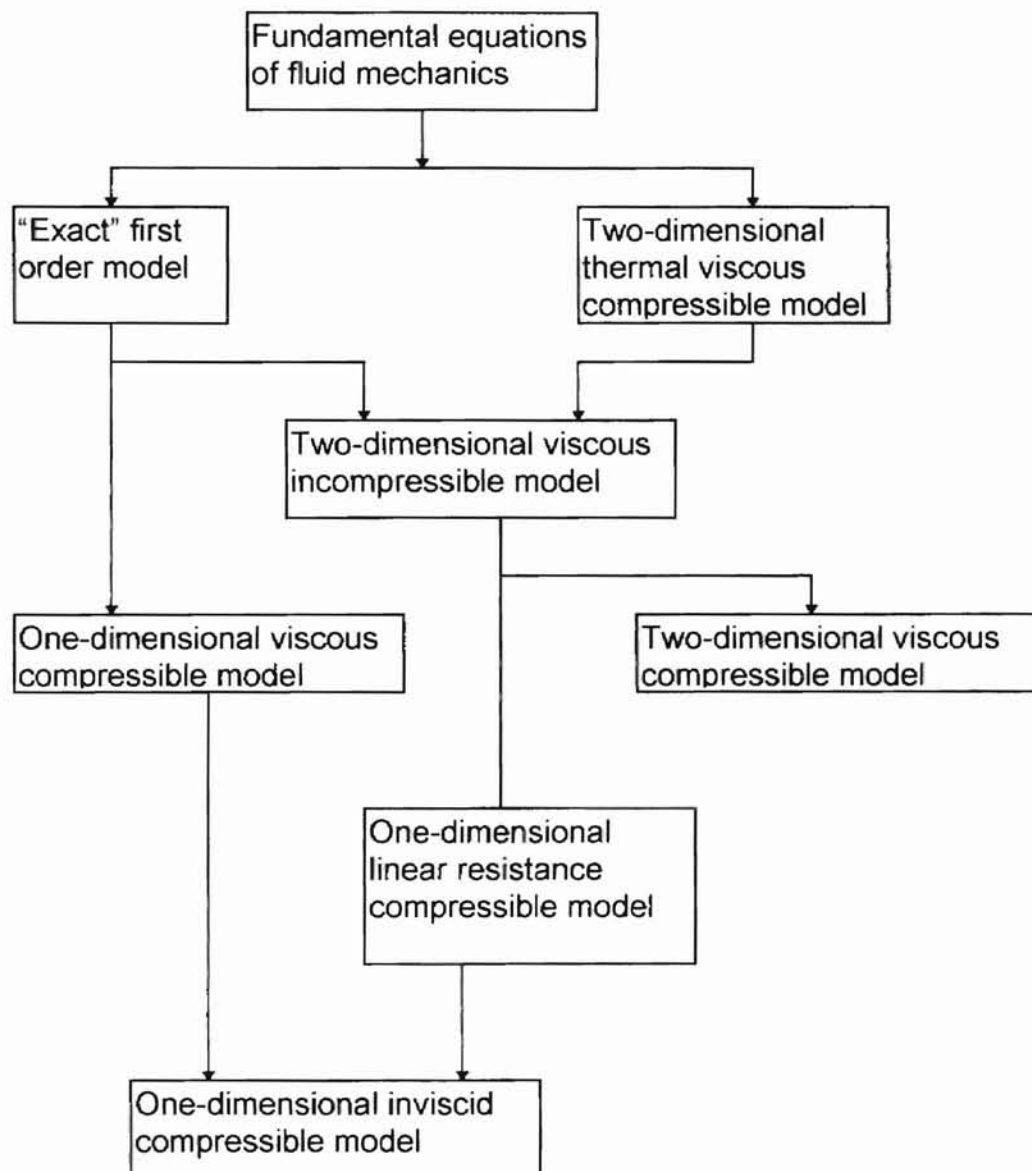


Figure 2.1 Structure of the Models

Prior to discussion of each of the seven models, it is useful to briefly describe their implementation in the Laplace operator domain. First, the input and output parameters for a fluid line are illustrated graphically in Figure 2.2.

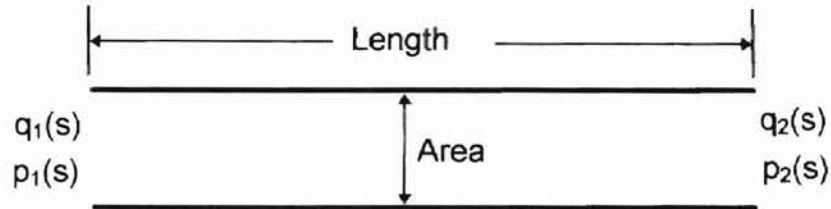


Figure 2.2 Nomenclature for Line

The Laplace transformed pressure and flow at the ends of the fluid line are represented in general form by the following expressions:

$$q_2(s) = q_1(s) \cosh \Gamma(s) - \frac{p_1(s)}{z_c(s)} \sinh \Gamma(s) \quad (2.1)$$

$$p_2(s) = p_1(s) \cosh \Gamma(s) - z_c(s) q_1(s) \sinh \Gamma(s) \quad (2.2)$$

The term  $\Gamma(s)$  is defined as the wave propagation operator, and  $z_c(s)$  is the characteristic impedance per unit length of the fluid in the line. The mathematical definitions of the wave propagation operator and the characteristic impedance increase substantially in sophistication with increasing hierarchy.

Gerlach [2] is credited with obtaining an exact solution of the complete first order Navier-Stokes equation which, when solved simultaneously with the continuity relation and a liquid equation of state, yielded an exact first order model for predicting the dynamics of a viscous, compressible fluid. Gerlach also theoretically predicted the presence of an infinite number of propagation modes.

The fundamental mode represents longitudinal propagation, while all additional modes correspond to radial modes of vibration. In appreciation of the difficulty in implementing the exact solution practically, Gerlach developed a rational approximate model suitable for most engineering problems. This simplified the treatment of the troublesome hyperbolic functions  $\sinh\Gamma(s)$  and  $\cosh\Gamma(s)$ .

Particularly, he represented the hyperbolic operators in terms of infinite products of second order polynomials. Gerlach compared the exact first order model with the approximate rational model for the case of a line termination impedance equal to zero. His comparison revealed that the use of a one term approximation gave excellent results up to somewhat beyond the first critical frequency. The use of two terms of the approximation improved the result up to just beyond the first critical frequency, but does not predict well the values around the second critical frequency. Utilizing additional terms would improve the result around the second critical frequency.

Oldenburger and Goodson [3] also developed an approximate model to simplify the calculation of system frequency characteristics. Their approach involved expanding functions containing the  $\sinh\Gamma(s)$  and  $\cosh\Gamma(s)$  operators in terms of infinite products of second order polynomials. This method, as indicated by Oldenburger [4], essentially amounts to modeling the line with lumped parameters based on resonant points, rather than on the basis of length, as is ordinarily done. This method of lumping results in a much less complicated model for a given desired accuracy.

Viersma [5] derived the so called “four-pole equations” utilizing lumped parameters for simulating line dynamics. However, he acknowledged that his method gives only practical solutions in the frequency domain. He stated that for analysis in the time domain, the complete pipeline, and not just the ends, should be considered. His four-pole equations correspond exactly to those of D’Souza and Oldenburger [6]. The four-pole equations imply that only two of the four variables:  $q_1$ ,  $p_1$ ,  $q_2$ , and  $p_2$ , should be regarded as independent variables. Blackburn [7] pointed out that the two independent variables are not located in the same end of the pipe.

Much theoretical and experimental work has been carried out in the area of predicting the frequency response of servovalve and line combinations. Woods [8] assessed a distributed parameter model with viscous losses. His model incorporated linear resistance and was compared to a wide variety of experimental responses with various source and load impedances. Watton [9] obtained a linearized solution in the frequency domain using an average friction model and a distributed friction model. The friction models are based upon the Hagen-Poiseuille equation for laminar, steady, fully developed, and incompressible flow. Watton also illustrated the use of an electrical analogy by implementing a series of  $\pi$  lumped networks. He concluded that for the frequencies dominant in hydraulic systems, the  $\pi$  lumped network approximation would be adequate.

Watton [10] also studied the effect of transmission line dynamics in a servovalve controlled actuator. His work demonstrates that even short lines may

have a significant effect on the response due to the effective low inertia of the actuator.

Hullender and Healey [11] formulated rational polynomial approximations for the hyperbolic Bessel functions of laminar flow distributed parameter models. For practical applications, they determined it was necessary to simplify the rational polynomial models to lower order models. This was accomplished using time domain state variable representations of modal approximations [12] and will be discussed in the following section.

Recently, a T-segment electrical analogy was successfully used in the modeling of a vehicle power steering system. Ferries and Arbanas [13] used the T-structure to model the lines connecting the valve, cylinder, pump, and reservoir. Each component was modeled separately and interconnected with a T-segment to create the complete hydraulic model. Although the resistance term used was not elaborated on in the model derivation, the simulation results successfully predicted power steering shudder frequency as measured in experiments.

## Time Domain Models

Several time domain studies have been conducted in the area of line dynamics. The approaches fall along the lines of modal approximations, finite difference approximations, the method of characteristics, and lumping by length using the  $\pi$  network electrical circuit analogy.

Starting with the one-dimensional wave equation, Healy and Hullender [12] developed a modal approximation method which includes four modes for each element. The resulting four modes are then solved using the linear state transition method. For the case of a blocked pneumatic transmission line, comparisons were made to a so called "exact" solution. It was found that four modes provided sufficient accuracy. The linear state transition method allowed for convenient coupling to other system elements.

The finite difference method has been applied to the solution of the first order wave equation. The method is restricted to the average friction model and is closely related to a lumping by length approach. Watton [14] determined that using greater than three nodes to analyze a line produced rapidly diminishing returns in accuracy. In addition, the mathematical stability of the method is extremely sensitive to proper time step selection.

The method of characteristics is used to solve two partial differential equations for wave propagation by combining them into a total differential equation. When laminar flow exists, the method of characteristics has been used for the lossless line model equations by Watton [9]. Zielke [15] extended the method of characteristics to include the effects of time dependent friction. Brown

[16] formulated the "quasi method" of characteristics which takes into account both time dependent friction and heat transfer.

Lee [17] investigated the computer control of transmission line dynamics for a servovalve and line hydraulic system. Lee modeled the distributed parameter line using the finite difference method (fdm) and the method of characteristics in his simulations. He agreed with Watton's conclusions that the method of characteristics is less time consuming and more stable with respect to time step selection. However, Lee found that if the line is divided into more than four sections, the response delay is abnormally long.

Krus et al. [18] mated the method of characteristics to the four-pole equations developed by Viersma. Krus first applied his method to the case of distributed resistance which utilized the well known Hagen-Poiseuille law for fully developed laminar flow in pipes. To extend his model to include frequency dependent resistance, Krus combined his expression for the case of purely distributed friction with a first order low pass filter to represent the frequency dependent friction. For numerical efficiency, the friction was lumped to the ends of the line, where the state variables were calculated.

Recently, Watton and Hawkey [19] presented an approach that uses the modal analysis technique as the foundation theory. This foundation established a set of discreet equations relating pressures and flow rates at both ends of the line. The unknown coefficients of each time domain equation were then determined for the practical line using measured test data. Thus, experimental data is required to complete the model.

## CHAPTER III

### THEORY OF EXACT FIRST ORDER MODEL

In any liquid fluid dynamics modeling endeavor, the ideal situation is to incorporate all equations of change describing the conservation of mass, the conservation of momentum, the conservation of energy, and various equations of state which may represent thermal and mechanical stresses. For fluid in a conduit, further expressions would be needed to describe boundary conditions and the interaction of the fluid with the conduit wall. Although the necessary mathematical expressions are available, simplifying assumptions and linearizations are needed so that solutions may be obtained. The simplifying and linearizing process requires great skill and experience in order to achieve reasonable results. The next challenge to the modeler is to successfully apply the simplified governing equations to practical engineering problems.

As presented in the literature survey, one of the most sophisticated fluid dynamics models available is the "Exact" first order model developed by Gerlach [2]. The intent of this section is to briefly present the formulation of the exact first order model as the foundation for the forthcoming rational approximate engineering model which will be utilized in this effort. The complete treatise for these two models may be found in reference [2]. The rational approximate model



will serve as a reference for the  $T^3$  model utilizing electrical analogies. The development of the  $T^3$  model will be presented in Chapter IV.

### Mathematical Formulation of Problem

The equations of change for fluid motion with respect to a fixed spatial coordinate system may be written as follows, according to [2]:

#### (a) Continuity Equation

The conservation of mass for a fluid is

$$\frac{\partial \rho}{\partial t} + \nabla \cdot (\rho \bar{v}) = 0 \quad (3.1)$$

where

$\rho$  = instantaneous fluid density

$\bar{v}$  = vector velocity in terms of spatial coordinate location and time

#### (b) Equation of Motion

The Navier-Stokes relation is

$$\rho \left\{ \frac{\partial \bar{v}}{\partial t} + (\bar{v} \cdot \nabla) \bar{v} \right\} = \rho \bar{F} - \nabla p + \mu \left\{ \frac{4}{3} \nabla (\nabla \cdot \bar{v}) - \nabla \times (\nabla \times \bar{v}) \right\} \quad (3.2)$$

In this equation,

$\bar{F}$  = vector body force per unit mass

$p$  = total fluid pressure

$\mu$  = shear viscosity

where each term is generally a function of the spatial coordinate position and time.

#### (c) Equation of State of Fluid

The equation of state of a fluid is the functional relationship between its pressure, density, and temperature. For a liquid, it is

$$dp = \beta \frac{d\rho}{\rho} \quad (3.3)$$

where  $\beta$  is the fluid bulk modulus of elasticity. The energy equation, which accounts for heat transfer effects, may be eliminated from the solution. Thermal effects have been shown to be negligible for liquids in many cases. The final assumption that the non-linear effects are probably minor or negligible will allow the following linearizations.

$$\bar{v} = \bar{v}_0 + \bar{v}_1 \quad (3.4)$$

$$p = p_0 + p_1 \quad (3.5)$$

$$\rho = \rho_0 + \rho_1 \quad (3.6)$$

The subscript "0" denotes steady state or slowly varying quantities, and the subscript "1" denotes first-order disturbance quantities. The substitution of equations 3.4, 3.5, and 3.6 into the continuity, motion, and state equations will linearize these equations and produce first order equations of change. In hydraulic applications, it may be assumed that buoyancy forces are extremely small compared to the enormous mechanical forces applied to the fluid.

Assuming no body force, the equations of change become

$$\rho_0 \frac{\partial \bar{v}_1}{\partial t} = -\nabla p_1 + \mu \left\{ \frac{4}{3} \nabla (\nabla \cdot \bar{v}_1) - \nabla \times \nabla \times \bar{v}_1 \right\} \quad (3.7)$$

which will be called the first-order Navier-Stokes equation,

$$\frac{\partial p_1}{\partial t} + \rho_0 \nabla \cdot \bar{v}_1 = 0 \quad (3.8)$$

for the first order continuity equation, and

$$dp_1 = \beta \frac{dp_1}{\rho_0} \quad (3.9)$$

for the liquid state equation.

Equations 3.7, 3.8, and 3.9 comprise the mathematical formulation of the problem. To describe the fluid conduit, the cylindrical coordinate system will be employed as shown in Figure 3.1. Introducing the isentropic speed of sound for the fluid under consideration

$$c_0 = \sqrt{\frac{\beta}{\rho_0}} \quad (3.10)$$

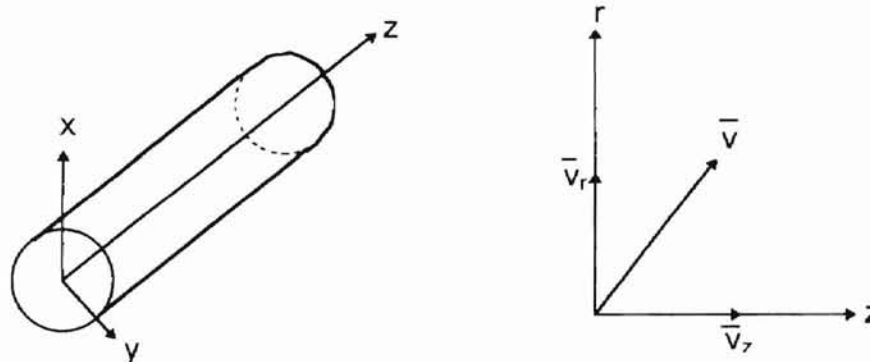


Figure 3.1. Coordinate system

and combining equations 3.8 and 3.9 gives

$$\frac{\partial p_1}{\partial t} + \rho_0 c_0^2 \nabla \cdot \bar{v}_1 = 0 \quad (3.11)$$

The Equations 3.7 and 3.11 are the equations of change in terms of the first order variables  $\bar{v}_1$  and  $p_1$  which represent small perturbations from the zero-order conditions  $\bar{v}_0$  and  $p_0$ . The restrictions on these equations are:

1. The fluid velocity ( $\bar{v} = \bar{v}_0 + \bar{v}_1$ ) at any point and time is much less than the velocity of sound in the fluid, thus justifying omission of the non-linear terms.
2. Perturbations in the density are negligible compared to the average density; that is  $\rho_1 \ll \rho_0$ .
3. Temperature effects are negligible.
4. Fluid viscosity is spatially independent.
5. The flow field is axi-symmetric

The first restriction is further supported by the fact that in fluid power systems, it is good design practice to size the components, fittings, and lines such that the fluid velocity does not exceed 15 feet per second.

### Solution Outline

The method of solution for equations 3.7 and 3.11 is lengthy, and again the reader is referred to reference [2] for the mathematical manipulations, most of which are omitted here. The key to unlocking the solution begins with the postulation that the vector velocity is composed of the gradient of the scalar potential  $\phi$  plus the curl of the vector potential  $\bar{\Psi}$ , or

$$\bar{v}_1 = \nabla\phi + \nabla \times \bar{\Psi} \quad (3.12)$$

In brief summary, the solution transforms the two coupled partial differential equations, 3.7 and 3.8, into two independent partial differential equations

$$\frac{\partial^2 \phi}{\partial t^2} = c_0^2 \nabla^2 \phi + \frac{4}{3} v \frac{\partial}{\partial t} \nabla^2 \phi \quad (3.13)$$

$$\frac{\partial \Psi}{\partial t} = v \nabla^2 \Psi \quad (3.14)$$

which are of known solvable form.

Assuming zero initial conditions, the Laplace transformation of equations 3.13 and 3.14 are obtained

$$s^2 \hat{\phi} = c_0^2 \nabla^2 \hat{\phi} + \frac{4}{3} \nu s \nabla^2 \hat{\phi} \quad (3.15)$$

$$s \hat{\Psi} = \nu \nabla^2 \hat{\Psi} \quad (3.16)$$

where  $\hat{\phi}$  and  $\hat{\Psi}$  are the transformed quantities. The solution to the above two equations was completed by

1. Application of method of separation of variables (creates separation constant  $\gamma$ )
2. Application of postulation that  $\bar{v}_1 = \nabla \hat{\phi} + \nabla \times \hat{\Psi}$ .
3. Specification of boundary conditions at the wall.

This led to the theoretical prediction of an infinite number of viscous modes of propagation. For purposes of hydraulic line modeling, it will be assumed that the zeroth mode, or fundamental mode, is predominant. The zeroth mode represents longitudinal vibrations. Furthermore, boundary conditions must be applied at the pipe ends. The boundary conditions necessary to satisfy are

$$\bar{v}_z \Big|_{z=0} = \bar{v}_1$$

and

$$\bar{p}_z \Big|_{z=0} = \bar{p}_1.$$

The bar notation indicates that the quantities have been averaged over the cross section by integration from  $r=0$  to  $r=r_0$ . Figure 3.2 shows a diagram of a fluid conduit with appropriate end conditions. Application of the pipe end conditions leads to the transfer relations

$$\bar{v}_z = \bar{v}_1 \cosh \gamma z - \frac{\bar{p}_1}{z_c} \sinh \gamma z \quad (3.17)$$

$$\bar{p} = \bar{p}_1 \cosh \gamma z - z_c \bar{v}_1 \sinh \gamma z \quad (3.18)$$

where

$$Z_c = \frac{\rho_0 C_0^2 \gamma}{s} \quad (3.19)$$

$Z_c$  is the characteristic impedance for the line.

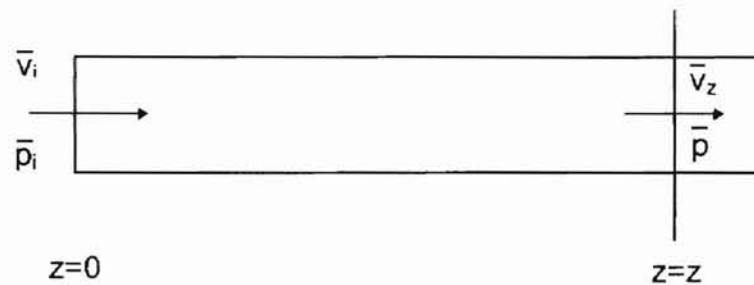


Figure 3.2. Diagram of Fluid Conduit for Fundamental Mode Transfer Equations

### Impedance Formulation

For convenience, equations 3.17 and 3.18 may be rewritten in a form relating conditions at two positions, where position 2 is oriented a  $+L$  distance from position 1 in the  $z$  direction. See Figure 3.3.

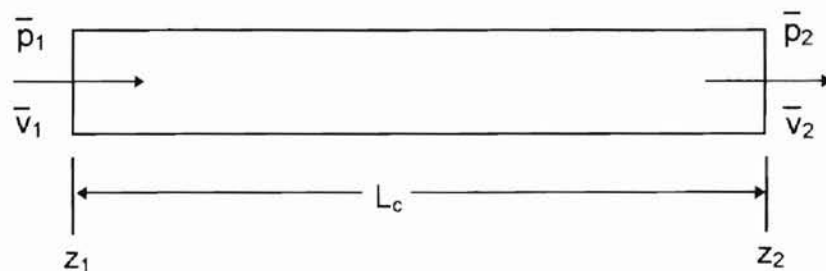


Figure 3.3 Diagram of a Fluid Conduit With Averaged Quantities at Each End.

This form is

$$\bar{v}_2 = \bar{v}_1 \cosh \Gamma - \frac{\bar{p}_1}{z_c} \sinh \Gamma \quad (3.20)$$

$$\bar{p}_2 = \bar{p}_1 \cosh \Gamma - z_c \bar{v}_1 \sinh \Gamma \quad (3.21)$$

The quantity  $\Gamma$  is often referred to as the wave propagation operator. It is related to  $\gamma$  by  $\Gamma = \gamma L_c$ . Equations 3.20 and 3.21 show that if one specifies the impedance at one end of the line, then the response of  $\bar{p}$  to  $\bar{v}$  or  $\bar{v}$  to  $\bar{p}$  for the other end can be found. Impedance is generally defined here as the ratio of pressure to velocity, or  $\bar{z} = \frac{\bar{p}}{\bar{v}}$ . Thus equations 3.20 and 3.21 may be written in impedance form as

$$\bar{z}_1 = \frac{\bar{z}_2 \cosh \Gamma + z_c \sinh \Gamma}{\cosh \Gamma + \frac{\bar{z}_2}{z_c} \sinh \Gamma} \quad (3.22)$$

where  $\bar{z}_1 = \frac{\bar{p}_1}{\bar{v}_1}$ .

For the special case of a termination impedance equal to the line characteristic impedance, equation 3.22 would become

$$\bar{z}_1 = z_c = \frac{\rho_0 c_0^2 \gamma}{s} \quad (3.23)$$

which means that the impedance looking into end 1 will be the same as the line characteristic impedance. The characteristic impedance is the impedance for which the load and input impedances are equal. For the case of a termination impedance other than  $z_c$ , such as  $z_2=0$ , equation 3.22 becomes

$$z_1 = z_c \tanh \Gamma \quad (3.24)$$

Qualitatively, equation 3.23 describes a matched impedance condition,  $\frac{z_1}{z_c} = 1$ .

This means there will be no standing wave patterns. No reflections are returned to the source in this case. Equation 3.24, which describes a blocked tube condition, will have large resonant peaks which depend on the values of the real and imaginary parts of the wave propagation operator.

#### Rational Approximate Engineering Model

Equations 3.20 and 3.21 are well known and have been obtained by several authors. The formula for the wave propagation operator merely varies according to the original equations of change. The definition of the gamma operator for the exact first order model is quite intricate and mathematically unwieldy for solving standard engineering problems. Fortunately, there are methods of approximating the gamma operators and the hyperbolic operators. From this point on, the bar operators will be omitted for brevity since it is understood that the fluid velocity and pressure are quantities averaged over the cross-sectional area of the line.

The simplified, or rational approximate engineering model [20] involves expanding the hyperbolic functions,  $\cosh \Gamma(s)$  and  $\sinh \Gamma(s)$ , as infinite products of second order polynomial terms

$$\cosh \Gamma(s) = \prod_{n=0}^{\infty} \left\{ 1 + \frac{2\zeta_{cn} s}{\omega_{cn}} + \frac{s^2}{\omega_{cn}^2} \right\} \quad (3.25)$$



$$\sinh \Gamma(s) = \Gamma(s) \prod_{n=1}^{\infty} \left\{ 1 + \frac{2\zeta_{sn}s}{\omega_{sn}} + \frac{s^2}{\omega_{sn}^2} \right\}. \quad (3.26)$$

The values of the constants  $\zeta_{cn}$ ,  $\zeta_{sn}$ ,  $\omega_{cn}$ , and  $\omega_{sn}$  are to be obtained by solving for the values of  $s_n$  at the zeroes of  $\cosh \Gamma(s)$  and  $\sinh \Gamma(s)$ .  $\zeta_n$  and  $\omega_n$  are found by noting that

$$s_n = -\zeta_n \omega_n \pm i\sqrt{1 - \zeta_n^2} \quad (3.27)$$

Figures 3.4, 3.5, 3.6, and 3.7 display plots of  $\zeta_{cn}$ ,  $\zeta_{sn}$ ,  $F_{cn}$ , and  $F_{sn}$  versus axial damping number. These plots are simply utilized by first calculating the dimensionless damping number for a line using

$$D_{nz} = \frac{vL_c}{c_0 f_0^2} \quad (3.28)$$

The corresponding values for  $\zeta_n$  and  $F_n$  are then read off of the plot. The frequency  $\omega_n$  is then given by equation 3.29.

$$\omega_n = \frac{F_n c_0}{L_c} \quad (3.29)$$

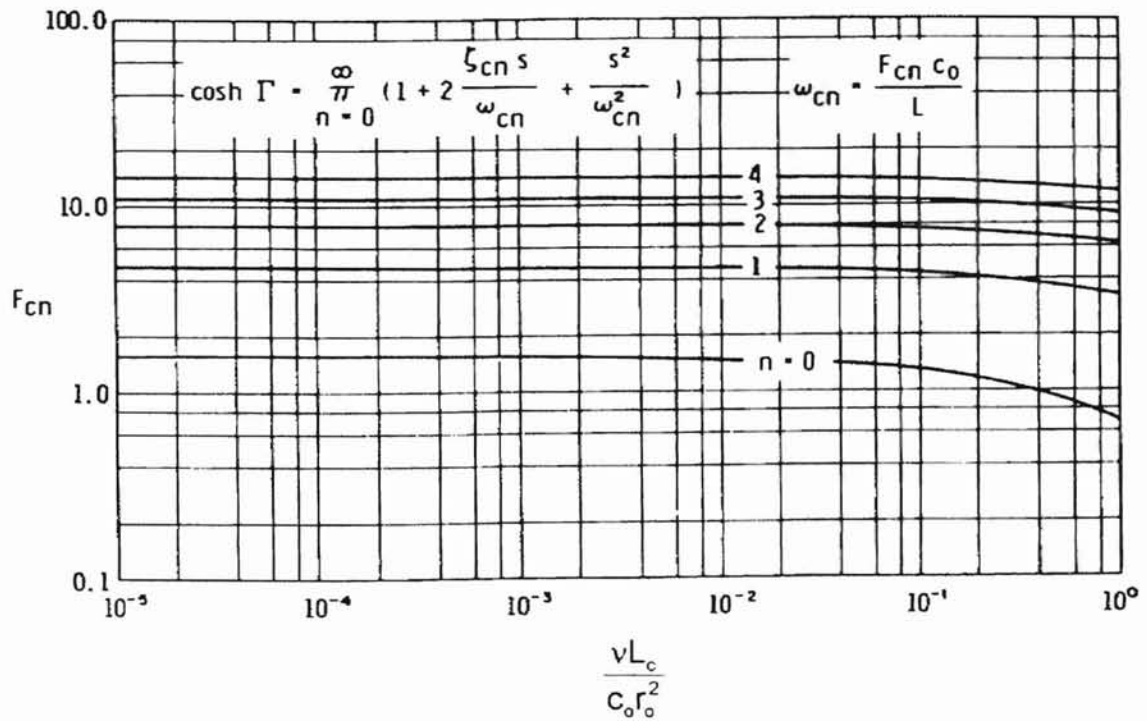


Figure 3.4 Variation of the Approximate Model Parameter  $F_{cn}$  with Axial Damping Number [20]

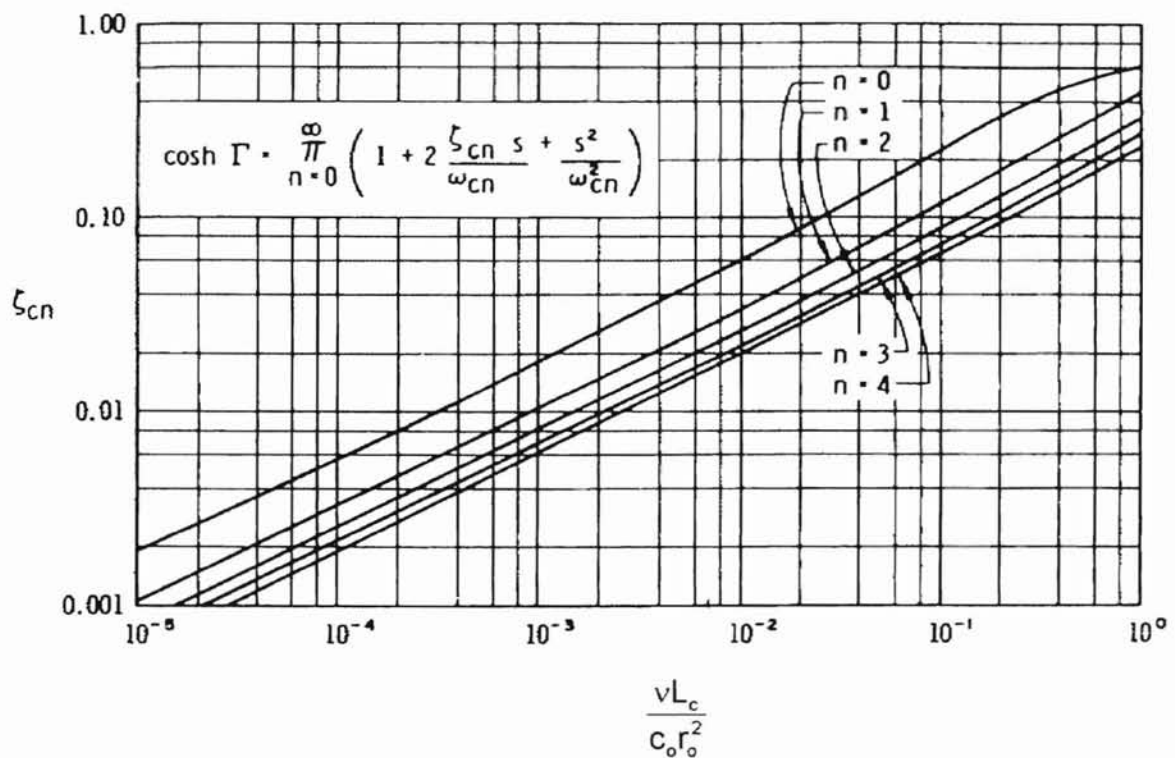


Figure 3.5 Variation of the Approximate Model Parameter  $\zeta_{cn}$  with Axial Damping Number [20]

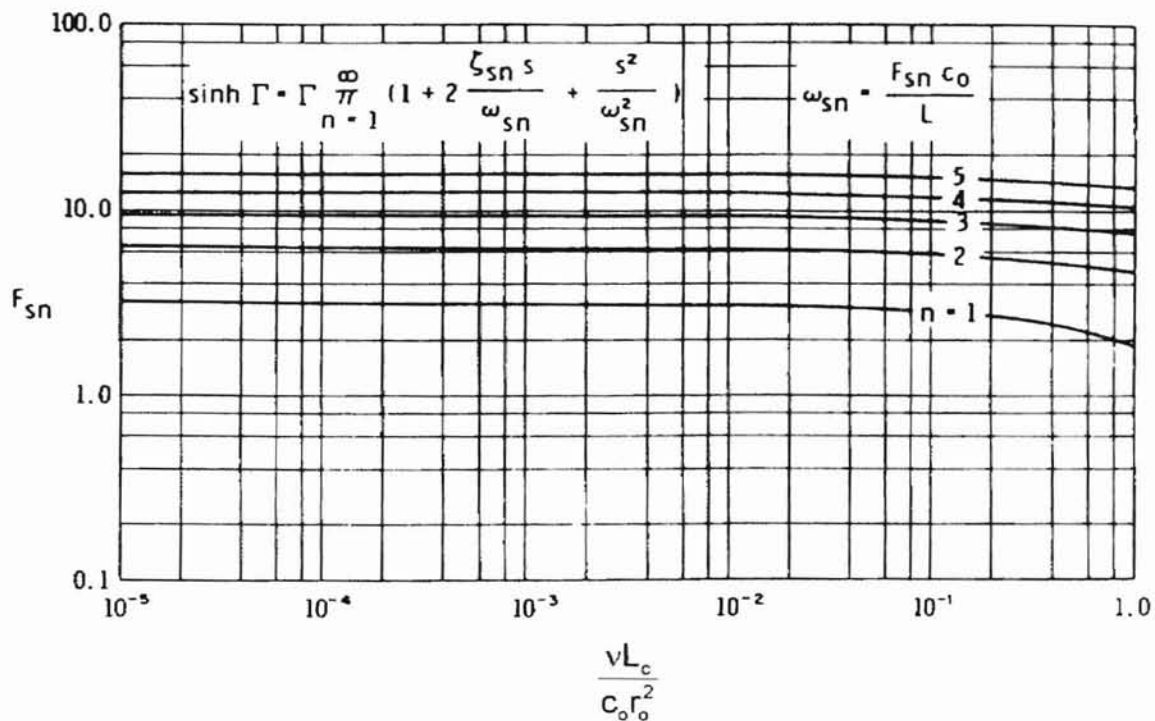


Figure 3.6 Variation of the Approximate Model Parameter  $F_{sn}$  with Axial Damping Number [20]

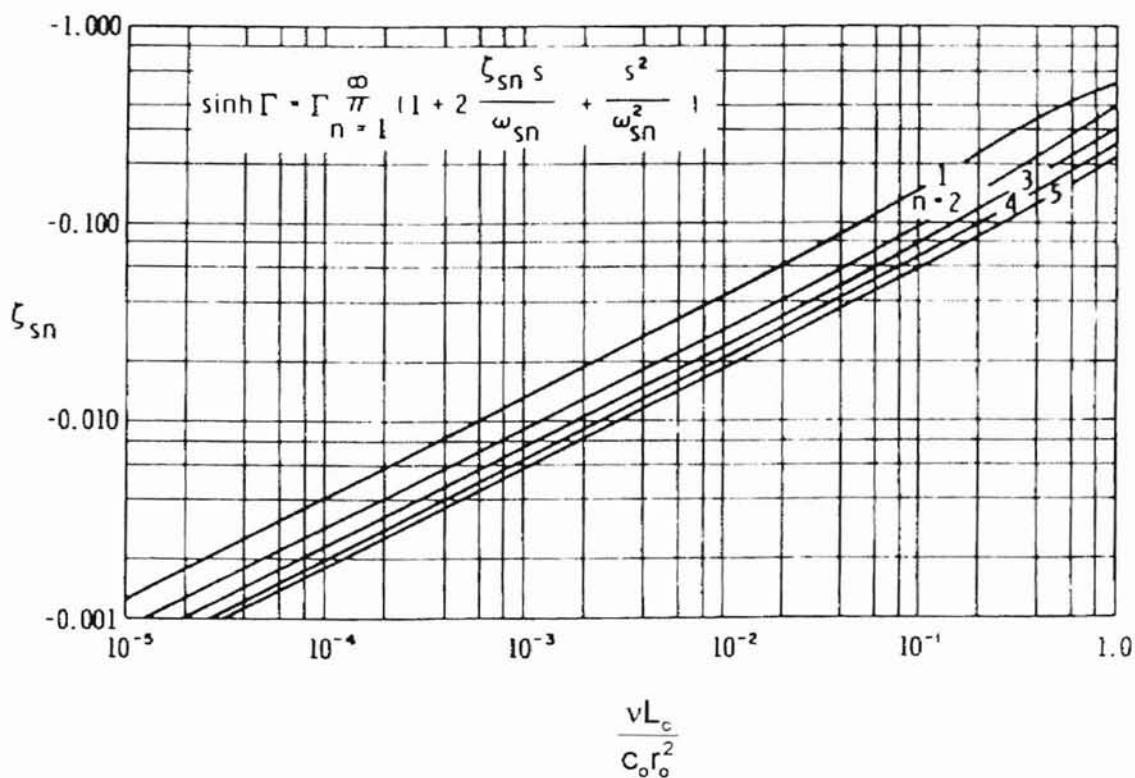


Figure 3.7 Variation of the Approximate Model Parameter  $\zeta_{sn}$  with Axial Damping Number [20]

For the case of a termination impedance equal to zero, equation 3.24 may be rewritten as (Laplace domain form)

$$z_1(s) = z_c(s) \frac{\sinh \Gamma(s)}{\cosh \Gamma(s)}. \quad (3.30)$$

For purposes of the approximate model, the wave propagation operator takes on the following form:

$$\Gamma(s) = \frac{sL_c}{C_0} \quad (3.31)$$

The characteristic impedance becomes

$$z_c = \frac{\rho_0 C_0^2 \Gamma(s)}{sL_c A} = \frac{\rho_0 C_0}{A}. \quad (3.32)$$

Substituting equations 3.25, 3.26, and 3.32 into equation 3.30 produces

$$\left( \frac{p_1(s)}{v_1(s)} \right) = \frac{\rho_0 C_0}{A} \cdot \frac{\Gamma(s) \prod_{n=1}^{n=\infty} \left\{ 1 + \frac{2\zeta_{sn} s}{\omega_{sn}} + \frac{s^2}{\omega_{sn}^2} \right\}}{\prod_{n=0}^{\infty} \left\{ 1 + \frac{2\zeta_{cn} s}{\omega_{cn}} + \frac{s^2}{\omega_{cn}^2} \right\}}. \quad (3.33)$$

Lastly, substituting equation 3.31 into equation 3.33 and simplifying results in the final amplitude ratio form of equation 3.34.

$$\left( \frac{p_1(s)}{v_1(s)} \right) = \frac{\rho_0 s L_c}{A} \cdot \frac{\prod_{n=1}^{n=\infty} \left\{ 1 + \frac{2\zeta_{sn} s}{\omega_{sn}} + \frac{s^2}{\omega_{sn}^2} \right\}}{\prod_{n=0}^{\infty} \left\{ 1 + \frac{2\zeta_{cn} s}{\omega_{cn}} + \frac{s^2}{\omega_{cn}^2} \right\}}. \quad (3.34)$$

### Simulation Results

The parameters in Table 3.1 were used in generating the magnitude response of equation 3.34 for the case of a termination impedance equal to zero. The

simulation results were obtained using MATLAB (Copyright The Mathworks). The MATLAB m-file listings containing the  $n=0$ ,  $n=1$ , and  $n=2$  approximate models are located in Appendix A.

Table 3.1  
Simulation Parameters for Rational Approximate Model

Parameter	Symbol	Value and Units
line length	$L_c$	70 inches
fluid density	$\rho_0$	$7.95 \times 10^{-5} \text{ lb}_f\text{sec}^2/\text{in}^4$
kinematic viscosity	$\nu$	$2.91 \times 10^{-2} \text{ in}^2/\text{sec}$
line radius	$r_0$	0.09 inches
sonic velocity	$c_0$	48965 in/sec

Figures 3.8 and 3.9 display the simulation results for the one term ( $n=0$ ) model. Figures 3.10 and 3.11 contain the simulation results for the two term ( $n=1$ ) model. It can be seen that the one term model predicts a fundamental frequency of approximately 1050 rad/sec. The two term model confirms the fundamental frequency prediction and shows a second critical frequency occurring at approximately 3200 rad/sec. The two term order model shows little attenuation at the second critical frequency. The simulation results of the three term ( $n=2$ ) model in Figures 3.12 and 3.13 yield a third critical frequency and show an improved amplitude prediction at the second critical frequency. In Figures 3.9, 3.11, and 3.13, the dimensionless frequency number on the horizontal axis is determined using equation 3.30.

$$F = \frac{\omega L_c}{c_0} \quad (3.30)$$

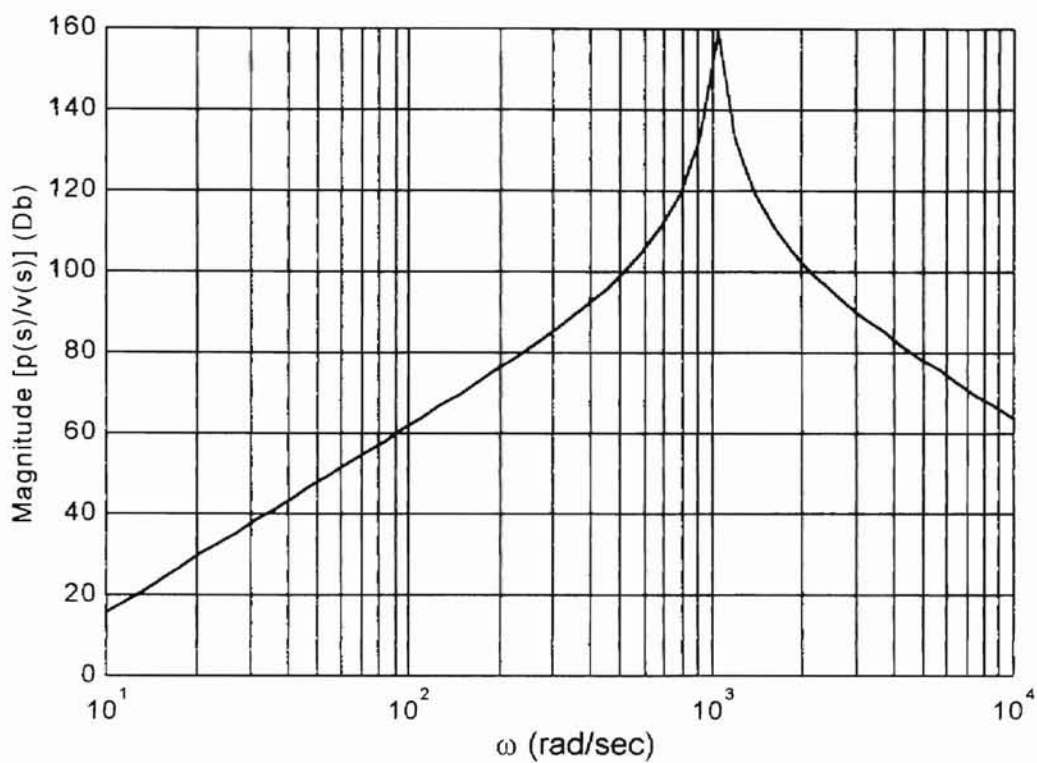


Figure 3.8  $n=0$  Amplitude Response vs. Angular Frequency

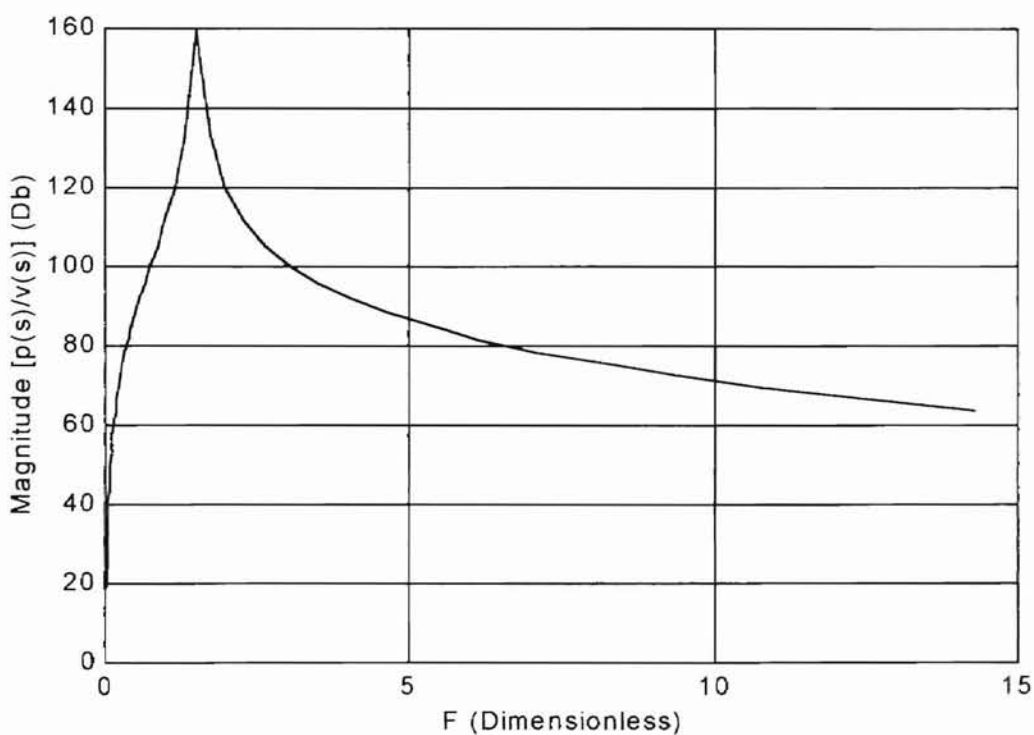


Figure 3.9  $n=0$  Amplitude Response vs Frequency Number

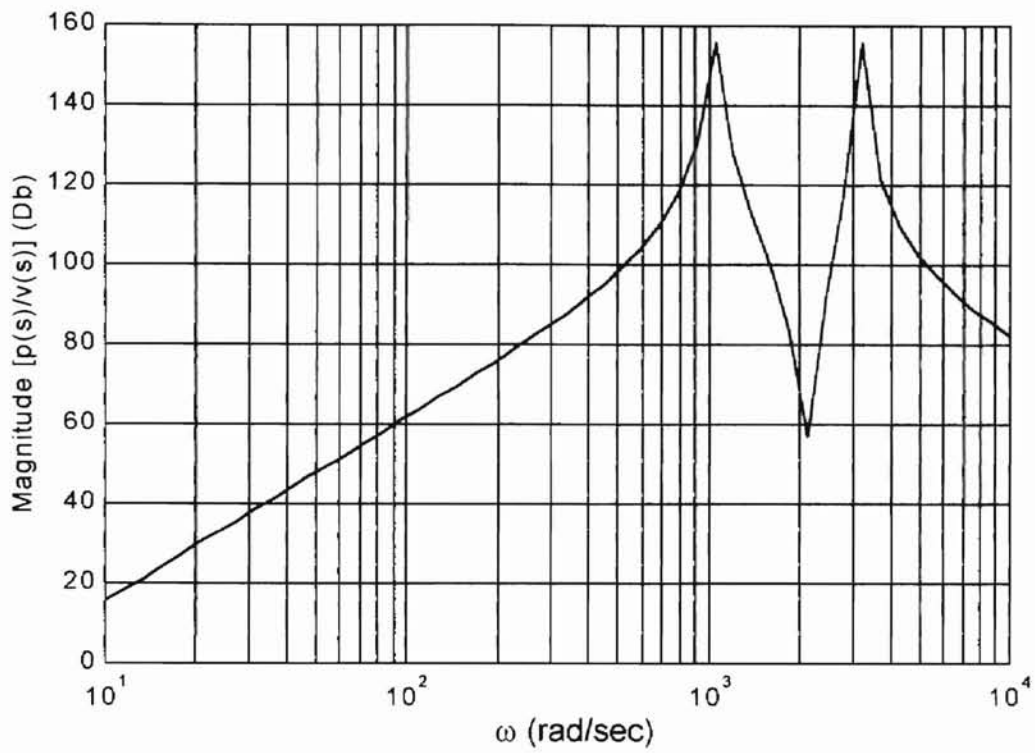


Figure 3.10  $n=1$  Amplitude Response vs. Angular Frequency

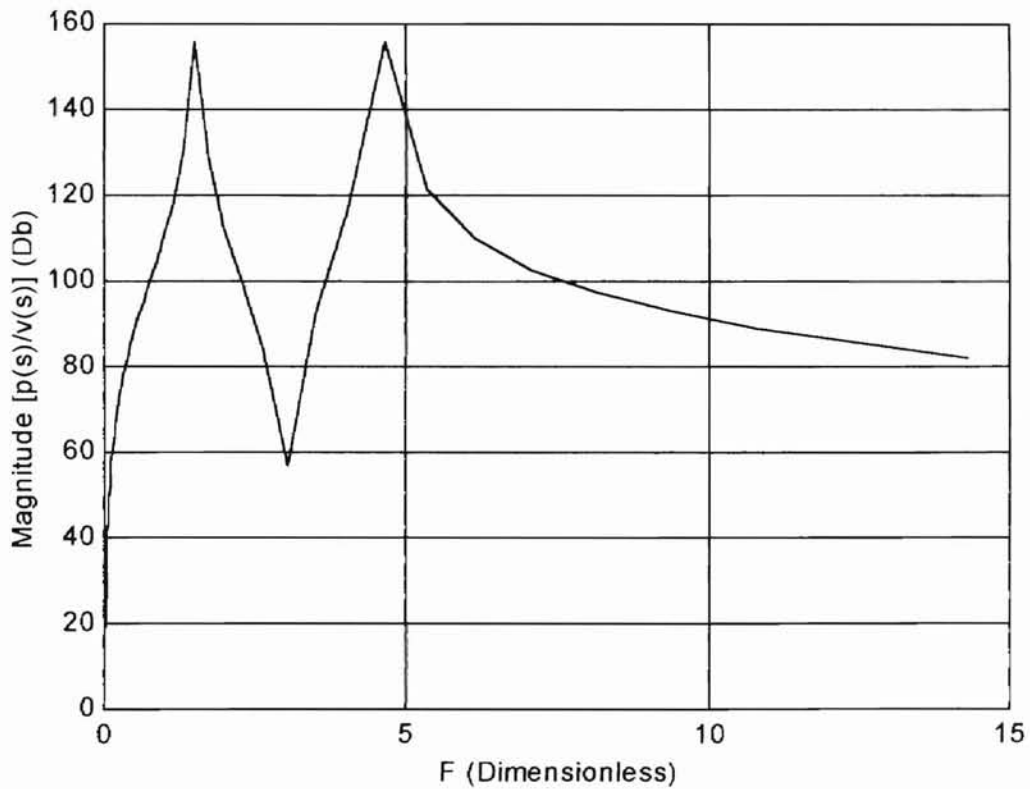


Figure 3.11  $n=1$  Amplitude Response vs Frequency Number

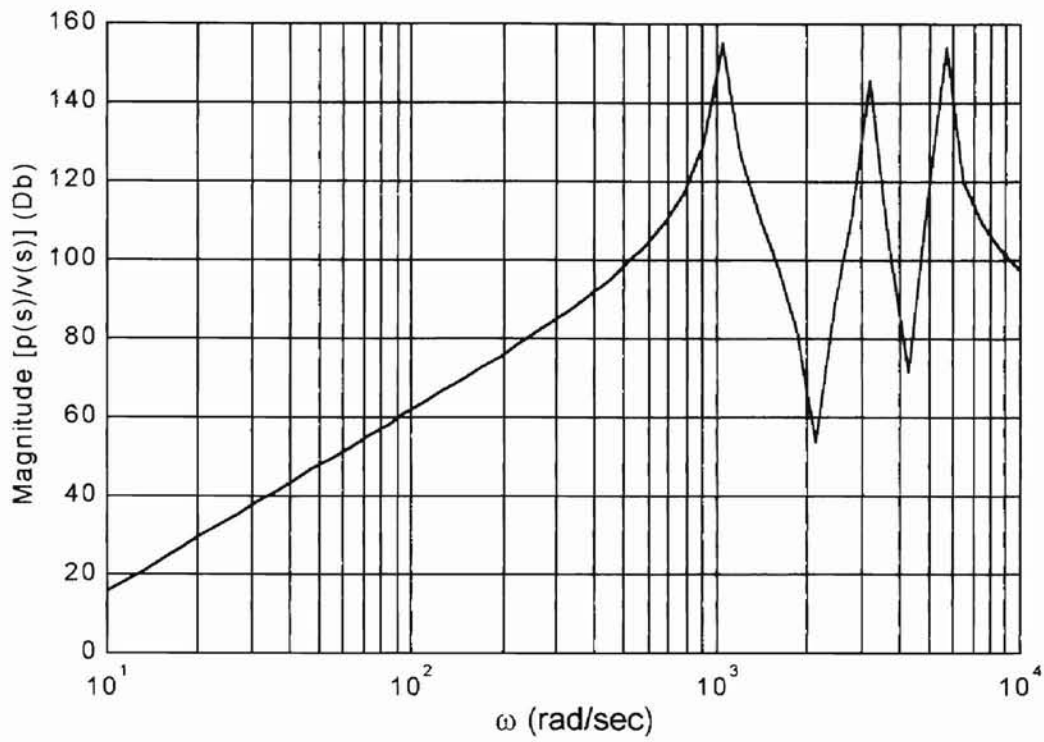


Figure 3.12  $n=2$  Amplitude Response vs. Angular Frequency

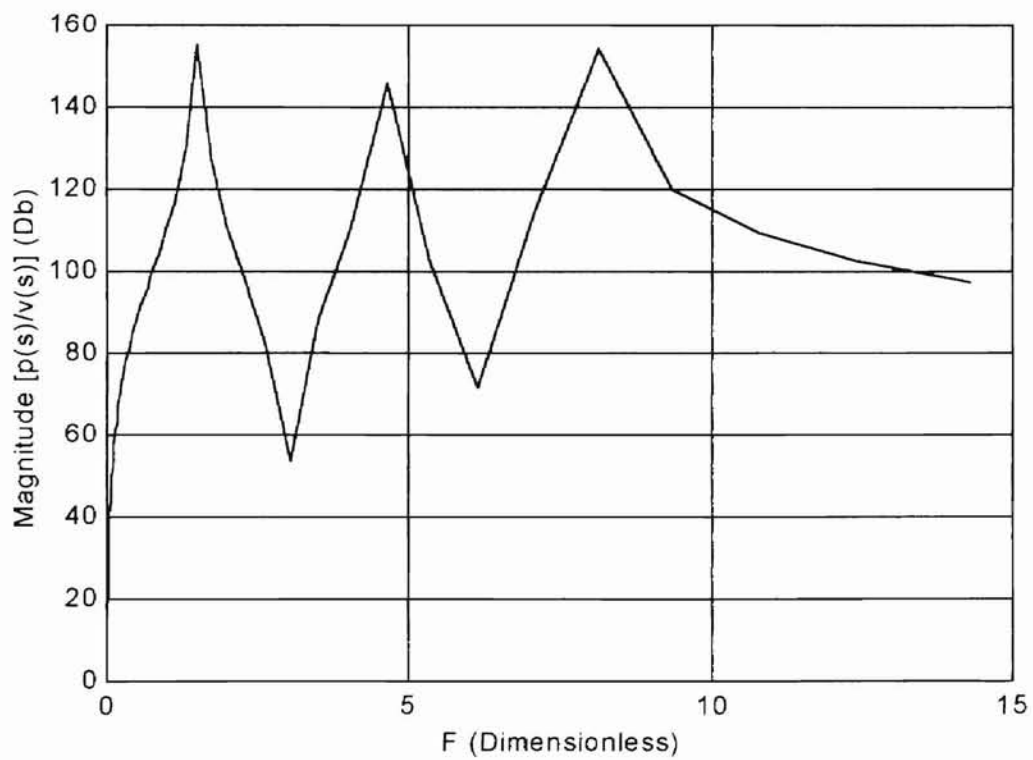


Figure 3.13  $n=2$  Amplitude Response vs. Frequency Number



## CHAPTER IV

### DEVELOPMENT OF ELECTRICAL ANALOGY FOR LINE DYNAMICS

Chapter III briefly summarized the fundamental fluid mechanics equations which are the foundation of the exact first order model. The subsequent and more easily applied rational approximate model was demonstrated in [2] to predict well the impedance amplitude response up to approximately the second critical line frequency when compared to the exact first order model and test data. This chapter will present the development of the  $T^3$  electrical analogy incorporating the S-T method. The intent will then be to compare the results of the  $T^3$  analogy with the rational approximate model. This will be completed in Chapter 5 through the solution of a fundamental engineering problem.

#### $T^3$ Network

The  $T^3$  lump is formulated from electrical circuit technology. In the modeling of a fluid transmission line, analogs between electrical properties and fluid mechanics properties must be defined. The analogs are:

$$\begin{array}{ll} \text{Pressure } P \text{ (psi)} & \leftrightarrow \text{Voltage } V \text{ (volts)} \\ \text{Volumetric Flow Rate } q \text{ (in}^3\text{/sec)} & \leftrightarrow \text{Current } I \text{ (amps)}. \end{array}$$

To describe the resistive, capacitive, and inductive properties of a fluid transmission line, the relations given in Table 4.1 may be employed. To illustrate how the fluid equations in Table 4.1 may be implemented, Figure 4.1 depicts one lump of the  $T^3$  network with fluid terms applied.

Table 4.1  
Describing Equations for Electrical Analogy of a Line

Property	Electrical Equation	Fluid Equation
Resistance (R)	$V=Ri$	$P=Rq$
Capacitance (C)	$i=C \cdot dV/dt$	$q=C \cdot dP/dt$
Inductance (L)	$V=L \cdot di/dt$	$P=L \cdot dq/dt$

A nodal method will be used so that the circuit components may be mathematically coupled. In Figure 4.1, the nodes are located at  $P_{in}$ ,  $P_2$ ,  $P_3$ ,  $P_4$ , and  $P_{out}$ .

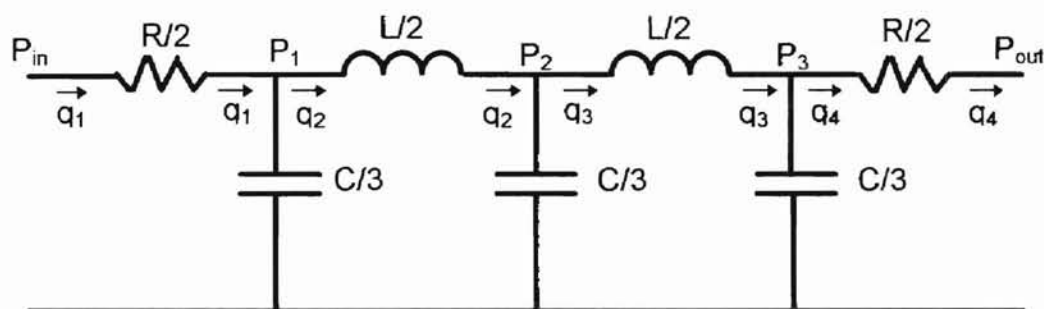


Figure 4.1 Schematic of  $T^3$  Lump

One school of thought is to lump the respective pressures and flows inside each resistor, capacitor, and inductor. However, the nodal method allows the effect of each component to be lumped at the node. In other words, the effective control volume is positioned at each node, rather than each component. By applying the fluid equations in Table 4.1 to the schematic in Figure 4.1, a set of five first order differential equations is obtained, which represents each of the five energy storing elements in the circuit.

#### Differential Equations for $T^3$ Lump

$$\frac{dP_1}{dt} = \frac{3}{C} \cdot (q_1 - q_2)$$

$$\begin{aligned}
 \frac{dP_2}{dt} &= \frac{3}{C} \cdot (q_2 - q_3) \\
 \frac{dP_3}{dt} &= \frac{3}{C} \cdot (q_3 - q_4) \\
 \frac{dq_2}{dt} &= \frac{2}{L} \cdot (P_1 - P_2) \\
 \frac{dq_3}{dt} &= \frac{2}{L} \cdot (P_2 - P_3)
 \end{aligned}
 \tag{4.1}$$

The typical equations for the resistance terms take on the following form assuming laminar flow.

$$P_{in} - P_1 = \frac{R}{2} \cdot q_1 \tag{4.2a}$$

$$P_3 - P_{out} = \frac{R}{2} \cdot q_4 \tag{4.2b}$$

Before the solution to equations 4.1 and 4.2 can proceed, it is necessary to first define the inductance, capacitance, and resistance terms, L, C, and R. Fluid inductance represents the mass of fluid in the line as

$$L = \frac{\rho \cdot \ell}{A_L} \quad (\text{lb}_f \text{sec}^2 / \text{in}^5) \tag{4.3}$$

where  $\rho$  = fluid density  
 $\ell$  = length of line segment  
 $A_L$  = inside cross-sectional area of line.

Fluid capacitance represents the compressibility of the fluid in the line and is given by

$$C = \frac{V_{line}}{\beta_{eff}} \quad (\text{in}^3 / \text{psi}) \tag{4.4}$$

where  $V_{line}$  = fluid volume in line  
 $\beta_{eff}$  = effective bulk modulus.

The effective bulk modulus is an extremely important parameter because it can reflect certain material properties of the pipe as well as the entrainment of air in

the oil. For this study, the effective bulk modulus is a combination of the fluid bulk modulus and the pipe bulk modulus. It is assumed that no vapor or entrained air is present, and a good mechanical design exists for the fluid passages, i.e. no holes or pockets exist which could collect air. Since the fluid bulk modulus and the conduit bulk modulus operate in parallel, they may be combined as resistors in parallel to yield

$$\beta_{\text{eff}} = \frac{\beta_{\text{pipe}} \cdot \beta_{\text{oil}}}{\beta_{\text{pipe}} + \beta_{\text{oil}}} \quad (\text{psi}) \quad (4.5)$$

where  $\beta_{\text{pipe}}$  = bulk modulus of pipe  
 $\beta_{\text{oil}}$  = bulk modulus of oil.

The bulk modulus for a thin walled pipe allows the use of the following formula which is generally used for hydraulic tubing.

$$\beta_{\text{pipe}} = \frac{W_t \cdot E}{d_o} \quad (\text{psi}) \quad (4.6)$$

where  $W_t$  = wall thickness  
 $E$  = elastic modulus of tube material  
 $d_o$  = outside diameter of tube

#### Resistance to Flow Calculation Methods

##### Hagen-Poiseuille Law

The resistance term,  $R$ , for flow through a circular conduit has historically been represented by the well known Hagen-Poiseuille law for the case of laminar flow. The presence of laminar, transition, or turbulent flow is determined by the Reynolds number,  $N_R$ .

$$N_R = \frac{\rho \cdot v \cdot d_i}{\mu} = \frac{u \cdot d_i}{\nu} \quad (4.7)$$

where  $\rho$  = fluid mass density  
 $v$  = fluid velocity  
 $\mu$  = absolute viscosity  
 $d_i$  = conduit inside diameter  
 $\nu$  = kinematic viscosity

The Reynolds number criteria for the various flow regimes is as follows:

<u>Flow Regime</u>	<u>Reynolds Criteria</u>
Laminar	$N_R \leq 2000$
Transition	$2000 < N_R < 4000$
Turbulent	$N_R \geq 4000$

The Hagen-Poiseuille law, shown in equation 4.8, may be applied over a given length of conduit to find the pressure drop and associated drag force on the conduit resulting from the flow of a viscous fluid.

$$\frac{\Delta P}{\ell} = \frac{8 \cdot \mu \cdot v}{r^2} = \frac{32 \cdot \mu \cdot v}{d_i^2} = \frac{128 \cdot \mu}{\pi \cdot d_i^4} \cdot q \quad (4.8)$$

where  $\Delta P$  = differential pressure

The assumptions for the fluid are that it is Newtonian and behaves as a continuum. The assumptions for the flow include laminar, steady, fully developed, and incompressible. When these assumptions exist, pure fluid resistance is of the form

$$\Delta P = R_{lam} \cdot q \quad (4.9)$$

where  $R_{lam}$  = resistance to laminar flow.

By equating coefficients between equations 4.8 and 4.9, the resistance term  $R_{lam}$  becomes

$$R_{lam} = \frac{128 \cdot \mu \cdot \ell}{\pi \cdot d_i^4} \quad (4.10)$$

In the case of turbulent flow conditions, equation 4.9 no longer holds, and the Hagen-Poiseuille equation cannot be applied. The resistance term becomes part of a square law formulation such as

$$\Delta P = R_{\text{turb}} \cdot q^2 \quad (4.11)$$

where  $R_{\text{turb}}$  = resistance to turbulent flow

which is obviously non-linear and more difficult to implement in a dynamic line model. Another way to account for pressure loss due to turbulent flow is the use of a pipe friction factor. For steady, one dimensional flow, a reduced form of the Bernoulli equation which includes a pipe friction factor can be used to calculate the pressure drop vs. flow relationship. One such equation is Darcy's empirical formula which includes a dimensionless friction factor,  $f_D$ . The Darcy equation is as follows:

$$\Delta P = f_D \cdot \frac{\ell \cdot \rho}{2 \cdot d_i} \cdot \left( \frac{q}{A_L} \right)^2 \quad (4.12)$$

### Moody Chart Method

The classical method of solution for calculating a flow rate given a pressure drop requires iteration and the use of the modified Moody chart as shown in Figure 4.2. The iteration process may be briefly summarized as follows:

#### Moody Chart Iteration Process

1. With  $\Delta P$  known, guess a value for friction factor
2. Calculate a flow rate using equation 4.12
3. Calculate a fluid velocity using  $v=q/A_L$ .
4. Calculate a Reynolds number using equation 4.7.
5. Using the modified Moody chart, find new friction factor.
6. Compare new friction factor to initial guess.
7. Replace initial guess with new friction factor.
8. Repeat steps 1-6 until new values for friction factor agree with previous iteration such that an error tolerance is satisfied.

One alternative to using the modified Moody chart is to use approximate relationships for smooth conduit. These relationships are:

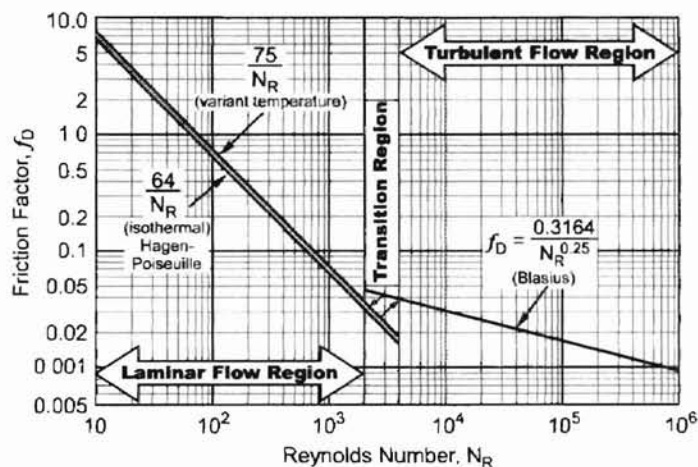


Figure 4.2 Modified Moody Chart [22]

$$\begin{aligned}
 f_D &= \frac{64}{N_R} && N_R \leq 2000 \text{ (isothermal)} \\
 &= \frac{75}{N_R} && N_R \leq 2000 \text{ (variant temperature)} \quad (4.13) \\
 &\approx 0.02 \text{ to } 0.045 && 2000 < N_R < 4000 \\
 &= \frac{0.3164}{N_R^{0.25}} && N_R \geq 4000 \text{ (Blasius solution)}
 \end{aligned}$$

For the transition region, a value for  $f_D$  of 0.0425 is often employed by hydraulic engineers. The same value will be used in this study. While these relationships

may replace the Moody chart, iteration is still the only method of solution. For a computer simulation, this would not be numerically efficient.

### S-T Method

Fortunately, a method exists which allows the fluid resistance to be taken into account for laminar or turbulent flow without the need for iteration. For the first time, this method will be implemented in the solution of fluid line dynamics. Known as the S-T method [21], it was first suggested by S.P. Johnson (ASME Summer Meeting, June, 1934). The terms "S" and "T" refer to two dimensionless numbers given as follows.

$$S = \frac{1}{v} \cdot \left( \frac{\Delta P \cdot d_i^3}{\ell \cdot \rho} \right)^{\frac{1}{2}} = N_R \cdot \left( \frac{f_D}{2} \right)^{\frac{1}{2}} \quad (4.14)$$

$$T = \frac{1}{v} \cdot \left( \frac{\Delta P \cdot q^3}{\ell \cdot \rho} \right)^{\frac{1}{5}} = \frac{N_R}{4} \cdot (8 \cdot \pi^3 \cdot f_D)^{\frac{1}{5}} \quad (4.15)$$

Furthermore, equation 4.12 is rearranged to yield the following.

$$f_D = \frac{\pi^2 \cdot \Delta P \cdot d_i^5}{8 \cdot \ell \cdot \rho \cdot q^2} \quad (4.16)$$

The two constants, S and T, are functions of the Reynolds number and the Darcy friction factor. Constant S may be used to calculate q if both  $\Delta P$  and  $d_i$  are known. Constant T may be used to find  $d_i$  if  $\Delta P$  and q are known. To avoid the iteration process, Fitch and Hong [22] reported that equation 4.13 may be substituted into equation 4.14 ( $N_R$  is eliminated) and solved for  $f_D$  to produce

$$f_D = \frac{2048}{S^2} \quad S \leq 200 \text{ (isothermal)} \quad (a)$$



$$= \frac{2812.5}{S^2} \quad S \leq 2000 \text{ (variant temperature)} \quad (b) \quad (4.17)$$

$$\approx 0.0425 \quad 200 < S < 400 \quad (c)$$

$$= \frac{0.2431}{S^{0.2857}} \quad S \geq 500 \text{ (Blasius solution)}. \quad (d)$$

Similarly, substituting equation 4.13 into equation 4.15 and solving for  $f_D$  in terms of  $T$  yields:

$$f_D = \frac{126.99}{T^{1.25}} \quad T \leq 550 \text{ (isothermal)}$$

$$= \frac{154.84}{T^{1.25}} \quad T \leq 550 \text{ (variable temperature)} \quad (4.18)$$

$$\approx 0.0425 \quad 550 < T < 1500$$

$$= \frac{0.277}{T^{0.263}} \quad T \geq 1500$$

Referring back to Figure 4.1, the S-T method will be used to calculate  $q_1$  and  $q_4$  and will in effect replace the resistance terms. Rearranging equation 4.12 to solve for flow rate  $q$  produces the following form of the Darcy equation.

$$q = \sqrt{\frac{2 \cdot \Delta P \cdot d_i}{\rho \cdot f_D \cdot \ell}} \cdot A_L \quad (4.19)$$

#### Comparison of Hagen-Poiseuille Law and S-T Method

It is useful at this point to compare the flow versus differential pressure predictions for the S-T method and the Hagen-Poiseuille formula. Table 4.2 lists the parameters used in generating the curves of Figure 4.3. From Figure 4.3, it can be seen that the S-T method and the Hagen-Poiseuille formula produce equivalent results in the laminar region. Data collected during the experimental

phase of this study will be used to test the accuracy of the S-T method in the laminar and turbulent regions.

Table 4.2  
Parameters Used For q vs.  $\Delta P$  Model Comparison

Parameter	Value	Units
diameter	0.18	inches
length	70	inches
fluid density	$8.10 \times 10^{-5}$	$\text{lb}_f\text{sec}^2/\text{in}^4$
kinematic viscosity	$3.84 \times 10^{-2}$	$\text{in}^2/\text{sec}$

The S-T method may be implemented in the modeling of fluid line dynamics by effectively replacing the resistance terms usually represented by the Hagen-Poiseuille formula. The limitation that the flow must always be laminar will be defeated through the application of the S-T method. One must realize, however, that the proposed  $T^3$  model in Figure 4.1 lumps the resistances as  $R/2$  and  $R/2$  at each end of the pipeline. For 1 lump of the  $T^3$  model, the following substitution for length is justified.

$$l_{\frac{R}{2}} = \frac{L_c}{2} \quad (4.20)$$

#### Application of S-T Method to $T^3$ Network

To demonstrate the utility of the S-T method, the solution of one lump of the  $T^3$  model will be considered. First, the appropriate differential equations are reiterated.

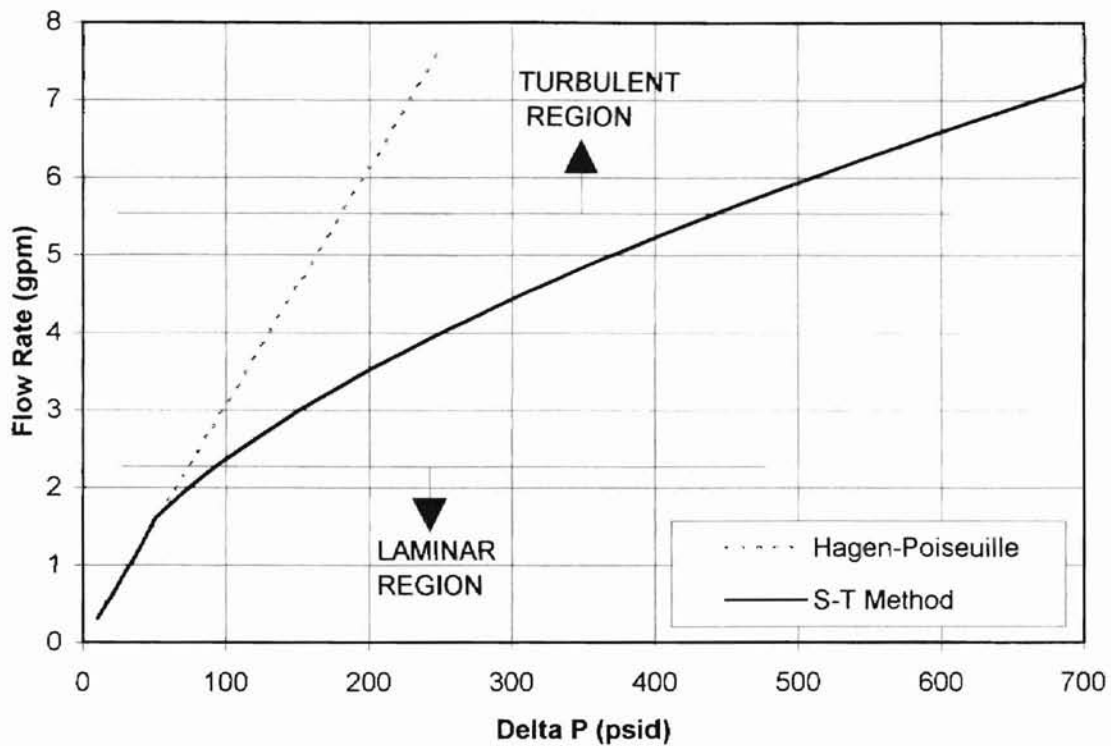


Figure 4.3 Comparison Plot of  $q$  vs.  $\Delta P$  Models

#### Differential Equations for $T^3$ Lump

$$\begin{aligned}
 \frac{dP_1}{dt} &= \frac{3}{C} \cdot (q_1 - q_2) \\
 \frac{dP_2}{dt} &= \frac{3}{C} \cdot (q_2 - q_3) \\
 \frac{dP_3}{dt} &= \frac{3}{C} \cdot (q_3 - q_4) \\
 \frac{dq_2}{dt} &= \frac{2}{L} \cdot (P_1 - P_2) \\
 \frac{dq_3}{dt} &= \frac{2}{L} \cdot (P_2 - P_3)
 \end{aligned} \tag{4.21}$$

The solution to the set of five differential equations will be carried out using MATLAB (copyright by The MathWorks, Inc.) and a Runge Kutta differential

equation solver routine by first converting the equations to state space form. The state variables are:

$$\begin{aligned}x_1 &= P_1 \\x_2 &= P_2 \\x_3 &= P_3 \\x_4 &= Q_2 \\x_5 &= Q_3\end{aligned}\tag{4.22}$$

Implementing the state variables creates the following set of state equations. The “dot” superscript indicates a differential with respect to time.

T<sup>3</sup> 1 lump model

$$\begin{aligned}\dot{x}_1 &= \frac{3}{C}(q_1 - x_4) \\ \dot{x}_2 &= \frac{3}{C}(x_4 - x_5) \\ \dot{x}_3 &= \frac{3}{C}(x_5 - q_4) \\ \dot{x}_4 &= \frac{2}{L}(x_1 - x_2) \\ \dot{x}_5 &= \frac{2}{L}(x_2 - x_3)\end{aligned}\tag{4.23}$$

The flow chart in Figure 4.4 graphically depicts the solution process incorporating the S-T Method. With the 1 lump model established, multiple lump models will be explored. Lumping by length is one of the advantages of the electrical analogy approach. It is a straightforward matter to generate a multiple lump model to increase the accuracy of the model from a dynamic standpoint. To assess the accuracy improvement, 2 and 4 lump models will be developed for comparison to the 1 lump model. For an n-lump model, the original formulation of the T<sup>3</sup> network becomes Figure 4.5 for multiple lumps.

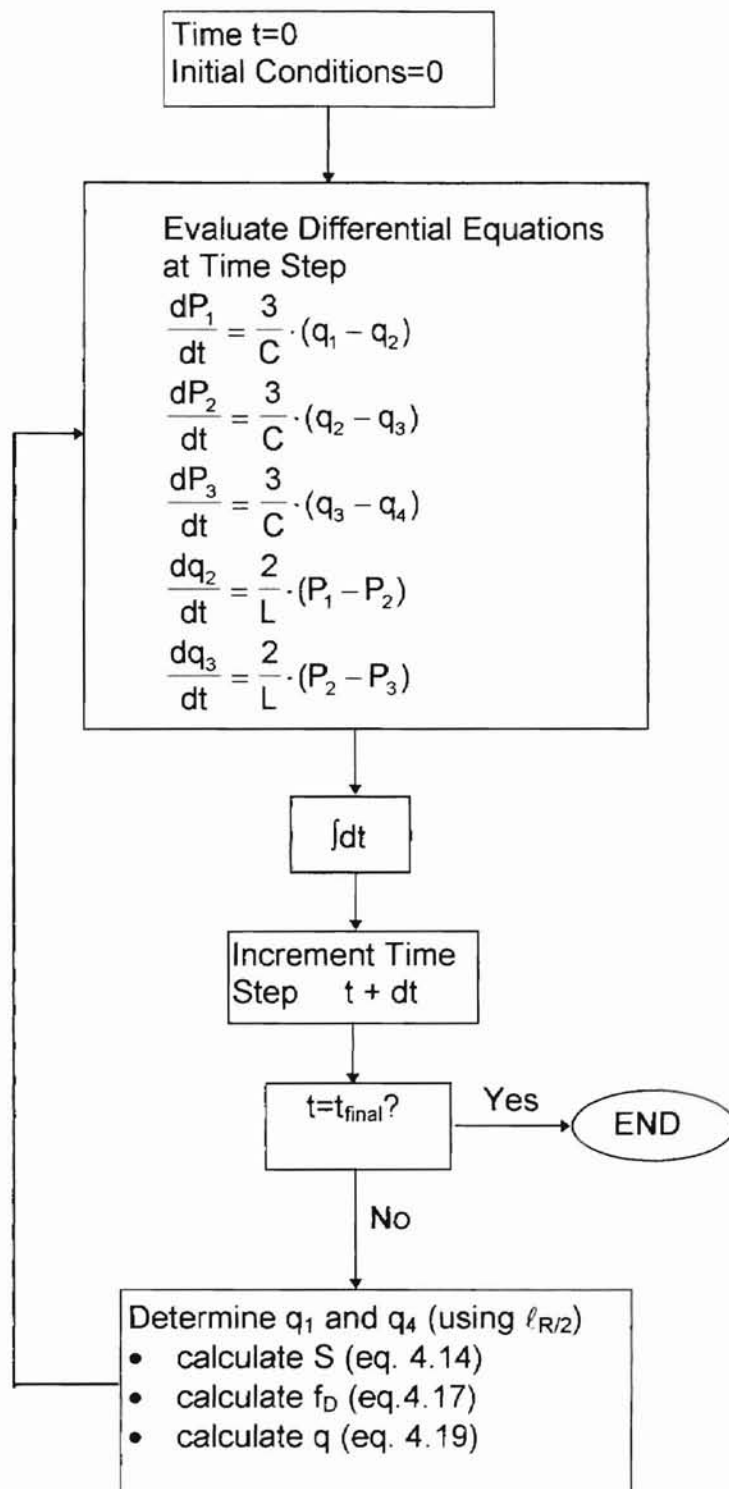


Figure 4.4 Flow Chart Demonstrating Solution of Differential Equations

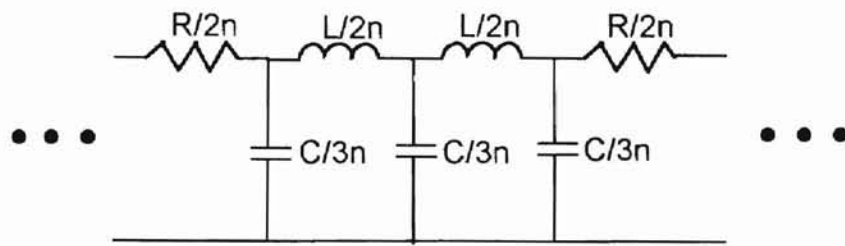


Figure 4.5 Schematic of  $n$ -Lump  $T^3$  Model

To discuss how the lumps can be interconnected, the schematic for  $n=2$  lumps is shown in Figure 4.6. To place a node at midpoint in Figure 4.6 would add an additional unknown to the describing set of equations. This would make them unsolvable because the number of unknowns would exceed the number of equations. Inputting a pressure at mid-point between the two central resistors as a known quantity like the input and output pressures to the line would not be practical. By not placing a node (or any other component) between the two central  $R/4$  resistances, they may be combined and simplified as resistors in series. The reduced 2 lump model becomes that shown in Figure 4.7.

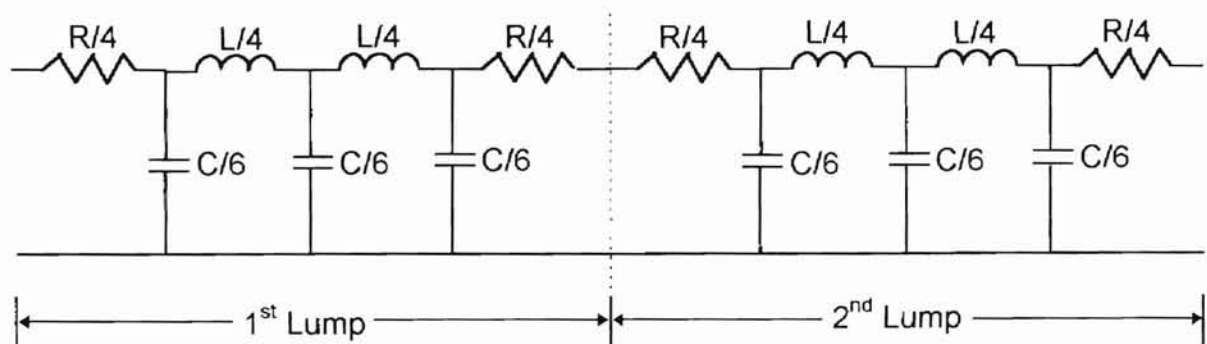


Figure 4.6 Schematic for 2 Lump  $T^3$  Model

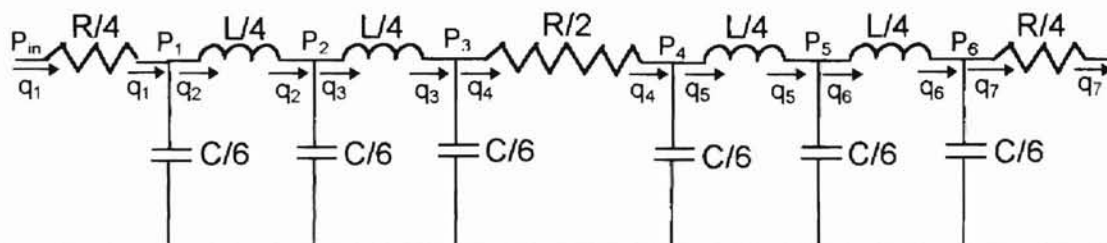


Figure 4.7 Reduced Form of 2 Lump Network

The differential equations, state variables, and state equations for the 2 lump  $T^3$  model are derived as follows:

#### Differential Equations for 2 Lump Model

$$\begin{aligned}
 \frac{dP_1}{dt} &= \frac{6}{C} \cdot (q_1 - q_2) \\
 \frac{dP_2}{dt} &= \frac{6}{C} \cdot (q_2 - q_3) \\
 \frac{dP_3}{dt} &= \frac{6}{C} \cdot (q_3 - q_4) \\
 \frac{dP_4}{dt} &= \frac{6}{C} \cdot (q_4 - q_5) \\
 \frac{dP_5}{dt} &= \frac{6}{C} \cdot (q_5 - q_6) \\
 \frac{dP_6}{dt} &= \frac{6}{C} \cdot (q_6 - q_7) \\
 \frac{dq_2}{dt} &= \frac{4}{L} \cdot (P_1 - P_2) \\
 \frac{dq_3}{dt} &= \frac{4}{L} \cdot (P_2 - P_3) \\
 \frac{dq_5}{dt} &= \frac{4}{L} \cdot (P_4 - P_5) \\
 \frac{dq_6}{dt} &= \frac{4}{L} \cdot (P_5 - P_6)
 \end{aligned} \tag{4.24}$$

$$\begin{aligned}
 x_1 &= P_1 \\
 x_2 &= P_2 \\
 x_3 &= P_3
 \end{aligned}$$

$$\begin{aligned}
 x_4 &= P_4 \\
 x_5 &= P_5 \\
 x_6 &= P_6 \\
 x_7 &= q_2 \\
 x_8 &= q_3 \\
 x_9 &= q_5 \\
 x_{10} &= q_6
 \end{aligned}
 \tag{4.25}$$

$$\begin{aligned}
 \dot{x}_1 &= \frac{6}{C}(q_1 - x_7) \\
 \dot{x}_2 &= \frac{6}{C}(x_7 - x_8) \\
 \dot{x}_3 &= \frac{6}{C}(x_8 - q_4) \\
 \dot{x}_4 &= \frac{6}{C}(q_4 - x_9) \\
 \dot{x}_5 &= \frac{6}{C}(x_9 - x_{10}) \\
 \dot{x}_6 &= \frac{6}{C}(x_{10} - q_7) \\
 \dot{x}_7 &= \frac{4}{L}(x_1 - x_2) \\
 \dot{x}_8 &= \frac{4}{L}(x_2 - x_3) \\
 \dot{x}_9 &= \frac{4}{L}(x_4 - x_5) \\
 \dot{x}_{10} &= \frac{4}{L}(x_5 - x_6)
 \end{aligned}
 \tag{4.26}$$

The length  $L_c/4$  must be used in the calculation of  $q_1$  and  $q_7$ , and length  $L_c/2$  must be used in the calculation of  $q_4$ . With the appropriate substitutions for length, the four lump models may be derived and solved in the same manner. The simulation results for a ramp input of inlet pressure for the 1, 2, and 4 lump models are presented in the simulation results section.



### Multiple Lump Dynamic Simulation Results

Simulations for 1, 2, and 4 lump models were completed using MATLAB. The m-files for each model are located in Appendix B. The parameters used for the simulation are given in Table 4.3

Table 4.3  
Multiple Lump Simulation Parameters

Parameter	Value	Units
inside diameter ( $d_i$ )	0.18	inches
outside diameter ( $d_o$ )	0.25	inches
length ( $L_c$ )	700	inches
fluid density ( $\rho$ )	$8.10 \times 10^{-5}$	$\text{lb}_f\text{sec}^2/\text{in}^4$
kinematic viscosity ( $\nu$ )	$3.84 \times 10^{-2}$	$\text{in}^2/\text{sec}$
tube elastic modulus ( $E$ )	$29 \times 10^6$	psi
inlet pressure ( $P_{in}$ )	ramp to 750 in 0.01 sec	psig
outlet pressure ( $P_{out}$ )	0	psig
fluid bulk modulus ( $\beta_{oil}$ )	200000	psi

The state variables for each model are plotted in the following graphs, Figures 4.8 through 4.17. Figures 4.8 and 4.9 display the results of the one lump model. Figure 4.8 shows  $P_1$ ,  $P_2$ , and  $P_3$  converging to the same pressure. This is to be expected because according to the  $T^3$  network, there are no resistive components between these three pressures. The fluid resistance is located at the ends of the line. Figures 4.10 and 4.11 contain the pressure and flow responses for the two lump model. From these figures, it can be seen that the higher frequency details of the response are more apparent.

Figures 4.12 through 4.17 represent the simulation results obtained from the 4 lump model. The propagation of pressure through the line can be discerned in Figures 4.12 through 4.15. Each of these graphs contains a group of three

pressure state variables and are presented in sequence. The delay in initial pressure rise as the input signal travels through the line is apparent in these graphs. The same trend is easily detected in the flow response graph of Figure 4.16. Figure 4.17 emphasizes the predicted delay by comparing the response of  $q_2$  and  $q_{12}$ .

#### A Note on Lumping by Length

One question that naturally arises is how many lumps are enough to adequately represent the frequency characteristics of a line? The natural frequency of a lump may be given by

$$\omega_n = \sqrt{\frac{1}{LC}} \quad (\text{rad/sec}) \quad (4.27)$$

or equivalently,

$$\omega_n = \frac{1}{\ell} \sqrt{\frac{\beta_{\text{eff}}}{\rho}} = \frac{1}{\ell} \cdot c_0 \quad (\text{rad/sec}). \quad (4.28)$$

If a line were to be divided into  $n$ -lumps, then equation 4.28 becomes

$$\omega_n = \frac{n}{L_c} \cdot c_0 \quad (\text{rad/sec}) \quad (4.29)$$

This does not represent the natural frequency of the line, but the highest frequency that the  $n$ -lumped line model can be expected to model. Thus, a 4-lump model for a 70 inch line using a sonic velocity of 48965 in/sec could be valid for frequencies up to approximately 2800 rad/sec (450 Hz). Although equation 4.29 is at best a crude estimate because it does not include viscous effects, it does represent the highest frequency for which the  $n$ -lumped model could have any validity.

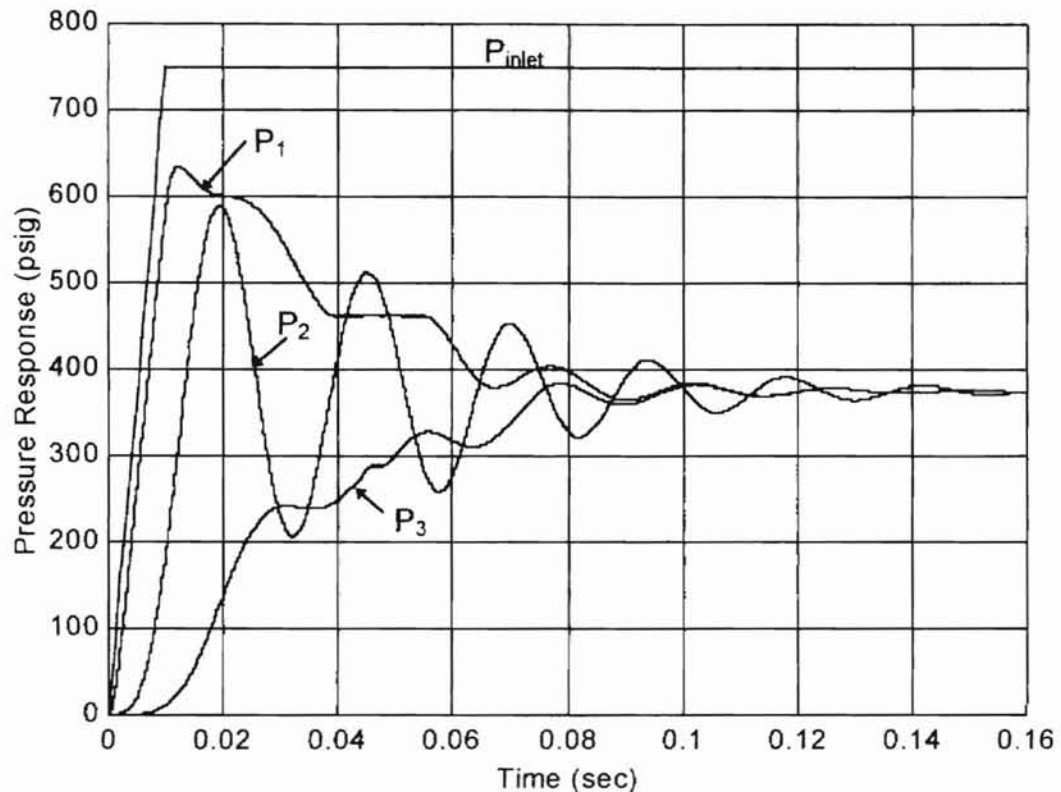


Figure 4.8 1 Lump Pressure Response Graph ( $P_1$ ,  $P_2$ , and  $P_3$ )

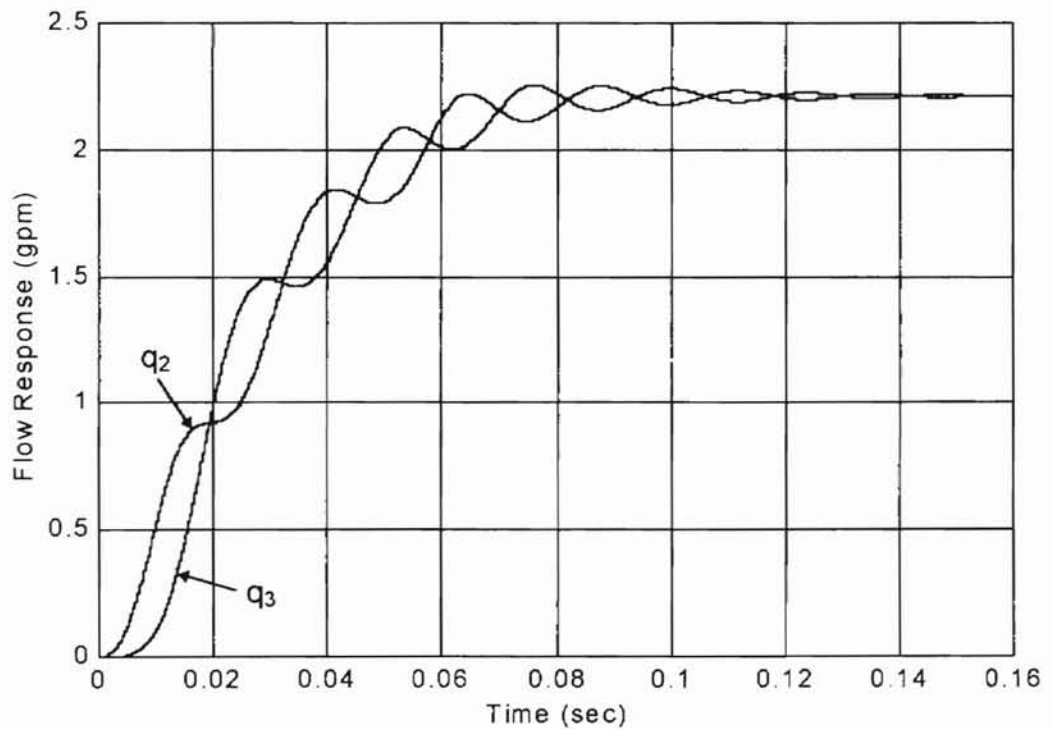


Figure 4.9 1 Lump Flow Response Graph ( $q_2$  and  $q_3$ )

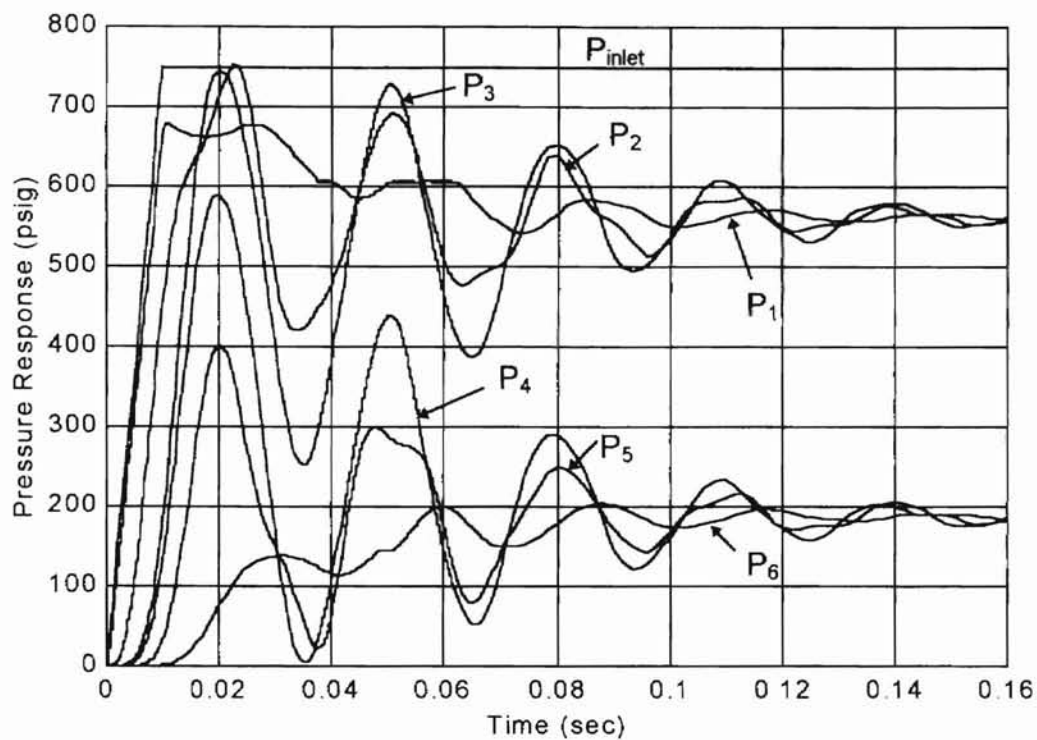


Figure 4.10 2 Lump Pressure Response Graph ( $P_1$  to  $P_6$ )

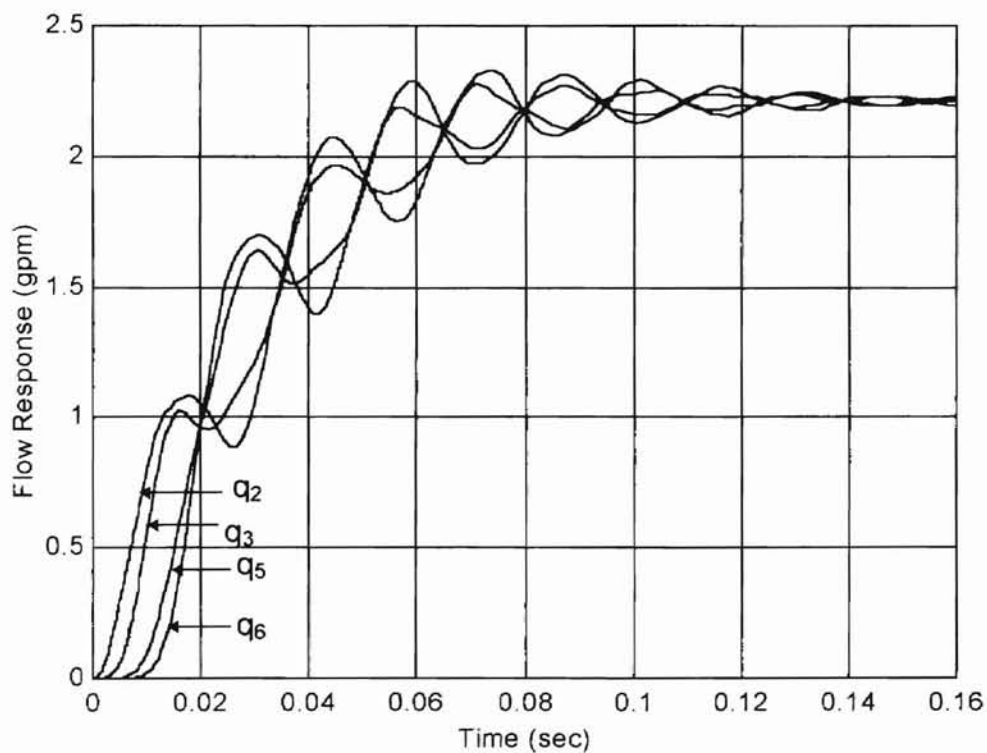


Figure 4.11 2 Lump Flow Response Graph ( $q_2$ ,  $q_3$ ,  $q_5$ , and  $q_6$ )

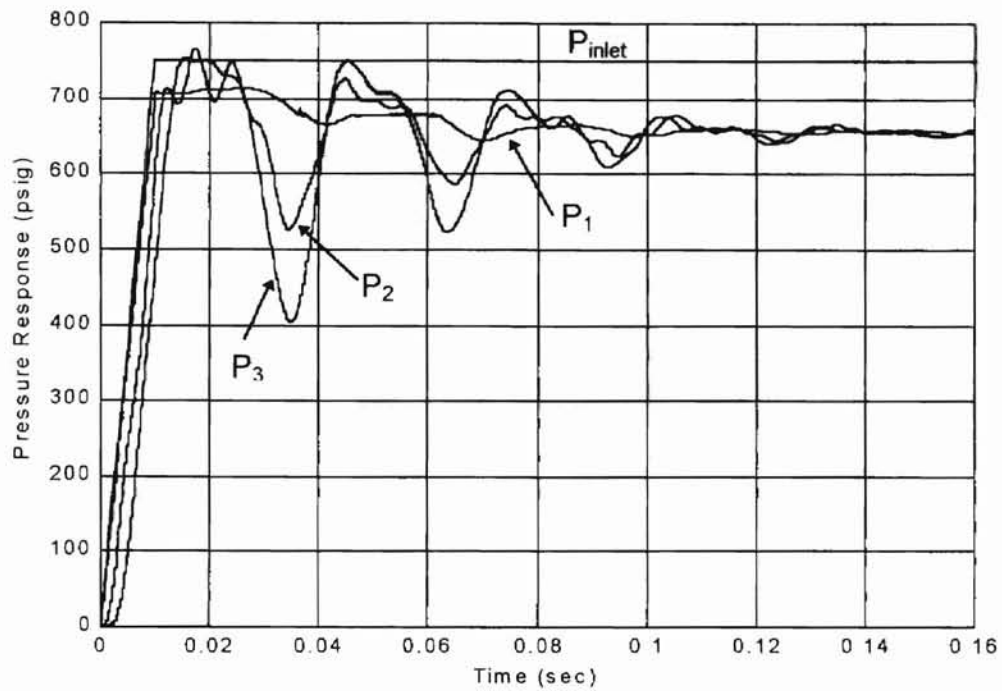


Figure 4.12 4 Lump Pressure Response Graph ( $P_1$ ,  $P_2$ , and  $P_3$ )

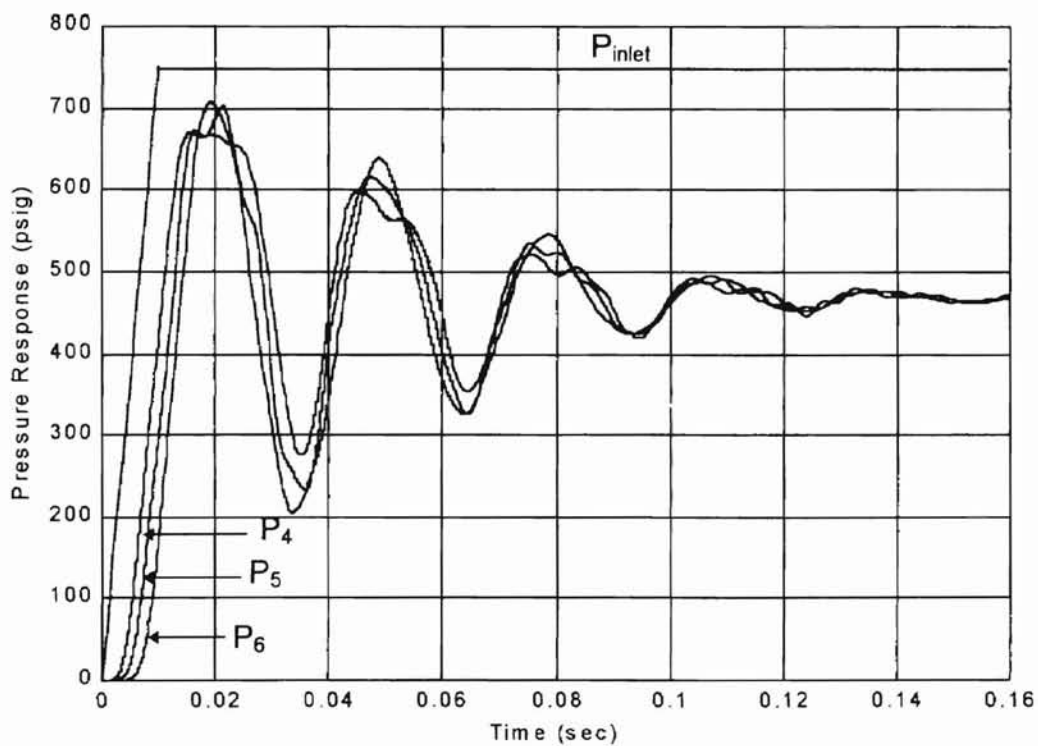


Figure 4.13 4 Lump Pressure Response Graph ( $P_4$ ,  $P_5$ , and  $P_6$ )

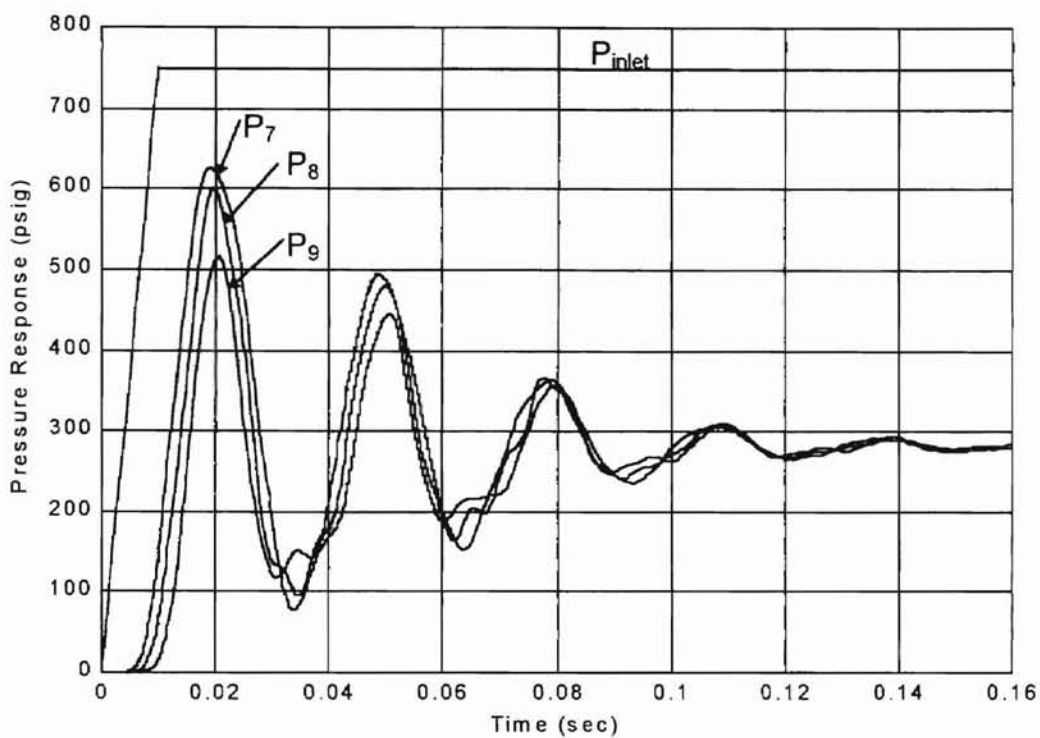


Figure 4.14 4 Lump Pressure Response Graph ( $P_7$ ,  $P_8$ , and  $P_9$ )

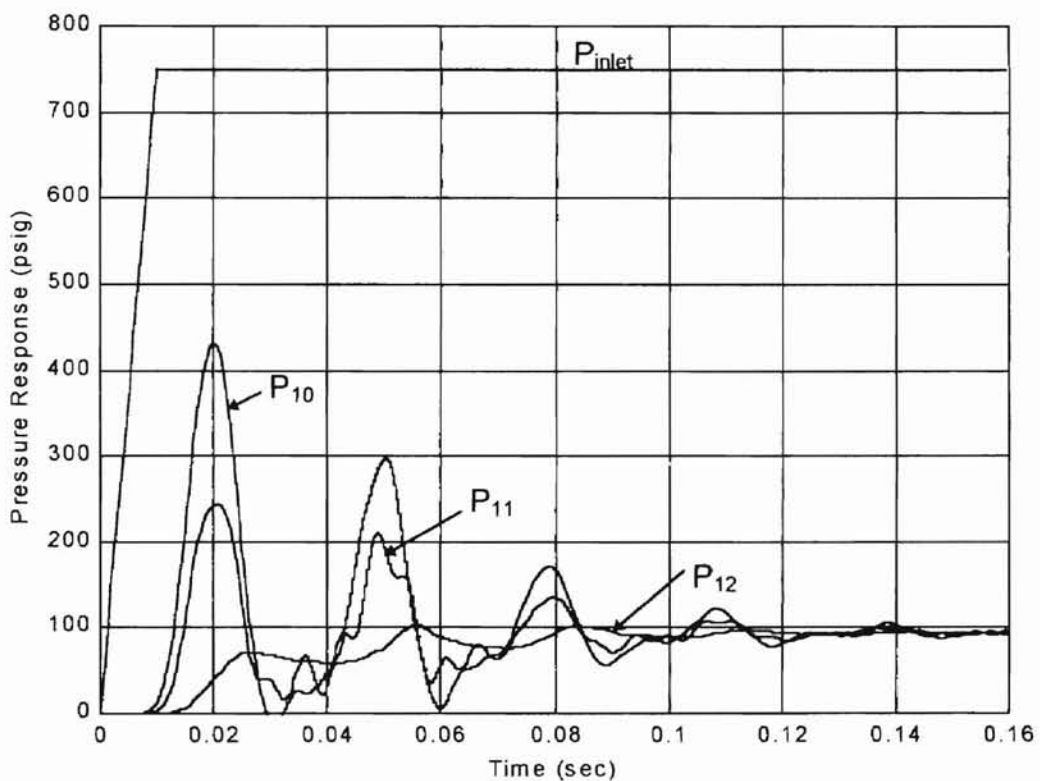


Figure 4.15 4 Lump Pressure Response Graph ( $P_{10}$ ,  $P_{11}$ , and  $P_{12}$ )

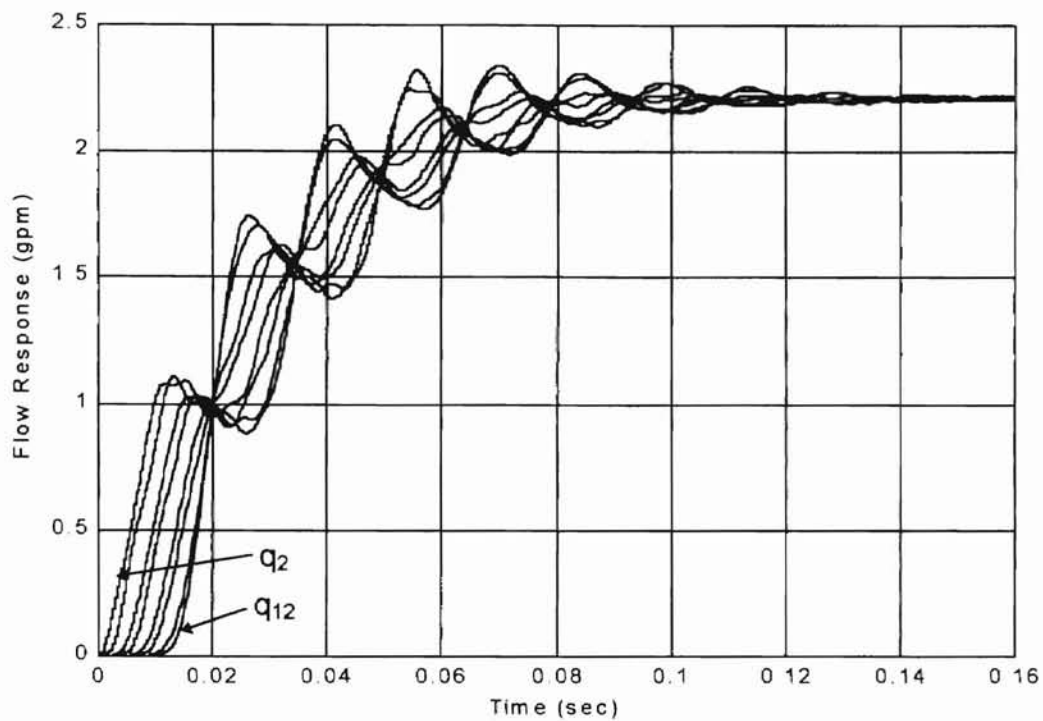


Figure 4.16 4 Lump Flow Response Graph ( $q_2$ ,  $q_3$ ,  $q_5$ ,  $q_6$ ,  $q_3$ ,  $q_9$ ,  $q_{11}$ , and  $q_{12}$ )

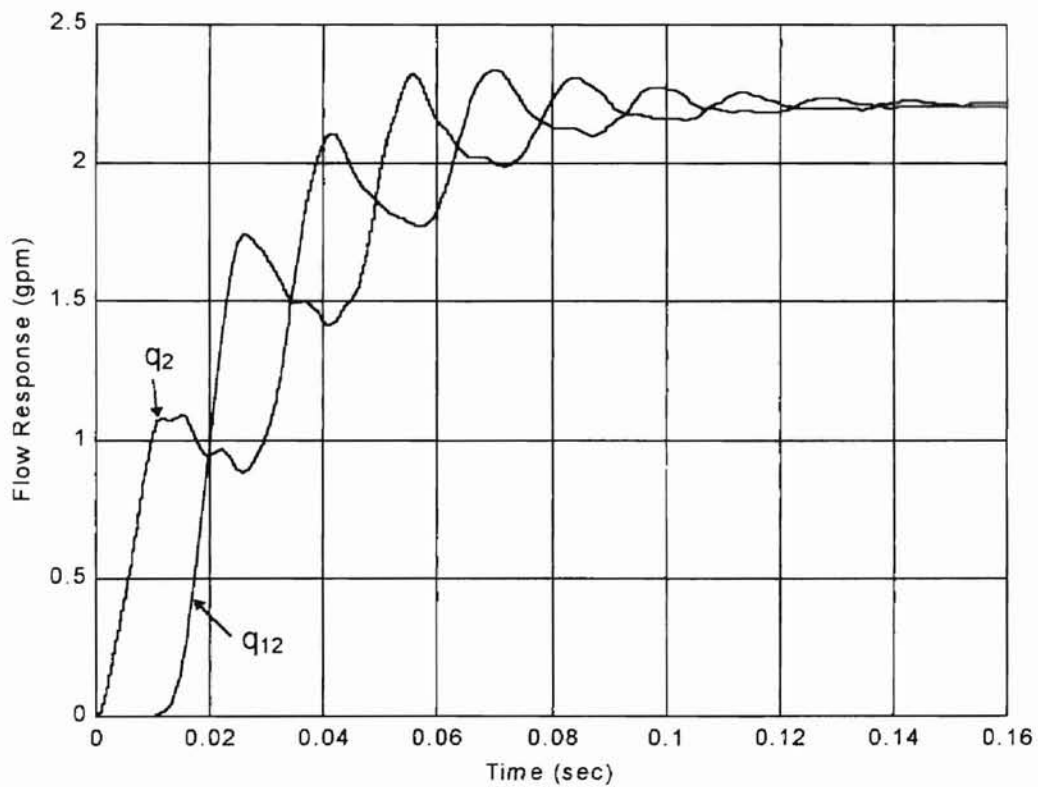


Figure 4.17 4 Lump Flow Response Graph ( $q_2$  and  $q_{12}$ )

### Dynamic Simulation of 4 Lump Models Comparing S-T and H-P Methods

The S-T and H-P methods for resistance to flow will now be compared from a dynamic standpoint through a direct comparison of the four lump model using an identical line length, diameter, and fluid parameters, but varying the inlet pressure. Table 4.4 reveals the parameters used for the dynamic simulations. Table 4.4 also reports the results of steady state calculations for predicted flow rate. This was done to verify that the dynamic flow rates converge to the steady state values calculated in Table 4.4 for each respective method.

Table 4.4  
Steady State Calculations for Volumetric Flow Rate

$$\begin{aligned} \nu &= 3.84 \times 10^{-2} \text{ in}^2/\text{sec} & \ell &= 700 \text{ inches} \\ \mu &= 3.11 \times 10^{-6} \text{ lb}_f\text{sec}/\text{in}^2 & d_i &= 0.18 \text{ inches} \\ \rho &= 8.10 \times 10^{-5} \text{ lb}_f\text{sec}^2/\text{in}^4 & A_L &= 2.54 \times 10^{-2} \text{ in}^2 \end{aligned}$$

$\Delta P$ (psid)	H-P Law q (gpm)	S-T Method			Flow Regime
		S <sup>*</sup>	$f_D$ <sup>**</sup>	q <sup>***</sup> (gpm)	
300	0.92	144.66	0.0978	0.92	Laminar
1500	4.61	323.47	0.0425	3.12	Transition
4500	13.83	560.26	0.0398	5.59	Turbulent

\*Equations 4.9 and 4.10

\*\*Equation 4.14

\*\*\*Equation 4.17

\*\*\*\*Equation 4.19

Consider first a step input inlet pressure of 300 psig. Figure 4.18 reveals the response of intermediate state variable  $P_5$  for the S-T and H-P methods, respectively. The results of these two methods cannot be distinguished because they are in fact identical. The plotted lines overlay one another. Likewise, the flow response curves of Figure 4.19 are also identical for each method and



cannot be distinguished from one another. The volumetric flow rates converge to approximately 0.92 gpm as foretold by the steady state calculations.

The next example was picked to fall in the transition region ( $2000 < N_R < 4000$ ). Figure 4.20 illustrates the results of each method for the intermediate pressure  $P_5$ . It can be seen that the response using the S-T method reaches a steady state value more quickly. This trend is further demonstrated in the flow response graph of Figure 4.21. In this plot, it can be seen that the H-P law converges to approximately 4.61 gpm, while the S-T Method converges to approximately 3.12 gpm. Because the H-P law is only valid for the laminar region, it is believed that the S-T Method provides the more correct answer for the transition region. This assumption will be tested against experimental data before conclusions can be drawn.

Finally, a comparison was made of the two methods in the turbulent region. An inlet pressure of 4500 psig yielded the pressure response curves shown in Figure 4.22. It is easy to see from this graph that the S-T method damping effect is even more pronounced than in the transition region. Figure 4.23 is a plot of the flow rate state variables and certainly demonstrates the deviation of the two methods in the turbulent flow regime. The H-P law converges to approximately 13.83 gpm, and the S-T method converges to approximately 5.59 gpm. Experiments will be conducted to determine which method is the more suitable predictor of volumetric flow rate in the transition and turbulent region.

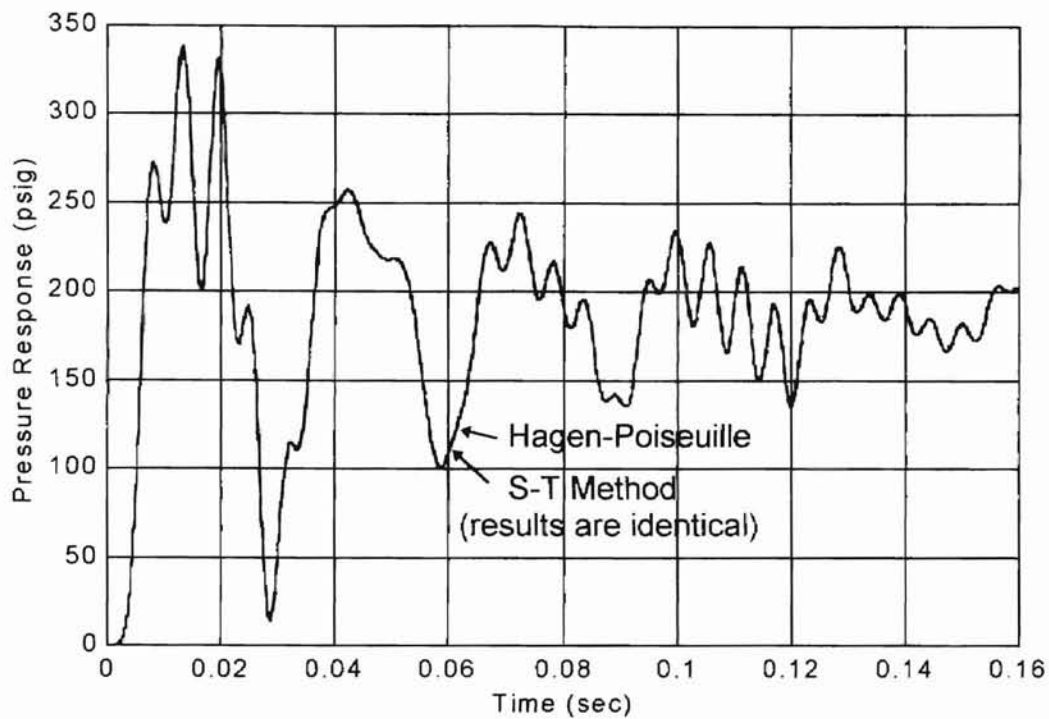


Figure 4.18 Comparison of H-P and S-T Pressure Response,  $P_5$   
Step Input: 300 psig, Laminar Flow Region

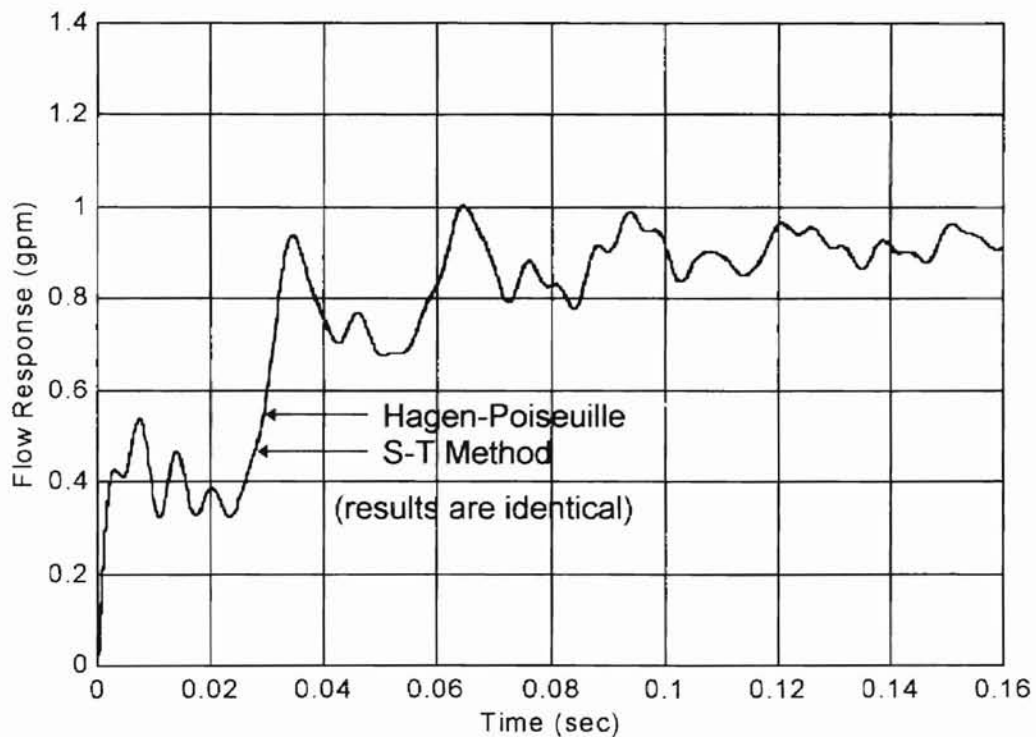


Figure 4.19 Comparison of H-P and S-T Flow Rate,  $q_2$ .  
Step Input: 300 psig, Laminar Flow Region

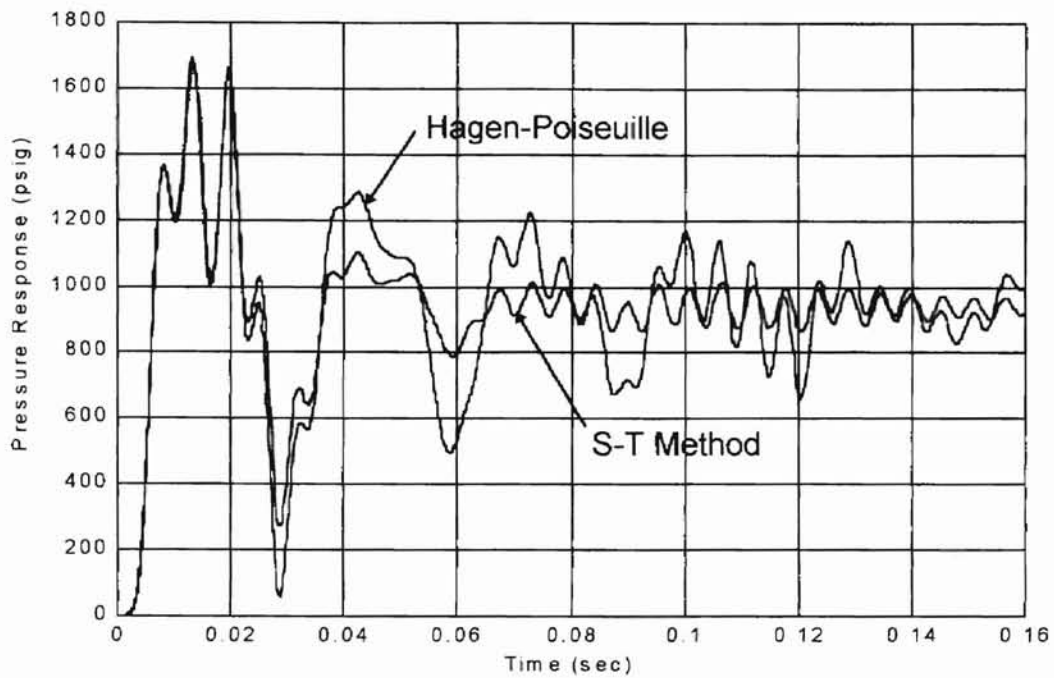


Figure 4.20 Comparison of S-T and H-P Pressure Response,  $P_5$   
Step Input: 1500 psig, Transition Flow Region

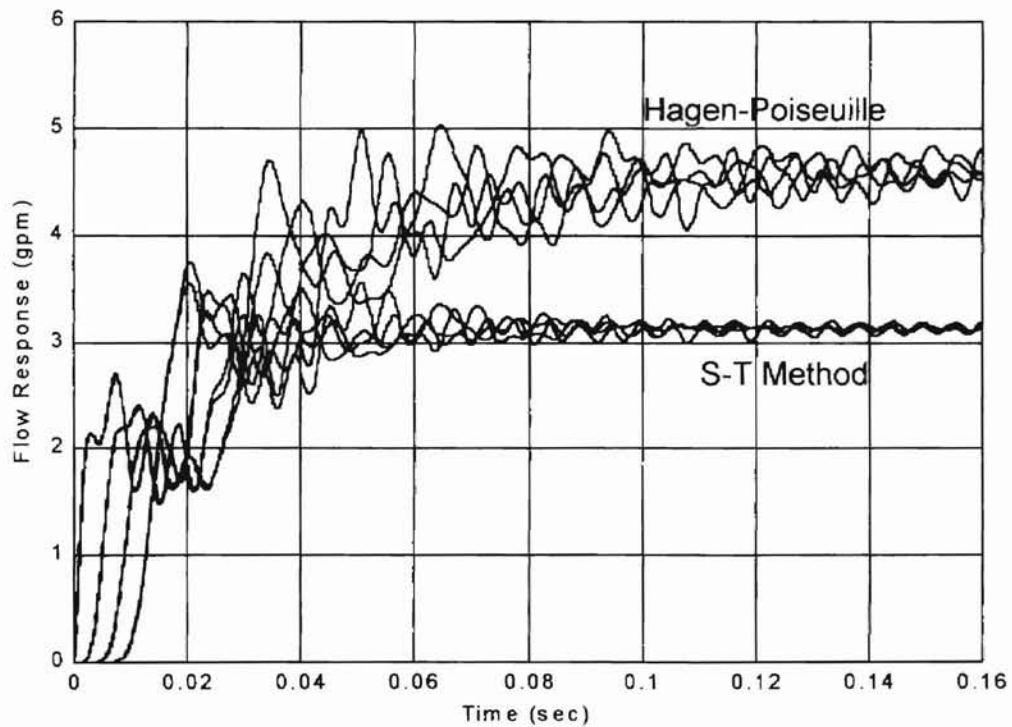


Figure 4.21 Comparison of S-T and H-P Flow Response  
Step Input: 1500 psig, Transition Flow Region

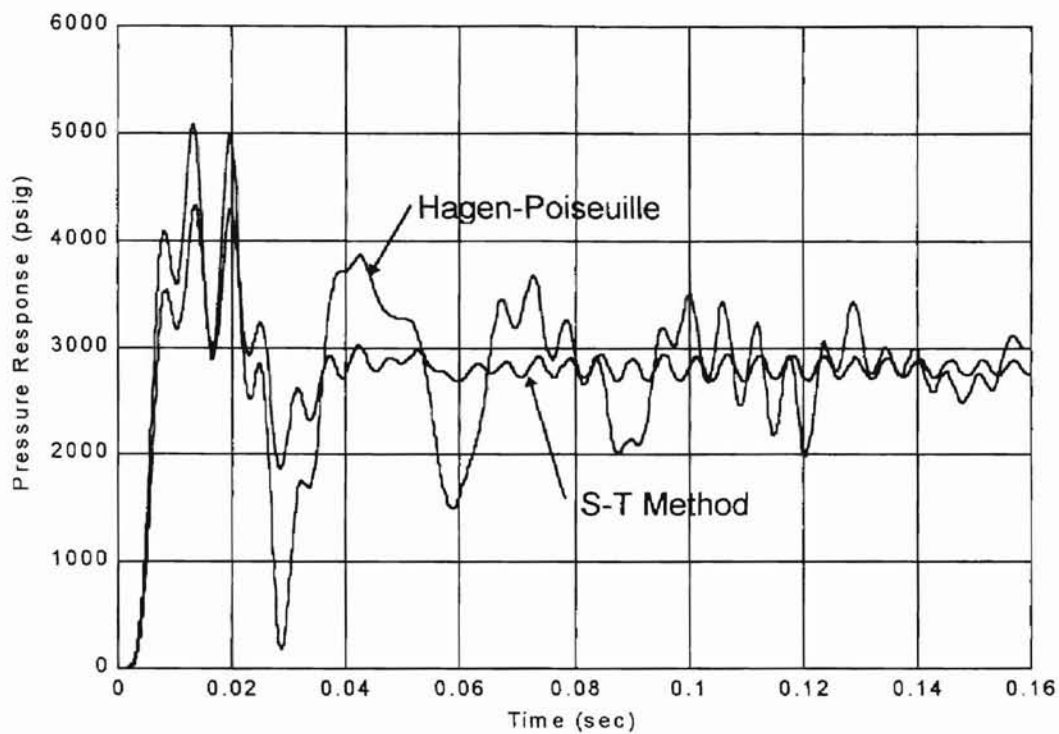


Figure 4.22 Comparison of S-T and H-P Pressure Response,  $P_5$   
Step Input: 4500 psig, Turbulent Flow Region

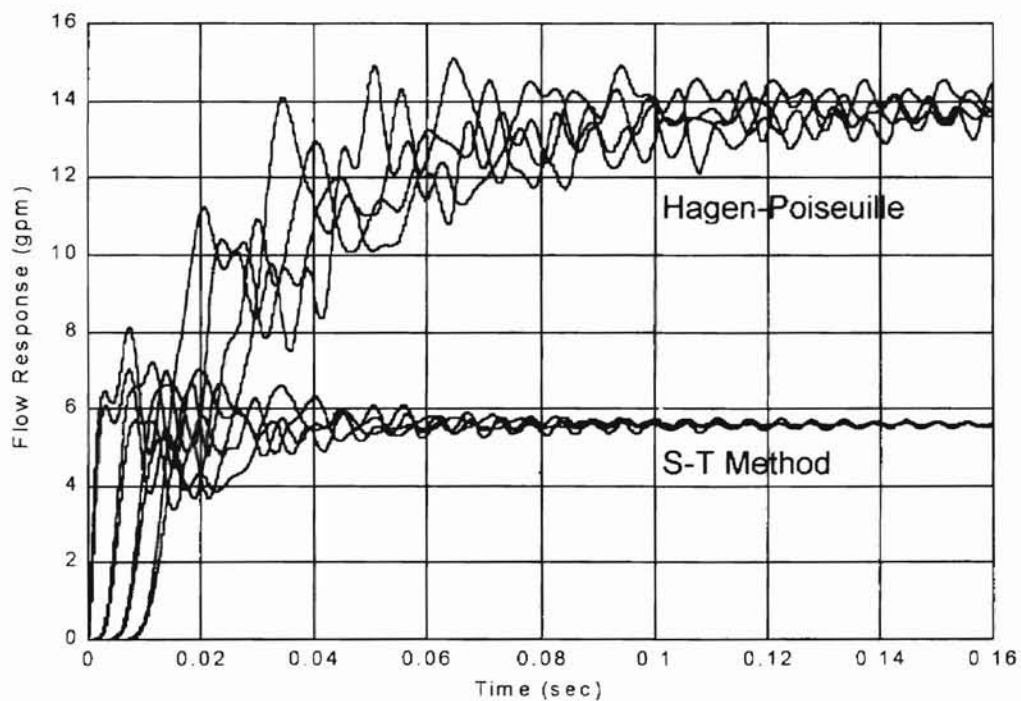


Figure 4.23 Comparison of S-T and H-P Flow Response  
Step Input: 4500 psig, Turbulent Flow Region

## CHAPTER V

### TRANSIENT RESPONSE COMPARISON OF RATIONAL APPROXIMATE MODEL AND $T^3$ MODEL

Individual simulation results have been obtained and discussed in Chapter III and Chapter IV for the rational approximate engineering model and the  $T^3$  network model, respectively. One way to directly compare the modeling approaches is to apply them in the solution of a common engineering system problem. The problem to be analyzed in this chapter is the classical water hammer problem.

Consider a fluid transmission line supplied by a constant pressure source and terminated by a valve. Figure 5.1 illustrates this situation using appropriate fluid power symbols.

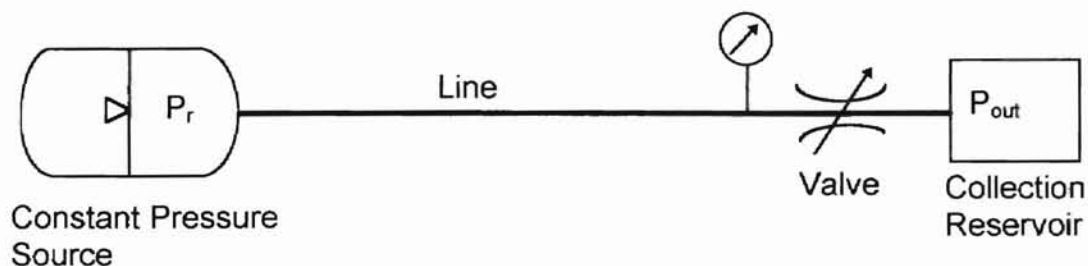


Figure 5.1 Illustration of Water Hammer Problem

Suppose a mass of fluid is traveling through the line at some velocity with the valve initially full open. Then suppose that the valve is suddenly demanded to close. When the valve is closed, a pressure wave will be reflected back to the source at the speed of sound in the fluid. Forward and backward traveling wave fronts are created and eventually dissipate. It is desired to know the pressure immediately upstream of the valve during this phenomenon.

To begin solving the problem, first the valve area history is introduced [20]. This data is tabulated in Table 5.1.

Table 5.1  
Effective Area of Valve vs. Time

Time (sec)	Area (in <sup>2</sup> )
0.00	8.34
0.01	8.30
0.03	7.49
0.05	6.36
0.078	4.74
0.110	3.47
0.142	2.39
0.175	1.57
0.205	0.84
0.236	0.35
0.261	0.00

An analytical expression for the data is given by the following ninth degree equation.

$$A_v(t) = 36098169 \cdot t^9 - 27651150 \cdot t^8 + 5290046 \cdot t^7 + 662432 \cdot t^6 - 210542 \cdot t^5 - 41747 \cdot t^4 + 16928 \cdot t^3 - 1707 \cdot t^2 + 9.226 \cdot t + 8.347 \quad (5.1)$$

The area data and curve fit equation are plotted in Figure 5.2. Furthermore, the flow through the valve may be modeled by the following equation [2].

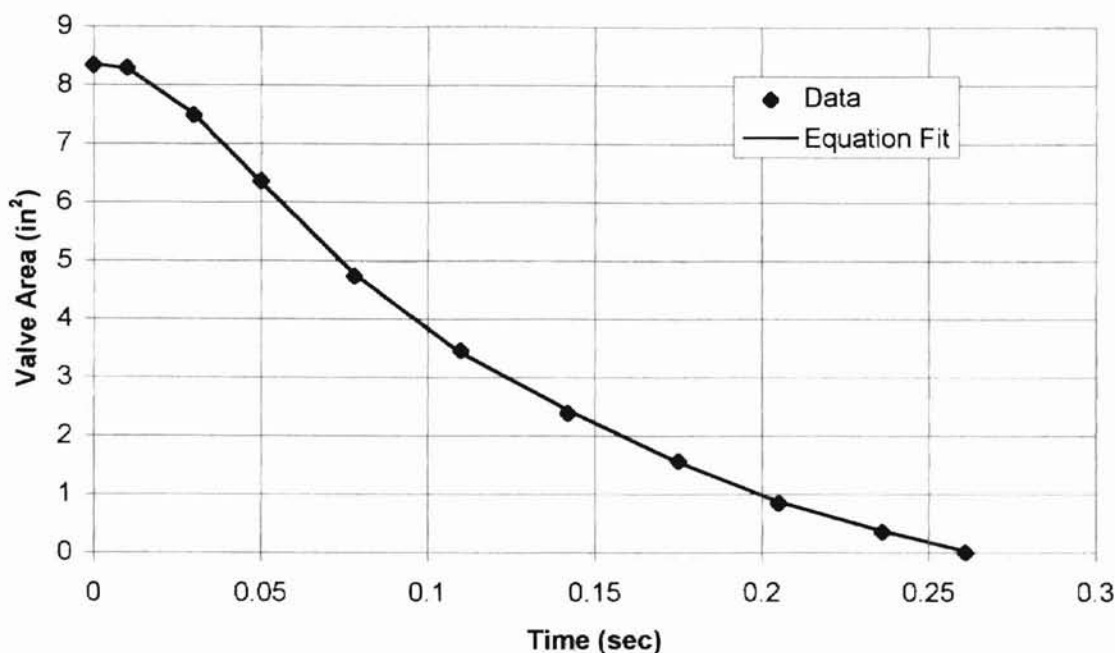


Figure 5.2 Graph of Valve Area Data and Curve Fit Equation

$$q_v(t) = A_v(t) \sqrt{\frac{2}{\rho} \cdot \frac{\Delta P(t)}{\left(1 - \frac{A_v^2(t)}{A_L^2}\right)}} \quad (5.2)$$

where  $q_v$  = valve flow rate (in<sup>3</sup>/sec)  
 $A_v$  = effective valve area (in<sup>2</sup>)  
 $\rho$  = fluid density (lb<sub>r</sub>sec<sup>2</sup>/in<sup>4</sup>)  
 $A_L$  = line inside cross-sectional area (in<sup>2</sup>)  
 $\Delta P$  = differential pressure across valve (psid)

#### Rational Approximate Model of Water Hammer Problem

The Laplace domain response equation [2] applicable to this water hammer problem is

$$\frac{p(s)}{v(s)} = -z_c A_L \tanh \Gamma(s). \quad (5.3)$$

Using one term of the rational approximate model allows  $\sinh \Gamma(s)$  and  $\cosh \Gamma(s)$  to become the following:

$$\sinh \Gamma(s) = \Gamma(s) = \frac{sL_c}{c_0} \quad (5.4)$$

$$\cosh \Gamma(s) = 1 + \frac{2\zeta_s s}{\omega_{c0}} + \frac{s^2}{\omega_{c0}^2} \quad (5.5)$$

For purposes of the approximate model, the characteristic impedance is once again

$$z_c = \frac{\rho c_0}{A_L} \quad (5.6)$$

Equation 5.3 will now be written with the appropriate substitutions.

$$\left( 1 + \frac{2\zeta_{sc0}s}{\omega_{c0}} + \frac{s^2}{\omega_{c0}^2} \right) \cdot p(s) = -\rho L_c s v(s) \quad (5.7)$$

Equation 5.7 represents a linear operator form. Because the valve pressure-flow relationship is a non-linear function, and the line will have a steady flow pressure drop which must be accounted for, equation 5.7 cannot readily be solved.

However, converting equation 5.7 to the time domain will allow incorporation of the valve non-linearity and the flow resistance. Expressing equation 5.7 in the time domain in terms of pressure and flow rate gives

$$\left( 1 + \frac{2\zeta_{sc0} \left( \frac{d}{dt} \right)}{\omega_{c0}} + \frac{\left( \frac{d}{dt} \right)^2}{\omega_{c0}^2} \right) \cdot p(t) = - \frac{\rho L_c \left( \frac{d}{dt} \right) q(t)}{A_L} \quad (5.8)$$

Equation 5.8 represents disturbance quantities. It is necessary to rewrite this expression in terms of total quantities. This can be done by adding to the right hand side of equation 5.8 the term  $(P_r - P_{ss})$  where  $P_r$  is the reservoir pressure at



the line inlet, and  $P_{ss}$  is the steady state pressure loss in the line. Including this term gives

$$\left( 1 + \frac{2\zeta_{c0} \left( \frac{d}{dt} \right) + \left( \frac{d}{dt} \right)^2}{\omega_{c0}^2} \right) \cdot p(t) = - \frac{\rho L_c \left( \frac{d}{dt} \right) q(t)}{A_L} + P_r - P_{ss}. \quad (5.9)$$

Equation 5.9 now relates the total pressure and total flow. The solution process carried out by this author will be to first rearrange equation 5.9 and use the "dot" superscript to denote differentials with respect to time. Equation 5.9 becomes the following:

$$\ddot{p}(t) = \omega_{c0}^2 \left( \frac{-\dot{p}(t) 2\zeta_{c0}}{\omega_{c0}} - p(t) - \frac{\rho L_c}{A_L} \dot{q}_v(t) + P_r - P_{ss} \right) \quad (5.10)$$

This second order differential equation will be solved by first separating it into two first order differential equations using the simple transformations

$$p_1 = \dot{p}$$

$$p_2 = p.$$

Applying the transformations to equation 5.10 produces the following two first order equations for one term of the rational approximate model.

$$\dot{p}_1(t) = \omega_{c0}^2 \left( \frac{-p_1(t) 2\zeta_{c0}}{\omega_{c0}} - p_2(t) - \frac{\rho L_c}{A_L} \dot{q}_v(t) + P_r - P_{ss} \right) \quad (5.11)$$

$$\dot{p}_2(t) = p_1(t) \quad (5.12)$$

The derivative with respect to time of the valve flow equation may be found analytically. It is (with the linear transformations applied):

$$\begin{aligned} \dot{q}_v = & \dot{A}_v(t) \frac{\sqrt{2(p_2(t) - p_{out})}}{\sqrt{\rho} \sqrt{1 - \frac{A_v^2(t)}{A_L^2}}} + \frac{A_v(t) p_1(t)}{\sqrt{2\rho(p_2(t) - p_{out})} \sqrt{1 - \frac{A_v^2(t)}{A_L^2}}} \\ & + \frac{A_v^2(t) \dot{A}_v(t) \sqrt{2(p_2(t) - p_{out})}}{\sqrt{\rho} \left(1 - \frac{A_v^2(t)}{A_L^2}\right)^2 A_L^2} \end{aligned} \quad (5.13)$$

The derivative of the valve area equation (equation 5.1) is easily obtained, and can be substituted into equation 5.13.

$$\begin{aligned} \dot{A}_v(t) = & 324883521 \cdot t^8 - 221209200 \cdot t^7 + 37030322 \cdot t^6 + 3974592 \cdot t^5 \\ & - 1052710 \cdot t^4 - 166988 \cdot t^3 + 50784 \cdot t^2 - 3414 \cdot t + 9.226 \end{aligned} \quad (5.14)$$

Substituting equations 5.13 and 5.14 into 5.10 will create a large expression solveable with a Runge Kutta routine. All that remains is a term for the steady state pressure drop,  $P_{ss}$ .

For comparison purposes, the resistance to flow will be calculated in three different ways, which include the Fanning friction factor, the S-T method, and the Hagen-Poiseuille law. Gerlach [2] implemented a Fanning friction factor ( $f_f$ ) for his particular example. The head loss due to pipe friction is given by

$$h_L = \frac{\Delta p}{\rho} = 2f_f \frac{L_c}{d_i} \cdot v^2 \quad (5.15)$$

So, the steady state pressure drop,  $P_{ss}$ , is equal to  $\Delta p$ , or

$$P_{ss} = 2f_f \frac{\rho L_c}{d_i} \cdot \left(\frac{q(t)}{A_L}\right)^2 \quad (5.16)$$

The alternative to using the Fanning friction factor, which requires a look up chart, is of course the S-T method. By calculating the constant S (eq. 4.14),

and the Darcy friction factor,  $f_D$  (eq. 4.17), the pressure drop vs. flow relationship may be calculated using eq. 4.12, which is repeated here.

$$P_{ss} = \frac{f_D}{2} \frac{\rho L_c}{d_i} \cdot \left( \frac{q(t)}{A_L} \right)^2 \quad (5.17)$$

These calculations are undertaken at each time step, so the value of the Darcy friction factor may not be constant throughout a simulation if the S-T method is employed during the solution of differential equations. Using MATLAB and a Runge Kutta routine, the solution of the water hammer problem using one term of the rational approximate model was completed. The difference between using the Fanning friction factor obtained by Gerlach [20], the S-T method, and the H-P law are readily apparent in Figure 5.3. The simulation parameters for the curves in Figure 5.3 are given in Table 5.2.

Table 5.2  
Simulation Parameters for Solution of  
Water Hammer Problem Using Rational Approximate Model

Parameter	Value and Units
$L_c$	276 inches
$d_i$	3.875 inches
$P_r$	45 psia
$P_{out}$	8.7 psia
Initial static pressure at valve	21.42 psia
$\rho$	$9.57 \times 10^{-5} \text{ lb}_f \text{sec}^2/\text{in}^4$
$v$	$0.001517 \text{ in}^2/\text{sec}$
$\beta$	320,000 psi
$\omega_{c0}$	293 rad/sec
$\zeta_{c0}$	0.001
$f_f$	0.012

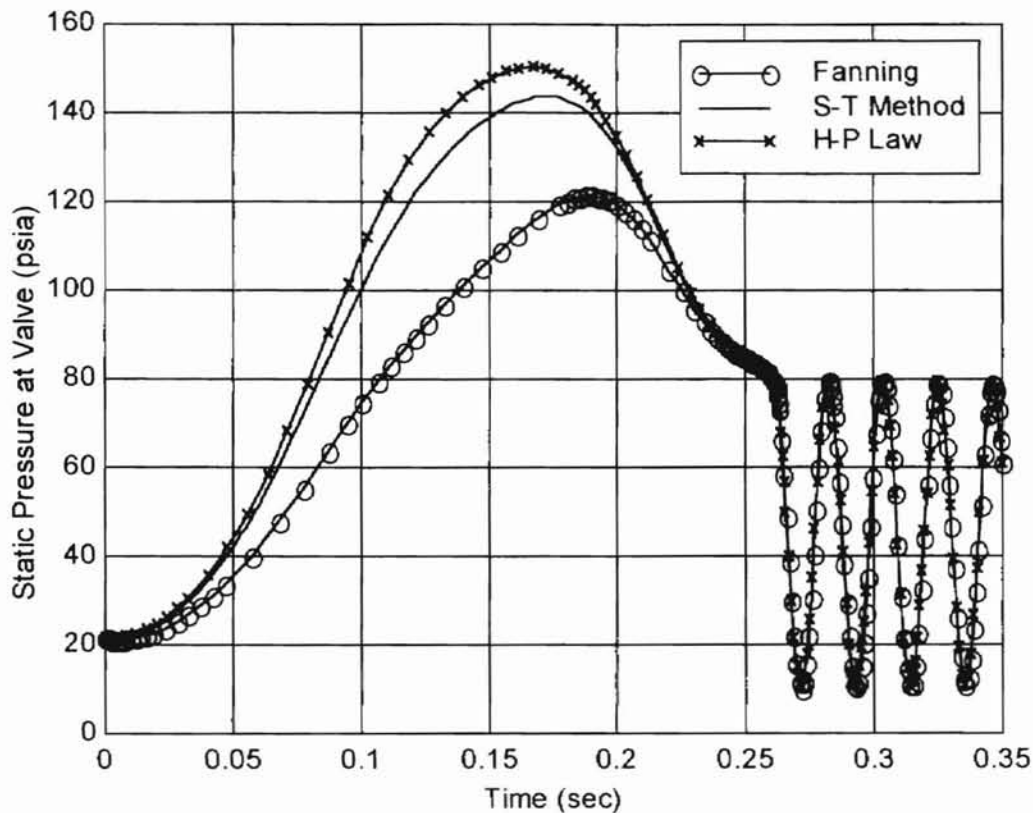


Figure 5.3 Water Hammer Effect, One Term Rational Approximate Model, Comparison of Fanning Factor, S-T Method, and H-P Law

It can be seen that the curves deviate significantly during the initial pressure rise. However, the three methods produce identical results upon complete closure of the valve at 0.26 seconds when the line is blocked. Now the  $T^3$  model with S-T method will be applied to the same water hammer problem.

#### $T^3$ Model of Water Hammer Problem

A schematic of the water hammer problem with a one lump  $T^3$  line representation is shown in Figure 5.4.

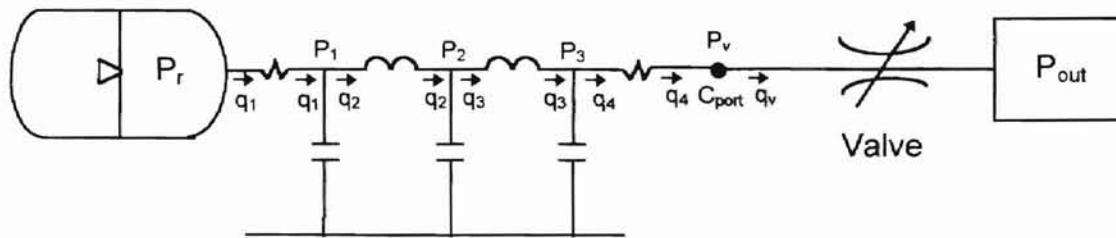


Figure 5.4 Schematic of Water Hammer Problem with Line Represented by 1 Lump  $T^3$  Network

In order to connect the line model to the valve model, a connecting node labeled  $P_v$  was created. Functioning as a small control volume, the node is a way for the flow values to be passed from the line to the valve, or vice versa.  $P_v$  corresponds to the pressure upstream of the valve and will be directly compared to the pressure history obtained using the rational approximate model. The parameter  $C_{port}$  is a nodal capacitance whose volume corresponds to the valve inlet port volume.

The dynamic equations for this system may be written as follows:

$$\begin{aligned}
 \dot{P}_1 &= \frac{3}{C} \cdot (q_1 - q_2) \\
 \dot{P}_2 &= \frac{3}{C} \cdot (q_2 - q_3) \\
 \dot{P}_3 &= \frac{3}{C} \cdot (q_3 - q_4) \\
 \dot{P}_v &= \frac{1}{C_{port}} \cdot (q_4 - q_v) \\
 \dot{q}_2 &= \frac{2}{L} \cdot (P_1 - P_2) \\
 \dot{q}_3 &= \frac{2}{L} \cdot (P_2 - P_3)
 \end{aligned} \tag{5.18}$$

Applying the state variable approach to the differential equations and using the S-T method to account for frictional losses in the pipe, simulation results were

obtained using MATLAB. The relevant simulation parameters given in Table 5.2 were employed. The connection node volume utilized was  $25 \text{ in}^3$ . The simulation results are shown in Figure 5.5 along with the simulation results previously obtained for the rational approximate model. In Figure 5.5, it can be seen that the 1 lump  $T^3$  model developed by this author agrees superbly with the well established 1 term rational approximate model derived from fundamental fluid mechanics theory. This result substantiates the  $T^3$  model with S-T method as an accurate way to represent the dynamic effect of a straight, rigid line coupled to a hydraulic system. The theoretical results in Figure 5.5 will be compared to test data in Chapter 6.

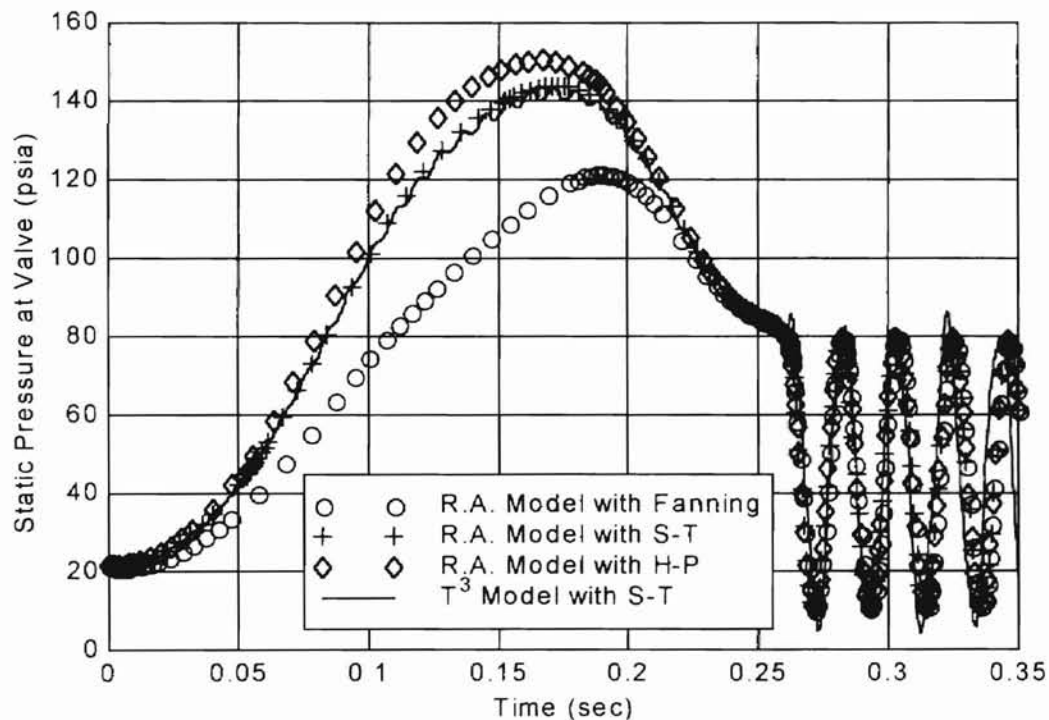


Figure 5.5 Theoretical Responses for Water Hammer Problem

## CHAPTER VI

### EXPERIMENT

#### Introduction

The experimental work is organized in three parts. The first part contains a description of the test setup and presentation of test data obtained from steady state testing. The steady state testing consists of  $\Delta P$  vs. flow testing on a rigid fluid line for the purpose of verifying the resistance to flow predictions of the S-T method. The second part of the experimental work presents dynamic line test data. The purpose of the dynamic testing is to assess the validity of the  $T^3$  model for a rigid fluid line installed in a hydraulic system. Test data [2] collected at the Marshall Space Flight Center located in Huntsville, Alabama from a water hammer experiment was used for comparison to simulation results. Lastly, to further verify the validity of the  $T^3$  model with S-T method, a final experiment was devised. In this experiment, the input and output pressures to a test line were sampled and recorded with respect to time. The flow generator provided a periodic, large amplitude flow signal to the line inlet. As a consequence of the restrictions caused by the test line and downstream load valve, a large amplitude pressure signal was created and measured at the test line inlet. The purpose of this testing was to compare the experimental pressure amplitude decay at the line

outlet to predictions obtained from the author's model. Data was collected at various load pressures and flow rates.

## PART 1: Steady State Testing to Verify S-T Method

### Experimental Apparatus

The schematic diagram for this experiment is shown in Figure 6.1. Figures 6.2 and 6.3 are photographs of the mechanical setup and the data acquisition instruments. As shown in Figure 6.1, a hydraulic system was constructed to generate a signal to a rigid transmission line. This was accomplished using a variable displacement check ball type piston pump coupled to a variable speed electric motor. Fluid conditioning was accomplished with a control filter and water cooled heat exchanger. The control filter removes particulate contaminants that may be introduced to the hydraulic system. The heat exchanger is of the shell and tube variety. The desired set point temperature is achieved by regulating the flow of cooling water through the heat exchanger. A relief valve set to a cracking pressure of 2500 psig was incorporated for pressure protection. Lastly, a turbine flowmeter with readout was installed to monitor mean flow rate through the test line.

To measure the pressure signals at the inlet and outlet of the test line, gage pressure transducers were connected to SAE/ARP 24B [23] pressure taps. Figure 6.4 is a photograph illustrating the installation of the outlet pressure transducer for the rigid, straight fluid transmission line. The short line connecting the pressure transducer to the pressure tap was 3.0 inches long for both the inlet



and outlet. The pressure transducers are of the bonded foil strain gage type with a range of 0 to 1000 psig. The analog pressure transducers provide infinite resolution (final resolution determined by the voltage measurement device) and a usable dynamic range from DC to 11 kHz as indicated by the manufacturer. Each transducer was powered by a constant voltage DC power supply. The output of each transducer was processed through a high bandwidth (DC to 20 kHz) amplifier.

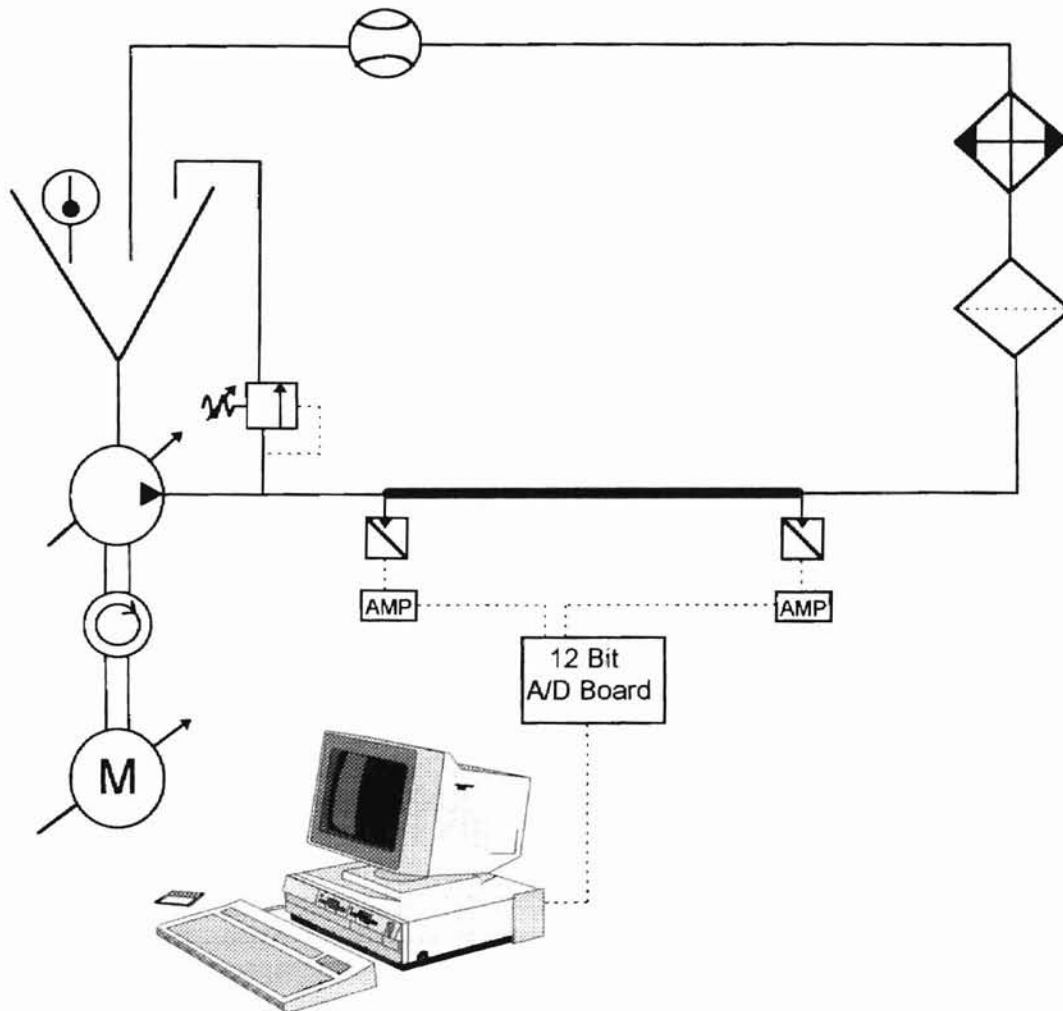


Figure 6.1 Schematic Diagram of Steady State Setup

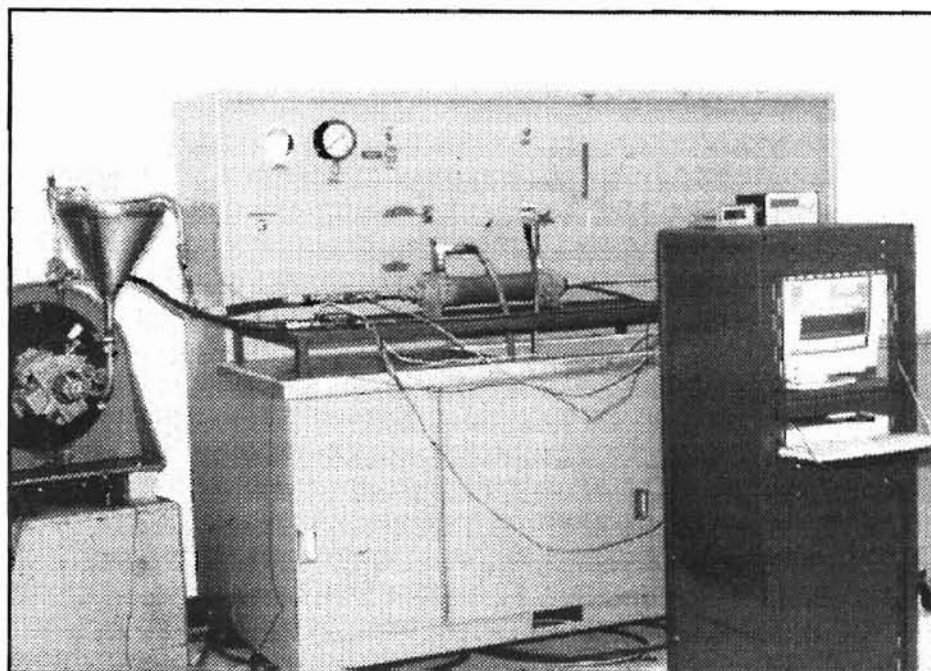


Figure 6.2 Photograph of Experimental Setup

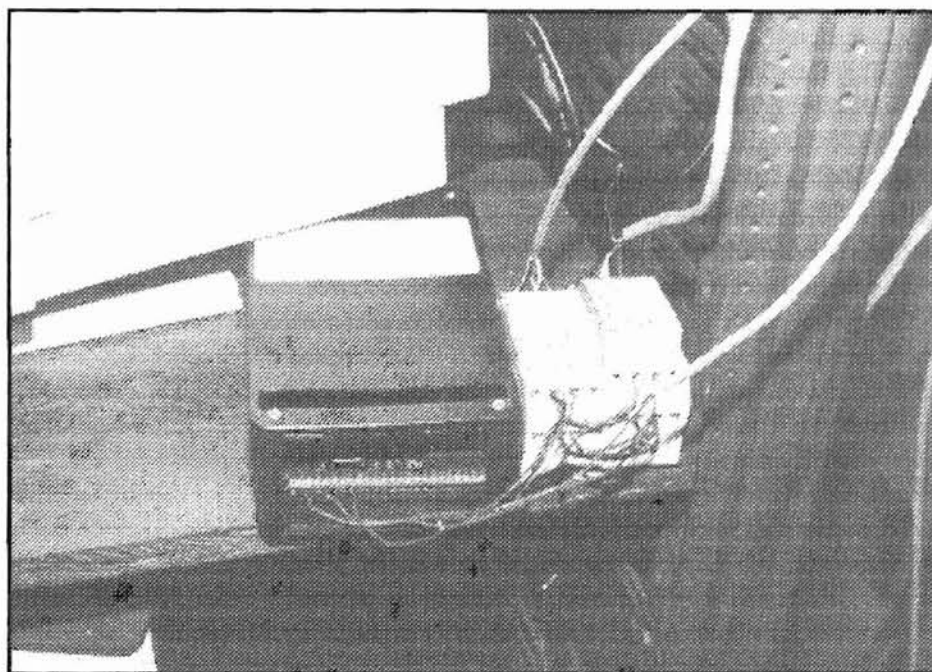


Figure 6.3 Photograph of Data Acquisition Terminal Card and Amplifiers

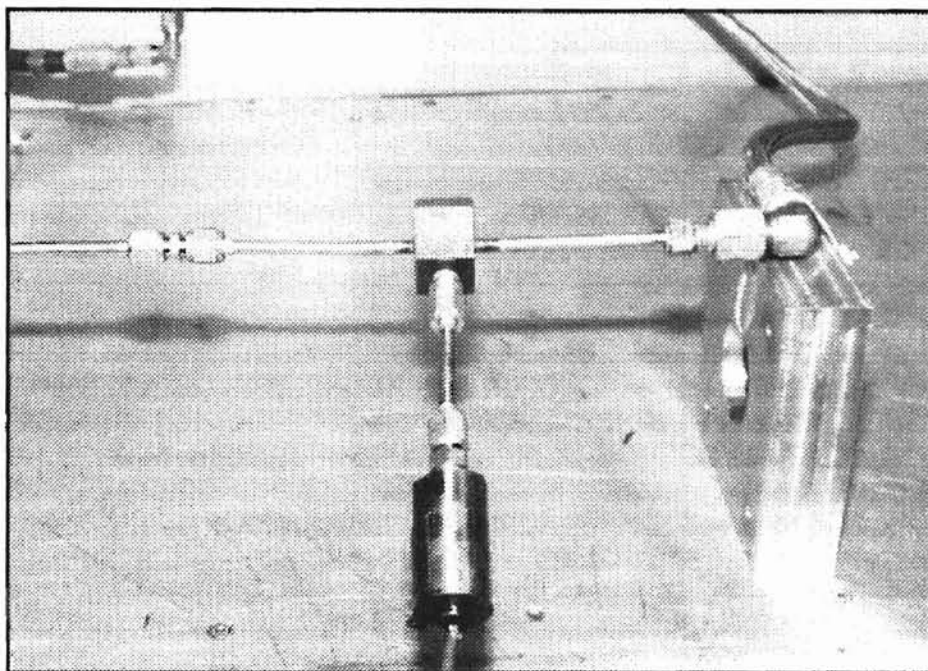


Figure 6.4 Photograph of Attachment of Outlet Pressure Transducer

#### Computer Data Acquisition

Each amplified pressure signal was collected and stored using a high speed data acquisition board connected to a personal computer. The two channels were sampled via a multiplexing A/D converter with 12 bits of resolution. Single ended inputs and a 0-10 VDC range were utilized. The resulting digital resolution was computed to be 0.00244 volts per bit. The sampling rate was fixed at 10,000 Hz. The primary components of the experimental apparatus are given in Table 6.1.

TABLE 6.1  
Primary Components of the Experimental Apparatus

Component Description	Manufacturer	Model Number
Hydraulic pump-7piston manual variable displacement	Hydro Rene Leduc	CR 084
Pressure transducers	Sensotec	Model LM
12 bit A/D data acquisition board	Intelligent Instrumentation	PCI-20377K-1
Personal computer	IBM	IBM compatible
Amplifiers	FES, Inc.	98 V/V
Thermocouple thermometer	Omega Instruments	Type F
Turbine flowmeter/readout Linearity: $\pm 0.1\%$ of reading over linear range Repeatability: $\pm 0.1\%$ of reading over repeatable range	Hoffer Flow Controls	Flowstar 2000A 0.15 to 15 gpm range Calibration traceable to NIST standards.
Working fluid	Phillips 66	Type F ATF
Power supply	Sorenson	Adjustable DC

#### Calibration and Identification

In order to convert the output voltage of the pressure measurement system (transducer and amplifier) to usable units, a calibration was performed using a certified dead weight tester. While applying a constant and known pressure to a pressure transducer, the output voltage was monitored and recorded with the data acquisition system. The linear relationship between output voltage and the applied pressure is given by the following equations:

*Inlet Pressure Transducer:*

$$\text{Pressure (psig)} = (\text{Input Voltage (volts)} - 1.61) \times 283.35 \quad (6.1)$$

*Outlet Pressure Transducer:*

$$\text{Pressure (psig)} = (\text{Input Voltage (volts)} + 0.0037) \times 282.32 \quad (6.2)$$

Figure 6.5 is a plot of the calibration data and linear fit line for the inlet pressure transducer. Figure 6.6 is a plot of the calibration data and linear fit line for the outlet pressure transducer.

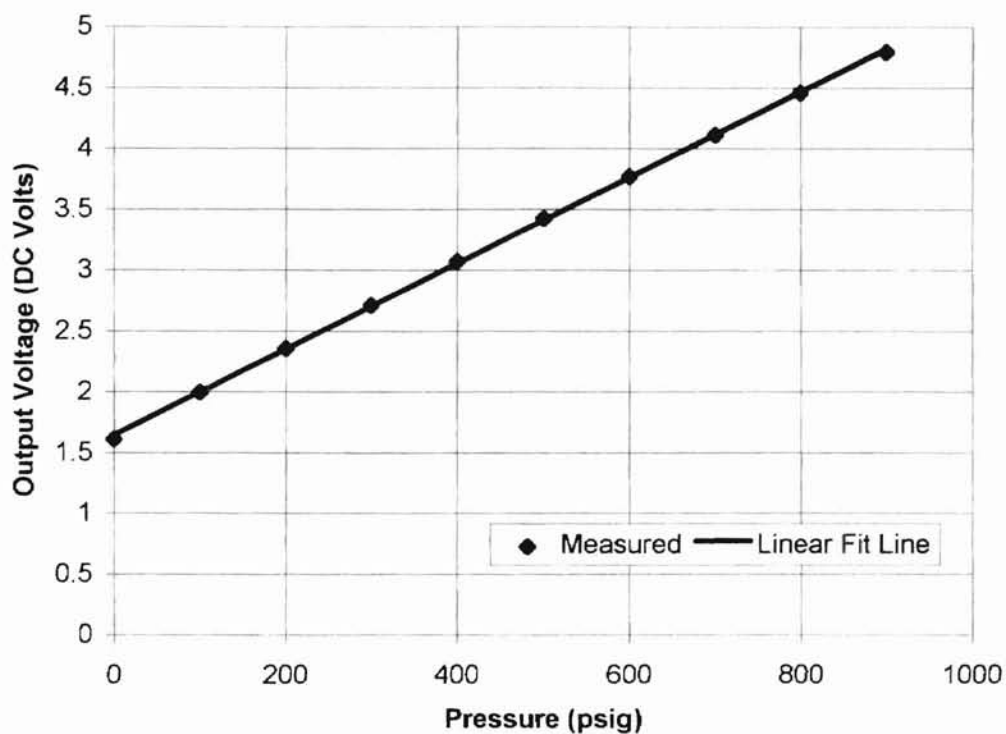


Figure 6.5 Plot of Calibration Data and Best Fit Line for Inlet Pressure Transducer

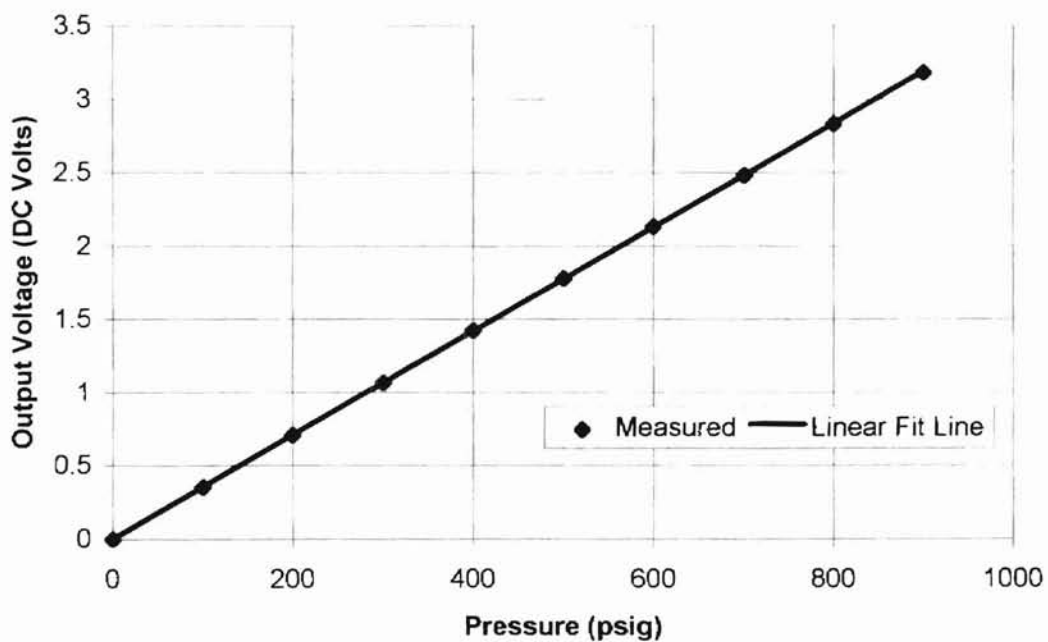


Figure 6.6 Plot of Calibration Data and Best Fit Line for Outlet Pressure Transducer

The fluid characteristic of viscosity was measured by means of a calibrated Brookfield viscometer. The viscosity was measured as the fluid temperature changed. The viscosity data was modeled using the Walther equation to obtain the relationship between the viscosity and temperature. Figure 6.7 is a plot of the viscosity data and the Walther equation model for the data.

*Walther Equation:*

$$\log_{10}[\log_{10}(v(\text{cSt}) + 0.6)] = -2.6617 \times \log_{10}T(\text{Rankin}) + 7.5091 \quad (6.3)$$

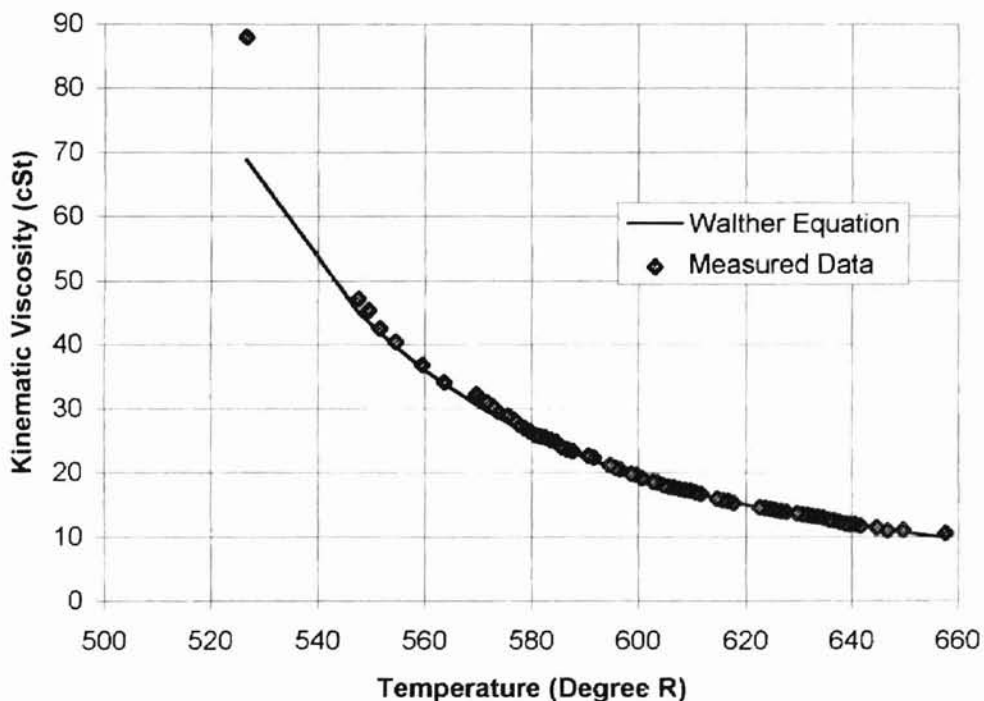


Figure 6.7 Plot of Viscosity Data and Walther Equation

The physical parameters for the test lines is given in Table 2. The construction material is type 304 stainless steel.

TABLE 6.2  
Physical Parameters for Test Line

Line ID	Length (in)	I.D. (in)	O.D. (in)	Wall thickness (in)
L-1	70	0.180	0.250	0.035

#### Procedure for Steady State Testing

The following test procedure was used for collecting data needed for comparison with the S-T model predictions. The output of the hydraulic piston pump is not constant. Each of the seven pistons stroke once per revolution, creating seven pulses per input shaft revolution. In addition, the action of the pump internal check valves and numerous other parameters contribute to the time varying periodic output flow of the pump. To remove many of the time varying aspects, simple averaging of the sampled pressure signals was used to obtain an average inlet pressure and an average outlet pressure to the test line.

The test procedure was as follows:

1. Calibrate all instruments.
2. Install test line.
3. Engage pump drive.
4. Maintain circulating fluid temperature of  $140^{\circ}\text{F} \pm 1^{\circ}\text{F}$ .
5. Adjust pump shaft speed to achieve desired mean flow rate.
6. With all test parameters stabilized, initiate data acquisition using a sample rate of 10,000 Hz. Average the data and record.
7. Repeat steps 2-7 as required with alternate flow rates.

#### Steady State Test Data

Figure 6.8 summarizes the experimental data collected for comparison to the Hagen-Poiseuille method and the S-T Method. For this comparison, the fluid density was  $7.91 \times 10^{-5} \text{ lb}_f\text{sec}^2/\text{in}^4$ , and the kinematic viscosity was  $3.03 \times 10^{-2} \text{ in}^2/\text{sec}$ .

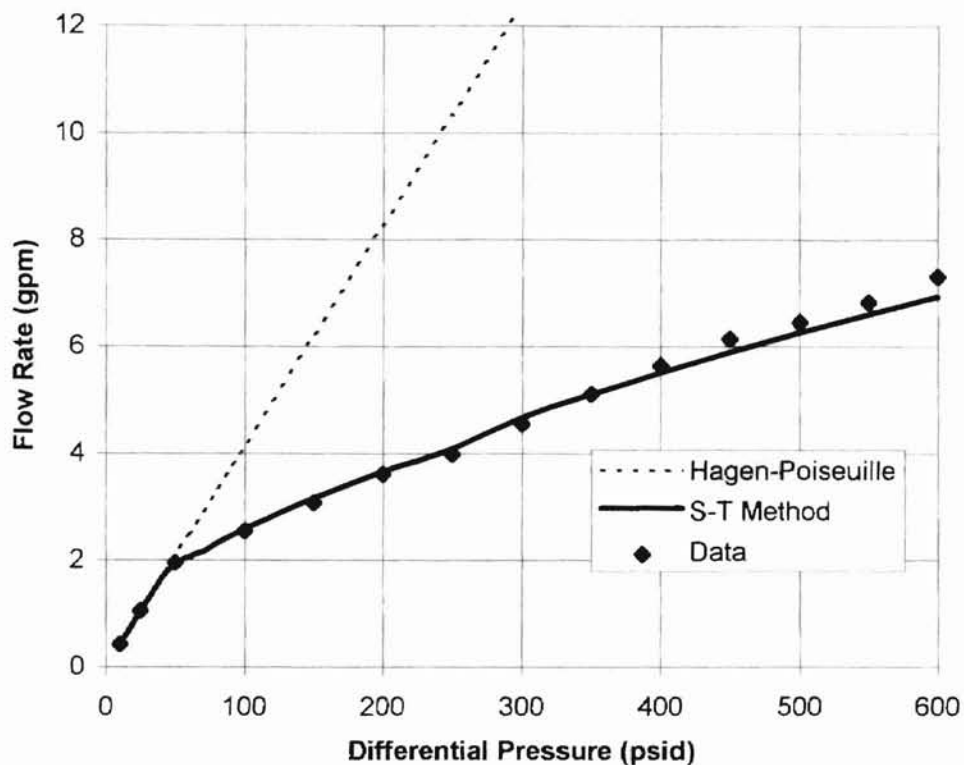


Figure 6.8 Comparison Plot of Steady State Data and Models

It can be seen in Figure 6.8 that the agreement between the data and the S-T method is excellent. The results of the steady state test substantiates the use of the S-T method for calculating resistance to flow. The Hagen-Poiseuille formula diverges quickly beyond the laminar region which terminates at 2.1 gpm. The slight inflection detected at 4.2 gpm in the curve for the S-T method is a characteristic of the crossover point from transition to turbulent flow.



## PART 2: Dynamic Testing

### Experimental Apparatus

The experimental setup for dynamic testing consisted of a pressurized reservoir, fluid line, pressure transducer, valve, and downstream collection reservoir. Figure 6.9 depicts the physical layout.

### Procedure and Results for Dynamic Testing

The basic premise for this test was to allow water to initially flow from the supply reservoir through the conduit and valve into the downstream reservoir. At time  $t=0$ , the valve was commanded to close. The valve area time history [20] corresponds to the data previously given in Table 5.1. When the valve finally closes, forward and backward traveling wave fronts are created in the test line. The pressure transducer located immediately upstream of the valve was used to measure pressure which was recorded. The test fluid was water. The line dimensions and fluid parameters are those given previously in Table 5.2. The experimental data collected at the Marshall Space Flight Center is plotted in Figure 6.10, along with the theoretical curves previously presented. From this figure, it can be seen that the rational approximate model with Fanning friction factor reported by Gerlach slightly undershoots the test data during the initial pressure rise. Conversely, the rational approximate model with S-T method and the  $T^3$  model with S-T method slightly overshoots the test data during the initial pressure rise. The rational approximate model with H-P law produced the largest peak pressure prediction of any of the models. The percent error between peak pressure prediction and experimental data is summarized in Table 6.3. The

deviation between data and theory is principally believed to be the result of errors in the analytical expression for valve area history compared with the actual valve area which occurred during the experiment.

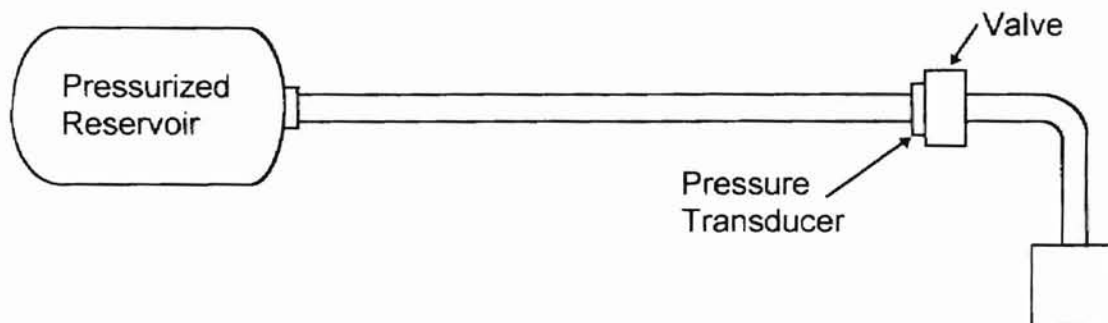


Figure 6.9 Physical Representation of Water Hammer Experiment

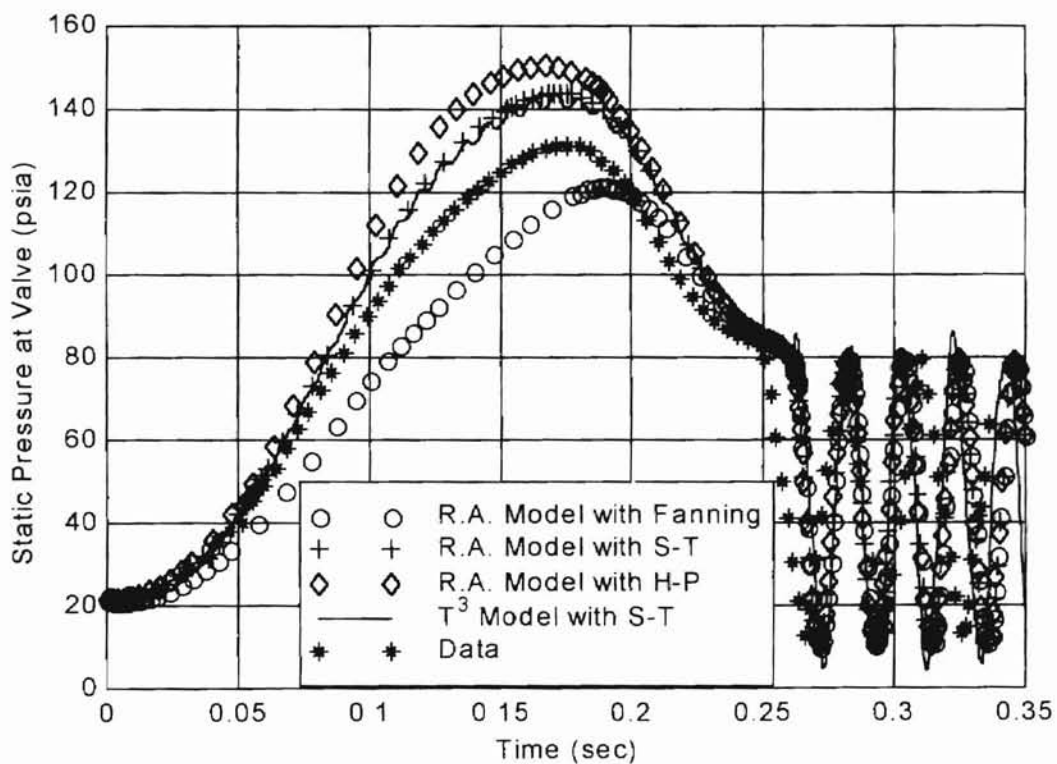


Figure 6.10 Comparison of Theoretical Curves and Experimental Data

Table 6.3  
Water Hammer Experiment  
Percent Error for Peak Pressure Predictions

$$\text{Error}(\%) = \frac{\text{Theoretical} - \text{Experimental}}{\text{Experimental}} \times 100$$

Modeling Approach	Error (%)
R.A. Model with Fanning Factor	-6.9
R.A. Model with H-P Law	15.4
R.A. Model with S-T Method	8.5
T <sup>3</sup> Model with S-T Method	8.5

Prior to valve closure, the primary dynamic contributors in the system are the line and the valve. The valve is represented by the valve flow equation and the valve effective flow area equation. These equations were developed through research conducted at the Fluid Power Research Center at Oklahoma State University. It can be seen that the majority of the error occurs between 0.05 seconds and 0.25 seconds. Upon valve closure, the conduit is effectively blocked and the valve is no longer a significant contributor to the pressure response. After 0.26 seconds, the theory agrees closely with the experimental data with respect to amplitude and period of the pressure wave. Conduit dynamics are thus primarily responsible for the transmission and attenuation of the pressure wave after valve closure. It can be deduced that during the first part of the pressure history, the principle source of error can be attributed to the valve area history and associated valve equation. During the latter part of the pressure history, the valve is no longer part of the analysis, and the agreement between theory and experiment is much improved.

## PART 3: Amplitude Decay Testing

### Experimental Apparatus

The fluid power system used for amplitude decay testing was nearly identical to that used for the steady state testing. The only exception was the addition of an adjustable valve (Marsh Instruments P/N N1514) located immediately after the test line. Figure 6.11 is a schematic diagram of the system. The valve was used to maintain a particular pressure load on the test line.

### Procedure for Amplitude Decay Testing

The procedure for this final stage of data collection was as follows:

1. Calibrate all instruments.
2. Install test line.
3. Engage pump drive.
4. Maintain circulating fluid temperature of  $120^{\circ}\text{F} \pm 1^{\circ}\text{F}$ .
5. Adjust pump shaft speed to achieve desired mean flow rate.
6. Adjust valve to achieve desired load pressure.
7. With all test parameters stabilized, initiate data acquisition using a sample rate of 10,000 Hz. Average the data and record.
8. Repeat steps 2-7 as required with alternate flow rates and load pressures.

The line was again 70 inches in length with an i.d. of 0.18 inches, and an o.d. of 0.25 inches. SAE 24B pressure taps were employed at the inlet and outlet to the line. The fluid was Phillips 66 Type F ATF.

### Modeling Approach

The fluid transmission line was modeled in conjunction with the load valve. The author's one-lump  $T^3$  line model with S-T method was utilized for the line. The valve was modeled using the following equation. The line and valve were connected by a node with a volume of  $1.5 \text{ in}^3$ . The remaining parameters used for the simulations are given in Table 6.4

$$q_v = C_d A_v \sqrt{\frac{2}{\rho} \cdot (\Delta P)} \quad (6.4)$$

where

$q_v$  = valve flow rate (in<sup>3</sup>/sec)

$C_d$  = discharge coefficient

$A_v$  = valve flow area (in<sup>2</sup>)

$\rho$  = fluid density (lb<sub>f</sub>sec<sup>2</sup>/in<sup>4</sup>)

$\Delta P$  = pressure differential across valve (psid)

A discharge coefficient of 0.60 is typically employed for all orifices [24]. The same value will be utilized for this study.

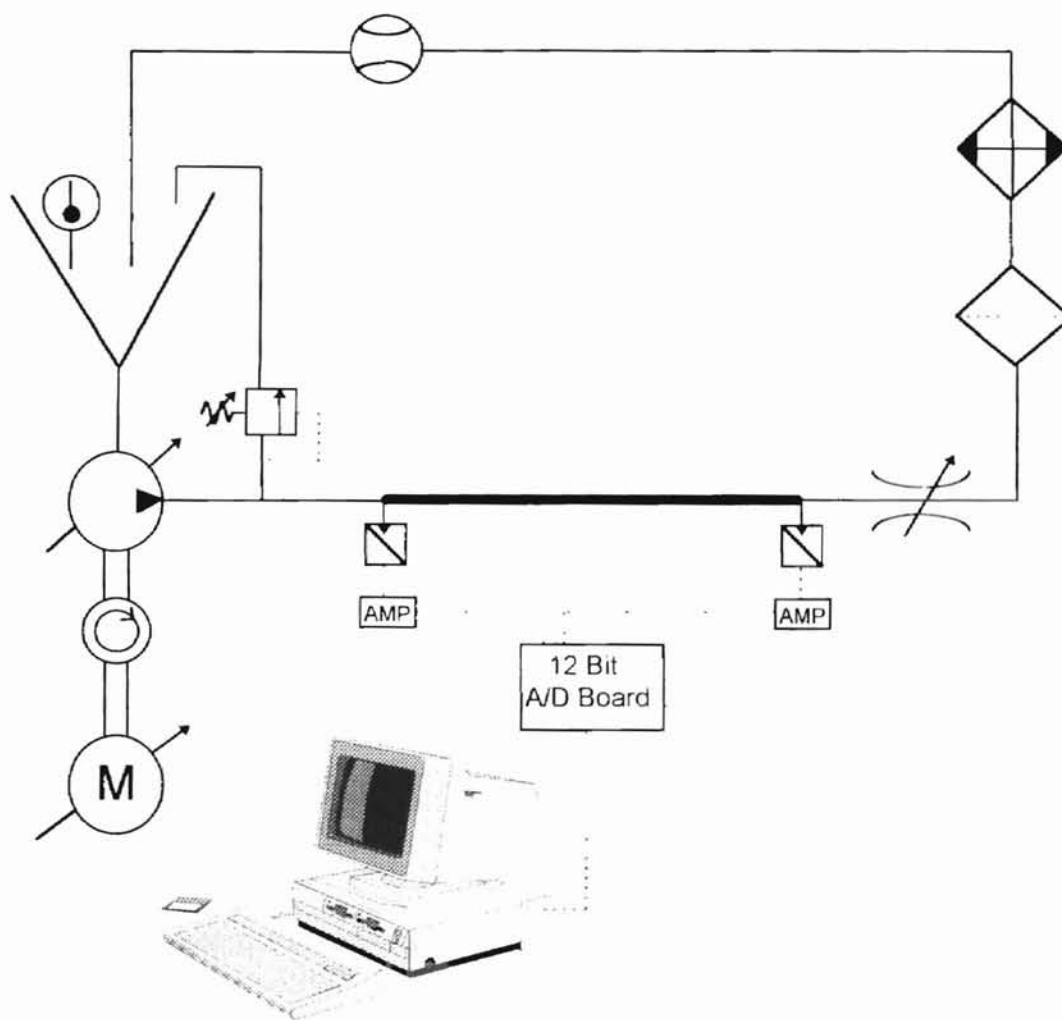


Figure 6.11 Schematic Diagram of System for Amplitude Decay Testing

### Comparison of Data and Author's Model

Upstream and downstream pressure traces were obtained at 2.25, 3.0, and 3.75 gpm mean flow rate. The upstream pressure trace was approximated using a representative equation which was used as the input to the author's model. The predicted downstream pressure trace computed at the node between the line and the valve was then compared to the actual experimental data collected at the downstream pressure tap. The experimental data presented in the following plots are the actual raw traces without any averaging or data smoothing.

Table 6.4  
Simulation Parameters

Parameter	Value and Units
$d_i$	0.18 in
$d_o$	0.25 in
$L_c$	70 in
$\rho$	$7.95 \times 10^{-5} \text{ lb}_f \text{ sec}^2 / \text{in}^4$
$\nu$	$0.0405 \text{ in}^2 / \text{sec}$
$E$	$29 \times 10^6 \text{ psi}$
$\beta_{oil}$	200,000 psi
$V_{node}$	$1.5 \text{ in}^3$

For the first case, data from the 3 gpm case was considered. The load valve was in the full open position. The trend of the inlet data follows a sine wave and was approximated as such as seen in Figure 6.12. The outlet data is plotted in Figure 6.13, with the predicted downstream pressure superimposed. The one lump  $T^3$  model predicts the downstream pressure quite well. For the next case, data from the 2.25 gpm case was analyzed. The load valve was partially closed to create back pressure on the test line. The back pressure changed the pump's output characteristics such that the line inlet data follows the pattern of a full wave

rectified sine, which is typically expected from a piston pump. The inlet pressure data superimposed with a full wave rectified sine for the model input are shown in Figure 6.14. The predicted line outlet pressure and associated test data are displayed in Figure 6.15. Again, the model agrees with the trend of the data. For the final case, a flow rate of 3.75 gpm was utilized. Figures 6.16 and 6.17 depict the test data and corresponding modeling effort. The model successfully emulates the pressure amplitude decay.

Applying a moving average to the inlet pressure data as it was collected would considerably smooth the data and allow for a much closer fit between the model input curve and the inlet data. This would in turn improve the outlet pressure prediction. At any rate, the error between predicted volumetric flow rate and measured volumetric flow rate is less than 5%. This error analysis is summarized in Table 6.5.

Table 6.5  
Amplitude Decay Experiment Flow Rate Error Analysis

$$\text{Error(\%)} = \left( \frac{\text{Predicted} - \text{Measured}}{\text{Measured}} \right) \times 100$$

Case	Predicted (gpm)	Measured (gpm)	Error (%)
1	3.10	3.00	3.3
2	2.30	2.25	2.2
3	3.85	3.75	2.7

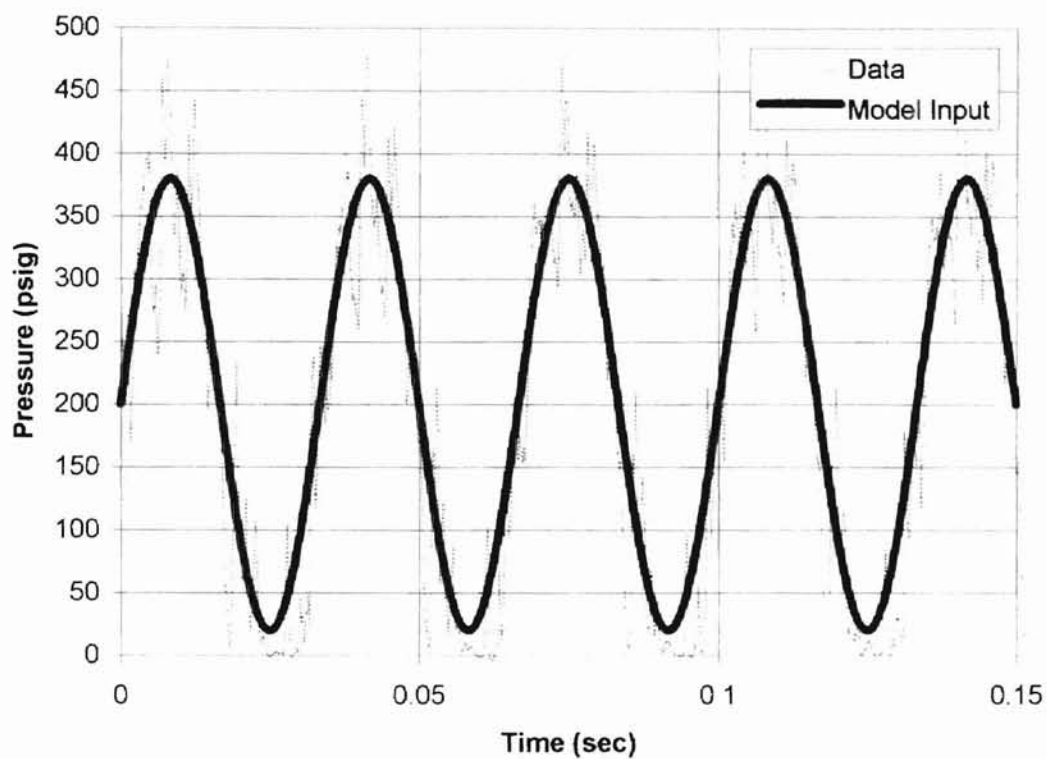


Figure 6.12 Inlet Data and Model Input Curve: 3 gpm

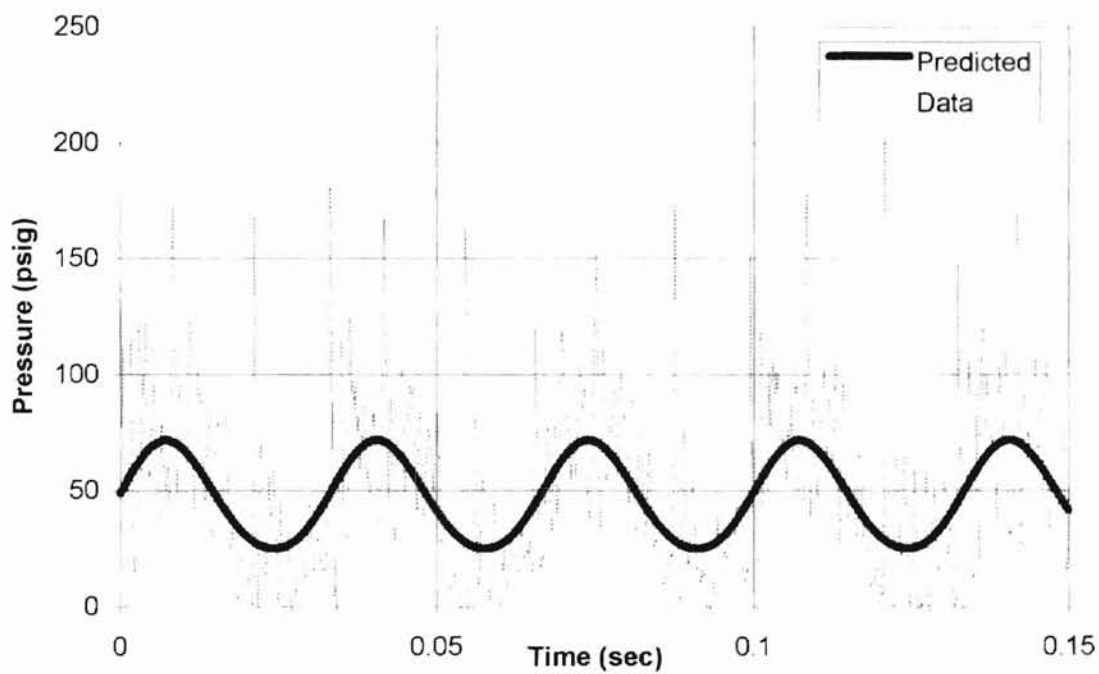


Figure 6.13 Outlet Data and Predicted Pressure: 3 gpm



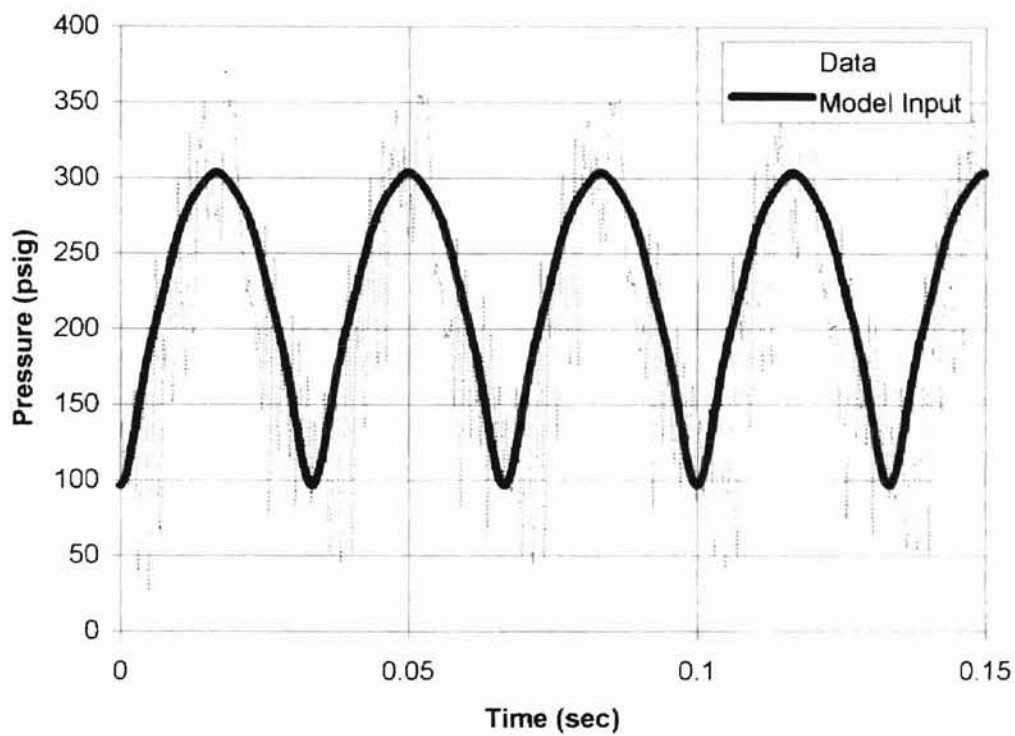


Figure 6.14 Inlet Data and Model Input Curve: 2.25 gpm

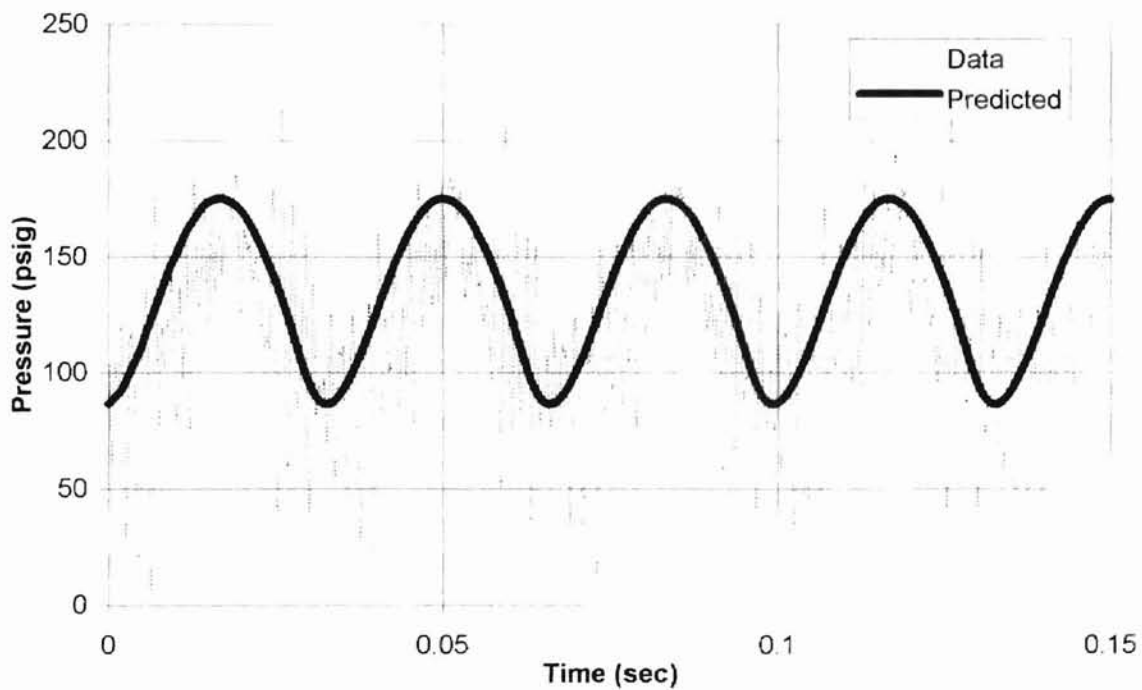


Figure 6.15 Outlet Data and Predicted Pressure: 2.25 gpm

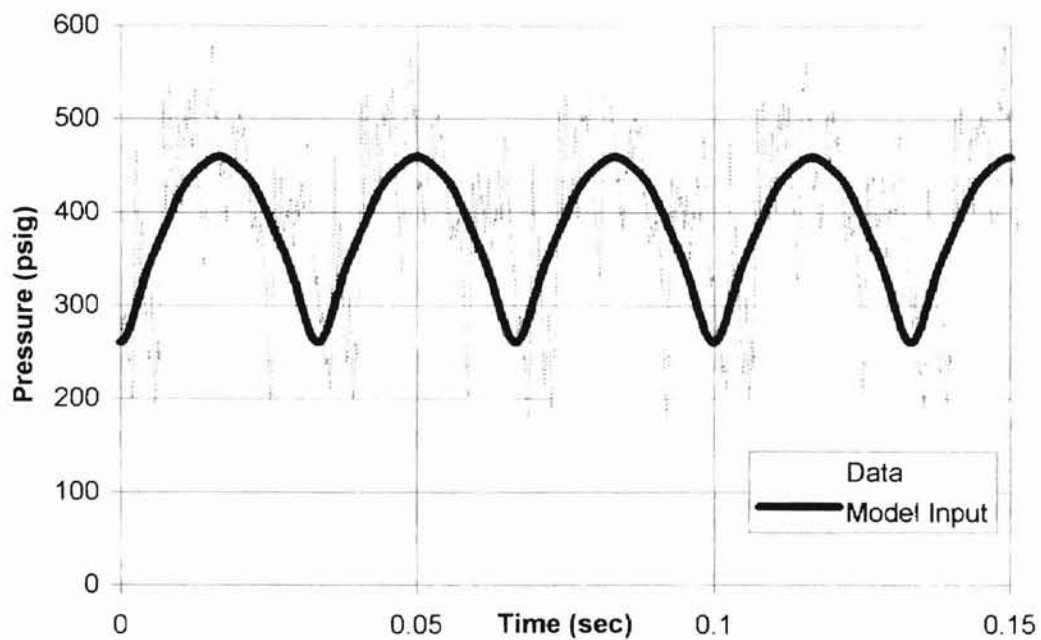


Figure 6.16 Inlet Data and Model Input Curve: 3.75 gpm

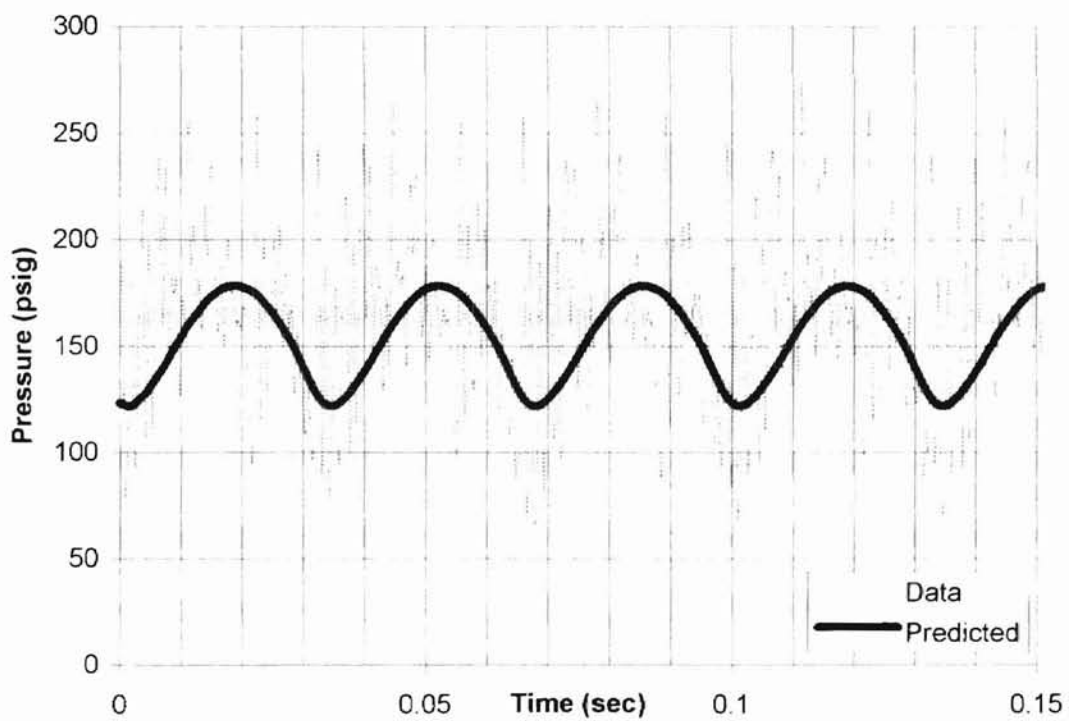


Figure 6.17 Outlet Data and Predicted Pressure: 3.75 gpm

## CHAPTER VII

### CONCLUSIONS AND RECOMMENDATIONS

This study successfully developed a new approach in the modeling of hydraulic transmission lines consisting of the  $T^3$  electrical analogy with S-T method. Through comparison with established models and test data, several conclusions and recommendations may be drawn. First, the scope of the model is summarized.

#### Scope of Model

1. The study was restricted to rigid, straight, circular lines with uniform cross-section.
2. Fluid density and viscosity were assumed to be uniform with respect to position and time.
3. This study encompassed smooth tubing.

#### Conclusions

1. One, two, and four lump models were derived and evaluated.
2. The rational approximate model is highly suitable for frequency domain analysis. It can be coupled to transfer functions for other components in a hydraulic system and integrated into a modern computer simulation package. The same can be said for the modal analysis technique discussed in the

literature review. However, both methods require tables for determining necessary coefficients.

3. The rational approximate model was shown to be derived from the fundamental equations of fluid dynamics, namely, a reduced and linearized form of the Navier Stokes relation, continuity equation, and liquid equation of state. The rational approximate model can be solved in the time domain for the limited case of a blocked line. One term of the rational approximate model was compared to 1 lump of the author's  $T^3$  model. The agreement between the two models was excellent and validates the use of the electrical analogy for a relatively large line with an internal diameter 3.875 inches and a length of 276 inches.
4. Many techniques rely on the Hagen-Poiseuille law for conduit friction. While valid for laminar fully developed flow, this formulation for friction effects in conduits must be used with caution. The approach developed in this investigation uses a method that is not limited to laminar flow. The S-T method for resistance to flow was experimentally verified for a 0.180 inch internal diameter line 70 inches long, in sharp contrast to the Hagen-Poiseuille law which deviated drastically beyond the laminar region. The experiment convincingly demonstrated the utility of the closed form solution provided by the S-T method.
5. The S-T method does not require cumbersome lookup charts. The first part of the experimental study verified the accuracy of the S-T method. This led to further exploration into the accuracy of the  $T^3$  model with S-T method from a

dynamic standpoint. The author's model agreed well with test data from a water hammer experiment in which a valve was suddenly commanded to close. The error between the theoretical prediction and the test data is due to a difference between the analytical expression for valve area history and the actual valve area history that occurred in the experiment.

6. The  $T^3$  analogy with S-T method was used to predict the pressure at the line/valve interface for a line/valve combination. Experimental data collected at different flow rates and pressures were obtained for a 70 inch test line with a 0.180 inch internal diameter. The inlet data was approximated with a representative function that served as the input pressure to the model. The  $T^3$  model with S-T method was shown to successfully predict the pressure amplitude decay caused by the test line.

#### Recommendations

1. Hydraulic lines are often composed of straight sections with intermediate bends, elbows, fittings, and various changes in cross-section. Pressure drops or minor losses associated with bends, elbows, fittings, or other sudden changes in diameter should be represented using equivalent length methodology.
2. The author's approach is not restricted to circular lines. It is feasible to use the concept of equivalent diameter, or hydraulic diameter, to represent non-circular cross-sections. Although, experiments should be carried out to confirm or deny the validity of using hydraulic diameter with the S-T method.

3. In this study, temperature variations along the 70 inch line were minimal as measured with non-intrusive surface temperature probes attached at the inlet and outlet of the line. At low Reynolds numbers, when variant temperature conditions are expected, it is recommended that equation 4.17 (b) be used in place of equation 4.17 (a) which was used in this study.

### Literature Cited

1. J.S. Stecki and D.C. Davis, "Fluid transmission lines-distributed parameter models Part 1: a review of the state of the art", *Proceedings of the Institution of Mechanical Engineers*, Vol 200, No. A4, 1986.
2. Gerlach, C.R., "The Dynamics of Viscous Fluid Transmission Lines with Particular Emphasis on Higher Mode Propagation," Ph.D. Dissertation, Oklahoma State University, July 1966.
3. Oldenburger, R. and Goodson, R.E. "Simplification of hydraulic line dynamics by use of infinite products", *Trans. ASME, J. Basic Engineering*, vol 86, pp 1-10, 1964.
4. Oldenburger, R., "Infinite-Product Analysis of Fluid Transmission Lines," *Proceedings of the Engineering Seminar on Fluid Control Systems at Pennsylvania State University*, March 1967.
5. Viersma, T.J., *Analysis, Synthesis and Design of Hydraulic Servosystems and Pipelines*, Elsevier, pp 129-229, 1980.
6. D'Souza, A.F., and Oldenburger, R., "Dynamic Response of Fluid Lines", *J. Basic Eng.*, *Trans. ASME*, Ser. D, pg 589, 1964.
7. Blackburn, J.F., Reethof, G., and Shearer, J.L., *Fluid Power Control*, Wiley, New York, Chapters 3 and 5, 1960.
8. Woods, R.L., Hsu, C.H., and Chung, C.H., "Comparison of Theoretical and Experimental Fluid Line Responses with Source and Load Impedances," *1983 Winter Annual Meeting ASME*, published in ASME Book H00278, pp. 1-36.
9. Watton, J., "The Simulation of Transmission Line Dynamics in Non-Linear Electrohydraulic Systems," *1983 Winter Annual Meeting ASME*, published in ASME Book H00278, pp. 98-112.
10. Watton, J., "The Effect of Transmission Line Dynamics on the Response of Servovalve Controlled Actuators," *1983 Winter Annual Meeting ASME*, published in ASME Book H00278, pp. 113-125.
11. Hullender, D.A., and Healey, A.J., "Rational Polynomial Approximations for Fluid Transmission Line Models," *Fluid Transmission Line Dynamics*, ASME H00200 1981, pp 33-56.

12. Healy, A.J., and Hullender, D.A., "State Variable Representation of Modal Approximations for Fluid Transmission Line Systems," *Fluid Transmission Line Dynamics*, ASME H00200 1981, pp 57-71
13. Ferries, G.R., and Arbanas, R.L., "Control/Structure Interaction in Hydraulic Power Steering Systems," *Proceedings of the American Control Conference*, Albuquerque, New Mexico, June, 1997.
14. Watton, J., Chapter 5, *Fluid Power Systems*, 1989 (Prentice-Hall, Englewood Cliffs, New Jersey).
15. Zielke, W., "Frequency dependent friction in transient pipe flow," *Journal of Basic Engineering*, ASME, pp109-114, 1968.
16. Brown, F.T., "A quasi method of characteristics with application to fluid lines with frequency dependent wall shear and heat transfer," *J. Basic Eng.*, ASME, pp. 217-227, 1969.
17. Lee, J.C., "An Investigation into the Computer Control of Transmission Line Dynamics for a Servo-Controlled Hydraulic System," M.S. Thesis, Oklahoma State University, 1989.
18. Krus, Weddfelt, and Palmberg, "Fast Pipeline Models for Simulation of Hydraulic Systems," *Transactions of the ASME, Journal of Dynamic Systems, Measurement, and Control*, Vol. 116, pp 132-136, March 1994.
19. Watton, J., and Hawkley, C.J., "An approach for the synthesis of oil hydraulic transmission line dynamics utilizing in situ measurements," *Institution of Mechanical Engineers, Journal of Systems and Control Engineering, Proceedings Part 1*, Vol. 210, No. 12, pp. 77-93, 1996.
20. Gerlach, Richard C., "Dynamic Models for Hydraulic Conduits," *Fluid Power Research Conference*, Oklahoma State University, Stillwater, Oklahoma, July 25 and 26, 1967.
21. Johnson, S.P., "A Survey of Flow Calculation Methods," *ASME Aeronautic and Hydraulic Division Summer Meeting*, June 19-21, 1934.
22. Fitch, E.C., and Hong, I.T., *Hydraulic Component Design and Selection*, Chapter 11, BarDyne, Inc., Stillwater, Oklahoma, 1997.
23. SAE/ARP 24B, "Determination of Hydraulic Pressure Drop," *Society of Automotive Engineers*, 485 Lexington Ave., New York, NY 10017.
24. Merritt, H.E., *Hydraulic Control Systems*, Chapter 3, John Wiley & Sons, Inc., 1967.



## Appendix A

Listing of MATLAB M-files for One, Two, and Three Terms  
of Rational Approximate Engineering Model

```

% Rational Approximate Model
% One term, n=0
% n0.m

t=0.035;
E=29e6;
do=0.25;
di=0.18;
ro=di/2;
Boil=200000;
Bpipe=t*E/do;
Beff=Boil*Bpipe/(Boil+Bpipe);
rho=7.95e-5;
nu=2.91e-2;
co=sqrt(Beff/rho);
l=70;
pi=3.14159;
Ai=pi*di*di/4;
Dn=nu*l/(co*ro*ro);
Fco=1.5;
Wco=Fco*co/l;
const=rho*l/Ai;
zetaco=0.04

num=const.*[0 1 0];
den=[1/Wco^2 2*zetaco/Wco 1];
w=logspace(1,4);
[mag,phase]=bode(num,den,w);
logmag=20*log(mag);
semilogx(w,logmag)
xlabel('w (rad/sec)'),ylabel('Magnitude [P(s)/V(s)] (Db)')
grid;
pause;
%%%%%%%%%%%%%%%%%%%%%%%%%%%%%%%%%%%%%%%%%%%%%%%%%%%%%%%%%%%%%%%%%%%%%%%%
% convert x-axis to dimensionless frequency number F
%%%%%%%%%%%%%%%%%%%%%%%%%%%%%%%%%%%%%%%%%%%%%%%%%%%%%%%%%%%%%%%%%%%%%%%%
F=w*l/co;
plot(F,logmag),grid;
xlabel('F=w*l/c (Dimensionless)');
ylabel('Magnitude [P(s)/V(s)] (Db)');

```

```

% Rational Approximate Model
% Two terms, n=1
% n1.m

t=0.035;
E=29e6;
do=0.25;
di=0.18;
ro=di/2;
Boil=200000;
Bpipe=t*E/do;
Beff=Boil*Bpipe/(Boil+Bpipe);
rho=7.95e-5;
nu=2.91e-2;
co=sqrt(Beff/rho);
l=70;
pi=3.14159;
Ai=pi*di*di/4;
Dn=nu*l/(co*ro*ro);

const=rho*l/Ai;
zetaco=0.04;
zetac1=0.023;
zetas1=0.03;
Fco=1.5;
Wco=Fco*co/l;
Fc1=4.6;
Wc1=Fc1*co/l;
Fs1=3.0;
Ws1=Fs1*co/l;

num=const.*[1/Ws1^2 2*zetas1/Ws1 1 0];
den1=[1/Wco^2 2*zetaco/Wco 1]; den2=[1/Wc1^2 2*zetac1/Wc1 1];
den=conv(den1,den2);
w=logspace(1,4);
[mag,phase]=bode(num,den,w);
logmag=20*log(mag);
semilogx(w,logmag),grid;
xlabel('w (rad/sec)'),ylabel('Magnitude [P(s)/V(s)] (Db)');
pause;
%%%%%%%%%%%%%%%%%%%%%%%%%%%%%%%%%%%%%%%%%%%%%%%%%%%%%%%%%%%%%%%%%%%%%%%%
% convert x-axis to dimensionless frequency number F
%%%%%%%%%%%%%%%%%%%%%%%%%%%%%%%%%%%%%%%%%%%%%%%%%%%%%%%%%%%%%%%%%%%%%%%%
F=w*l/co;
plot(F,logmag),grid;
xlabel('F=w*l/c (Dimensionless)'),ylabel('Magnitude [P(s)/V(s)] (Db)');

```

```

% Rational Approximate Model
% Three terms, n=2
% n2.m
t=0.035;
E=29e6;
do=0.25;
di=0.18;
ro=di/2;
Boil=200000;
Bpipe=t*E/do;
Beff=Boil*Bpipe/(Boil+Bpipe);
rho=7.95e-5;
nu=2.91e-2;
co=sqrt(Beff/rho);
l=70;
pi=3.14159;
Ai=pi*di*di/4;
Dn=nu*l/(co*ro*ro);
const=rho*l/Ai;
zetaco=0.04; zetac1=0.023; zetac2=0.018;
zetas1=0.03; zetas2=0.02;
Fco=1.5; Wco=Fco*co/l;
Fc1=4.6; Wc1=Fc1*co/l;
Fc2=8.0; Wc2=Fc2*co/l;
Fs1=3.0; Ws1=Fs1*co/l;
Fs2=6; Ws2=Fs2*co/l;
sn1=[1/(Ws1)^2 2*zetas1/Ws1 1];
sn2=[1/(Ws2)^2 2*zetas2/Ws2 1];
gam=(rho*l/Ai).*[1 0];
sa=conv(sn1,sn2);
num=conv(gam,sa);
cn0=[1/Wco^2 2*zetaco/Wco 1];
cn1=[1/Wc1^2 2*zetac1/Wc1 1];
cn2=[1/Wc2^2 2*zetac2/Wc2 1];
ca=conv(cn0,cn1); den=conv(ca,cn2);
w=logspace(1,4);
[mag,phase]=bode(num,den,w);
logmag=20*log(mag);
semilogx(w,logmag),grid,xlabel('w (rad/sec)'),ylabel('Magnitude [P(s)/V(s)] (Db)');
pause;
%%%%%%%%%%%%%%%%%%%%%%%%%%%%%%%%%%%%%%%%%%%%%%%%%%%%%%%%%%%%%%%%%%%%%%%%
% convert x-axis to dimensionless frequency number F
%%%%%%%%%%%%%%%%%%%%%%%%%%%%%%%%%%%%%%%%%%%%%%%%%%%%%%%%%%%%%%%%%%%%%%%%
F=w*l/co;
plot(F,logmag),grid,xlabel('F=w*l/c (Dimensionless)');
ylabel('Magnitude [P(s)/V(s)] (Db)');

```

## Appendix B

Listing of Matlab M-Files for One, Two,  
and Four Lump  $T^3$  Models with S-T Method

```
% out1.m
% tee cubed 1 lump time domain solution
% S-T method
global l di do Pout;
di=0.18;
do=0.25;
l=700;
Pout=0;
y0=[0 0 0 0 0];
t0=0;
tf=0.16;
t1=0:0.001:0.01;
Pramp=75000*t1;
t2=0.01:0.01:0.16;
Pconst=1*t2/t2+750;
tspan=0:0.0001:0.16;
[u,y]=ode23('stline1',tspan,y0);
plot(t1,Pramp,t2,Pconst,u,y(:,1),u,y(:,2),u,y(:,3)),grid
xlabel('Time (sec)'); ylabel('Pressure Response (psig)');
pause;
y(:,4)=y(:,4)*(60/231); y(:,5)=y(:,5)*(60/231);
plot(u,y(:,4),u,y(:,5)),grid;
xlabel('Time (sec)');ylabel('Flow Response (gpm)');
```

```

% time domain solution
% stline1.m 1 lump line model
% S-T Method

function ydot=stline1(u,y);
global I di do Pout;

thick=(do-di)/2;           %tube thickness (in)
em=29*10^6;               %tube elastic modulus (psi)
Btube=thick*em/do;       %tube bulk modulus (psi)
Boil=200000;             %oil bulk modulus (psi)
Beff=Boil*Btube/(Boil+Btube); %effective bulk modulus (psi)
a=3.14159*di*di/4;       %inside cross-sectional area (in^2)
mu=3.1159e-6;           %absolute viscosity
rho=8.0978e-5;          %fluid density
nu=mu/rho;               %kinematic viscosity
V=a*I;                   %volume
C=V/Beff;                %capacitance
L=rho*I/a;                %inductance
if u<=0.01
    Pin=75000*u;
end
if u>0.01
    Pin=750;
end
for i=1:2,
    if i==1
        deltap=Pin-y(1);
    end
    if i==2
        deltap=y(3)-Pout;
    end
    s(i)=(1/nu)*sqrt((abs(deltap)*di^3)/(rho*(l/2)));
    if s(i)==0
        s(i)=0.01;
    end
    if s(i)<=200
        fd(i)=2048/s(i)^2;
    end
    if s(i)<500 & s(i)>200
        fd(i)=.0425;
    end
    if s(i)>=500
        fd(i)=.2431/(s(i)^.2857);
    end
    q(i)=sqrt((2*abs(deltap)*di)/(rho*fd(i)*(l/2)))*a;

```

```
    if deltap>=0
        q(i)=q(i);
    else
        q(i)=-q(i);
    end
end
```

```
ydot(1)=(3/C)*(q(1)-y(4));
ydot(2)=(3/C)*(y(4)-y(5));
ydot(3)=(3/C)*(y(5)-q(2));
ydot(4)=(2/L)*(y(1)-y(2));
ydot(5)=(2/L)*(y(2)-y(3));
ydot=ydot';
```



```

% out2.m
% output file
% S-T method two lump line model

y0=[0 0 0 0 0 0 0 0 0 0];
global I di do Pout
di=.18;
do=.25;
I=700;
Pout=0;
t0=0;
tf=0.16;
tspan=[t0 tf];
t1=0:0.001:0.01;
Pramp=75000*t1;
t2=0.01:0.01:0.16;
Pconst=1*t2/t2+750;
[u,y]=ode23s('stline2',tspan,y0);
plot(t1,Pramp,'-',t2,Pconst,':',u,y(:,1),u,y(:,2),u,y(:,3), ...
    u,y(:,4),u,y(:,5),u,y(:,6)),grid
xlabel('Time (sec)'),ylabel('Pressure Response (psig)');
pause;
y(:,7)=y(:,7)*60/231; y(:,8)=y(:,8)*60/231;
y(:,9)=y(:,9)*60/231; y(:,10)=y(:,10)*60/231;
plot(u,y(:,7),u,y(:,8),u,y(:,9),u,y(:,10)),grid
xlabel('Time (sec)'),ylabel('Flow Response (gpm)')

```

```

% m-file containing 2 lump t-cubed model
% stline2.m
% S-T Method

function ydot=stline2(u,y);
global l di do Pout
thick=(do-di)/2;           %tube thickness (in)
em=29*10^6;               %tube elastic modulus (psi)
Btube=thick*em/do;       %tube bulk modulus (psi)
Boil=200000;              %oil bulk modulus (psi)
Beff=Boil*Btube/(Boil+Btube);%effective bulk modulus (psi)
a=3.14159*di*di/4;       %inside cross-sectional area (in^2)
mu=3.1159e-6;            %absolute viscosity
rho=8.0978e-5;           %fluid density
nu=mu/rho;               %kinematic viscosity
V=a*l;                   %volume
C=V/Beff;                %capacitance
L=rho*l/a;               %inductance
if u<=0.01
    Pin=75000*u;
end
if u>0.01
    Pin=750;
end
for i=1:3,
    if i==1
        deltap=Pin-y(1);
        n=2;
    end
    if i==2
        deltap=y(3)-y(4);
        n=1;
    end
    if i==3
        deltap=y(6)-Pout;
        n=2;
    end
    s(i)=(1/nu)*sqrt((abs(deltap)*di^3)/(rho*(l*(2*n))));
    if s(i)==0
        s(i)=0.01;
    end
    if s(i)<=200
        fd(i)=2048/s(i)^2;
    end
    if s(i)<500 & s(i)>200
        fd(i)=.0425;
    end
end

```

```

end
if s(i)>=500
    fd(i)=.2431/(s(i)^.2857);
end
q(i)=sqrt((2*abs(deltap)*di)/(rho*fd(i)*(l/(2*n))))*a;
if deltap>=0
    q(i)=q(i);
else
    q(i)=-q(i);
end
end
if y(4)<0
    y(4)=0;
end;
if y(5)<0
    y(5)=0;
end;
if y(6)<0
    y(6)=0;
end;
ydot(1)=(6/C)*(q(1)-y(7));
ydot(2)=(6/C)*(y(7)-y(8));
ydot(3)=(6/C)*(y(8)-q(2));
ydot(4)=(6/C)*(q(2)-y(9));
ydot(5)=(6/C)*(y(9)-y(10));
ydot(6)=(6/C)*(y(10)-q(3));
ydot(7)=(4/L)*(y(1)-y(2));
ydot(8)=(4/L)*(y(2)-y(3));
ydot(9)=(4/L)*((y(4))-y(5));
ydot(10)=(4/L)*((y(5))-y(6));
if y(1)>=y(2)
    y(7)=y(7);
else
    y(7)=-y(7);
end
if y(2)>=y(3)
    y(8)=y(8);
else
    y(8)=-y(8);
end
if y(4)>=y(5)
    y(9)=y(9);
else
    y(9)=-y(9);
end
if y(5)>=y(6)

```

```
    y(10)=y(10);  
else  
    y(10)=-y(10);  
end  
ydot=ydot';
```

```
% out4.m
% output file for 4 lump line model
% tee cubed with S-T
global I di do Pout
I=700;
di=0.18;
do=0.25;
Pout=0;
y0=[0 0 0 0 0 0 0 0 0 0 0 0 0 0 0 0 0 0];
t0=0;
tf=0.16;
t1=0:0.001:0.01;
Pramp=75000*t1;

[u,y]=ode23('stline4',t0,tf,y0);
plot(t1,Pramp,u,y(:,1),u,y(:,2),u,y(:,3),u,y(:,4),u,y(:,5),u,y(:,6), ...
    u,y(:,7),u,y(:,8),u,y(:,9),u,y(:,10),u,y(:,11),u,y(:,12)),grid
xlabel('Time (sec)'),ylabel('Pressure Response (psig)');
pause;
for i=13:20
    y(:,i)=y(:,i)*60/231;
end
plot(u,y(:,13),u,y(:,15),u,y(:,17),u,y(:,19)),grid
xlabel('Time (sec)'),ylabel('Flow Response (gpm)');
```

```

% m-file containing 4 lump t-cubed model
% stline4.m
% S-T Method

function ydot=stline4(u,y);
global l di do Pout
thick=(do-di)/2;           %tube thickness (in)
em=29*10^6;                %tube elastic modulus (psi)
Btube=thick*em/do;        %tube bulk modulus (psi)
Boil=200000;              %oil bulk modulus (psi)
Beff=Boil*Btube/(Boil+Btube); %effective bulk modulus (psi)
a=3.14159*di*di/4;        %inside cross-sectional area (in^2)
mu=3.1159e-6;             %absolute viscosity
rho=8.0978e-5;            %fluid density
nu=mu/rho;                %kinematic viscosity
V=a*l;                    %volume
C=V/Beff;                 %capacitance
L=rho*l/a;                %inductance
if u<=0.01
    Pin=75000*u;
end
if u>0.01
    Pin=750;
end

for i=1:5;
    if i==1
        deltap=Pin-y(1);
        n=4;
    end
    if i==2
        deltap=y(3)-y(4);
        n=2;
    end
    if i==3
        deltap=y(6)-y(7);
        n=2;
    end
    if i==4
        deltap=y(9)-y(10);
        n=2;
    end
    if i==5
        deltap=y(12)-Pout;
        n=4;
    end
end

```

```

s(i)=(1/nu)*sqrt((abs(deltap)*di^3)/(rho*(l/(2*n))));
if s(i)==0
    s(i)=0.01;
end
if s(i)<=200
    fd(i)=2048/s(i)^2;
end
if s(i)<500 & s(i)>200
    fd(i)=.0425;
end
if s(i)>=500
    fd(i)=.2431/(s(i)^.2857);
end
q(i)=sqrt((2*abs(deltap)*di)/(rho*fd(i)*(l/(2*n))))*a;
end
ydot(1)=(12/C)*(q(1)-y(13));
ydot(2)=(12/C)*(y(13)-y(14));
ydot(3)=(12/C)*(y(14)-q(2));
ydot(4)=(12/C)*(q(2)-y(15));
ydot(5)=(12/C)*(y(15)-y(16));
ydot(6)=(12/C)*(y(16)-q(3));
ydot(7)=(12/C)*(q(3)-y(17));
ydot(8)=(12/C)*(y(17)-y(18));
ydot(9)=(12/C)*(y(18)-q(4));
ydot(10)=(12/C)*(q(4)-y(19));
ydot(11)=(12/C)*(y(19)-y(20));
ydot(12)=(12/C)*(y(20)-q(5));
ydot(13)=(8/L)*(y(1)-y(2));
ydot(14)=(8/L)*(y(2)-y(3));
ydot(15)=(8/L)*(y(4)-y(5));
ydot(16)=(8/L)*(y(5)-y(6));
ydot(17)=(8/L)*(y(7)-y(8));
ydot(18)=(8/L)*(y(8)-y(9));
ydot(19)=(8/L)*(y(10)-y(11));
ydot(20)=(8/L)*(y(11)-y(12));
ydot=ydot';

```

## Appendix C

### Listing of MATLAB M-Files Comparing S-T and H-P Methods for a Four Lump Model



```

% out4.m
% output file for 4 lump line models
% comparison of S-T and H-P methods
global I Pin Pout
I=700;
Pin=750;
Pout=0;
y0=[0 0 0 0 0 0 0 0 0 0 0 0 0 0 0 0 0 0];
x0=[0 0 0 0 0 0 0 0 0 0 0 0 0 0 0 0 0 0];
t0=0;
tf=0.25;
%[t,x]=ode23s('hpline4',tspan,x0);
%[u,y]=ode23s('stline4',tspan,y0);
[t,x]=ode23('hpline4',t0,tf,x0);
[u,y]=ode23('stline4',t0,tf,y0);
%[u,y]=ode23('stline4',t0,tf,y0);
%plot(u,y(:,1),u,y(:,2),u,y(:,3),u,y(:,4),u,y(:,5),u,y(:,6)),grid
%plot(u,y(:,13),u,y(:,20)),grid
plot(u,y(:,1),u,y(:,4),u,y(:,7),u,y(:,10),t,x(:,1),t,x(:,4), ...
     t,x(:,7),t,x(:,10)),grid
xlabel('Time (sec)'),ylabel('Pressure Response (psig)');
pause;
for i=13:20
    x(:,i)=x(:,i)*60/231;
    y(:,i)=y(:,i)*60/231;
end
plot(u,y(:,13),u,y(:,15),u,y(:,17),u,y(:,19), ...
     t,x(:,13),t,x(:,15),t,x(:,17),t,x(:,19)),grid
xlabel('Time (sec)'),ylabel('Flow Response (gpm)');
%plot(u,y(:,4)),grid
%xlabel('Time (sec)'),ylabel('Flow rate (in^3/sec)')

```

```

% m-file containing 4 lump t-cubed model
% stline4.m
% S-T Method

function ydot=stline4(u,y);
global l Pin Pout
di=0.18;           %inside diameter (in)
do=0.25;           %outside diameter (in)
thick=(do-di)/2;  %tube thickness (in)
em=29*10^6;        %tube elastic modulus (psi)
Btube=thick*em/do; %tube bulk modulus (psi)
Boil=200000;      %oil bulk modulus (psi)
Beff=Boil*Btube/(Boil+Btube); %effective bulk modulus (psi)
a=3.14159*di*di/4; %inside cross-sectional area (in^2)
mu=3.1159e-6;     %absolute viscosity
rho=8.0978e-5;    %fluid density
nu=mu/rho;        %kinematic viscosity
V=a*l;            %volume
C=V/Beff;         %capacitance
L=rho*l/a;        %inductance
for i=1:5;
    if i==1
        deltap=Pin-y(1);
        n=4;
    end
    if i==2
        deltap=y(3)-y(4);
        n=2;
    end
    if i==3
        deltap=y(6)-y(7);
        n=2;
    end
    if i==4
        deltap=y(9)-y(10);
        n=2;
    end
    if i==5
        deltap=y(12)-Pout;
        n=4;
    end
    end
    s(i)=(1/nu)*sqrt((abs(deltap)*di^3)/(rho*(l/(2*n))));
    if s(i)==0
        s(i)=0.01;
    end
    if s(i)<=200

```

```

    fd(i)=2048/s(i)^2;
end
if s(i)<500 & s(i)>200
    fd(i)=.0425;
end
if s(i)>=500
    fd(i)=.2431/(s(i)^.2857);
end
q(i)=sqrt((2*abs(deltap)*di)/(rho*fd(i)*(l/(2*n))))*a;
end
ydot(1)=(12/C)*(q(1)-y(13));
ydot(2)=(12/C)*(y(13)-y(14));
ydot(3)=(12/C)*(y(14)-q(2));
ydot(4)=(12/C)*(q(2)-y(15));
ydot(5)=(12/C)*(y(15)-y(16));
ydot(6)=(12/C)*(y(16)-q(3));
ydot(7)=(12/C)*(q(3)-y(17));
ydot(8)=(12/C)*(y(17)-y(18));
ydot(9)=(12/C)*(y(18)-q(4));
ydot(10)=(12/C)*(q(4)-y(19));
ydot(11)=(12/C)*(y(19)-y(20));
ydot(12)=(12/C)*(y(20)-q(5));
ydot(13)=(8/L)*(y(1)-y(2));
ydot(14)=(8/L)*(y(2)-y(3));
ydot(15)=(8/L)*(y(4)-y(5));
ydot(16)=(8/L)*(y(5)-y(6));
ydot(17)=(8/L)*(y(7)-y(8));
ydot(18)=(8/L)*(y(8)-y(9));
ydot(19)=(8/L)*(y(10)-y(11));
ydot(20)=(8/L)*(y(11)-y(12));
ydot=ydot';

```

```

% m-file containing 4 lump t-cubed model
% hpline4.m
% Hagen-Poiseuille Law
function xdot=stline4(t,x);
global I Pin Pout
di=0.18;           %inside diameter (in)
do=0.25;           %outside diameter (in)
thick=(do-di)/2;  %tube thickness (in)
em=29*10^6;        %tube elastic modulus (psi)
Btube=thick*em/do; %tube bulk modulus (psi)
Boil=200000;       %oil bulk modulus (psi)
Beff=Boil*Btube/(Boil+Btube); %effective bulk modulus (psi)
a=3.14159*di*di/4; %inside cross-sectional area (in^2)
mu=3.1159e-6;      %absolute viscosity
rho=8.0978e-5;     %fluid density
nu=mu/rho;         %kinematic viscosity
V=a*I;             %volume
C=V/Beff;          %capacitance
L=rho*I/a;         %inductance
R=128*mu*I/(3.14*di^4); %resistance
for i=1:5;
    if i==1
        deltap=Pin-x(1);
        n=4;
    end
    if i==2
        deltap=x(3)-x(4);
        n=2;
    end
    if i==3
        deltap=x(6)-x(7);
        n=2;
    end
    if i==4
        deltap=x(9)-x(10);
        n=2;
    end
    if i==5
        deltap=x(12)-Pout;
        n=4;
    end
    q(i)=(2*n/R)*abs(deltap);
end
xdot(1)=(12/C)*(q(1)-x(13));
xdot(2)=(12/C)*(x(13)-x(14));
xdot(3)=(12/C)*(x(14)-q(2));

```

```
xdot(4)=(12/C)*(q(2)-x(15));  
xdot(5)=(12/C)*(x(15)-x(16));  
xdot(6)=(12/C)*(x(16)-q(3));  
xdot(7)=(12/C)*(q(3)-x(17));  
xdot(8)=(12/C)*(x(17)-x(18));  
xdot(9)=(12/C)*(x(18)-q(4));  
xdot(10)=(12/C)*(q(4)-x(19));  
xdot(11)=(12/C)*(x(19)-x(20));  
xdot(12)=(12/C)*(x(20)-q(5));  
xdot(13)=(8/L)*(x(1)-x(2));  
xdot(14)=(8/L)*(x(2)-x(3));  
xdot(15)=(8/L)*(x(4)-x(5));  
xdot(16)=(8/L)*(x(5)-x(6));  
xdot(17)=(8/L)*(x(7)-x(8));  
xdot(18)=(8/L)*(x(8)-x(9));  
xdot(19)=(8/L)*(x(10)-x(11));  
xdot(20)=(8/L)*(x(11)-x(12));  
xdot=xdot';
```

## Appendix D

### Listing of MATLAB M-Files for Solution of Water Hammer Problem

```
% output file, 1 term R.A. model with Fanning, H-P, and S-T
% 1 lump T^3 with S.T. comparisons
% hammer.m
```

```
P0=[0 21.42];
x0=[0 0 0 21.42 6087 6087];
```

```
global di length Pr Pvout l nu rho beta
```

```
beta=320000;    %fluid bulk modulus (psi)
rho=9.574e-5;   %fluid density (lbfsec^2/in^4)
nu=0.001517;    %kinematic viscosity (in^2/sec)
di=3.875;       %pipe id (inches)
length=276;     %pipe length (inches)
l=length;
Pr=45;          %supply reservoir pressure (psia)
Pvout=8.7;      %downstream reservoir pressure (psia)
```

```
t0=0;
tf=0.35;
tspan=[t0 tf];
options=odeset('abstol',1e-6,'reltol',1e-3);
[t,P]=ode15s('approxfan',tspan,P0);
v=t;
z=P;
[t,P]=ode15s('approxst',tspan,P0);
k=t;
j=P;
[t,P]=ode15s('approxhp',tspan,P0);
[u,y]=ode15s('st1',tspan,x0);
plot(v,z(:,2),'ko',k,j(:,2),'k+',t,P(:,2),'d',u,y(:,4),'k-'),grid
legend('R.A. Model with Fanning','R.A. Model with S-T', ...
'R.A. Model with H-P','T^3 Model with S-T')
xlabel('Time (sec)'),ylabel('Static Pressure at Valve (psia)')
```

```

%solve water hammer problem
%approxfan.m
%Fanning friction factor

function pdot=approxfan(t,P);
global l di nu rho beta Pr Pvout
ro=di/2;           % pipe inside radius (inches)
a=3.14159*di*di/4; % pipe inside crosssectional area (in^2)
ff=0.012;         % fanning friction factor
Co=sqrt(beta/rho); % sonic velocity (in/sec)
Dn=nu*l/(Co*ro^2);
Fco=1.4;
wco=Fco*Co/l;
zco=0.001;
Av=36098169*t^9-27651150*t^8+5290046*t^7+662432*t^6-210542*t^5 ...
    -41747*t^4+16928*t^3-1707*t^2+9.226*t+8.347;
if t>=0.261
    Av=0;
end
Avdot=324883521*t^8-221209200*t^7+37030322*t^6+3974592*t^5 ...
    -1052710*t^4-166988*t^3+50784*t^2-3414*t+9.226;
if t>=0.261
    Avdot=0;
end

q=Av*sqrt(2*(P(2)-Pvout)/(rho*(1-(Av^2)/a^2)));
if P(2)>=Pvout
    q=q;
else
    q=-q;
end

Pss=2*ff*(l/di)*rho*(q/a)^2; % steady state pressure drop
num=rho*(1-(Av^2/a^2))*2*P(1)-2*(P(2)-Pvout)*(-2*rho*Av*Avdot)/a^2;
den=(rho*(1-(Av^2/a^2)))^2;
dirA=0.5*((2*(P(2)-Pvout))/(rho*(1-(Av^2/a^2))))^(-0.5)*num/den;

qdot=Av*dirA+sqrt(2*(P(2)-Pvout)/(rho*(1-Av^2/a^2)))*Avdot;

pdot(1)=(wco^2)*(-P(1)*2*zco/wco -P(2) -(rho*l/a)*qdot +Pr -Pss);
pdot(2)=P(1);
pdot=pdot';

```



```

%1 term water hammer problem with S-T method
%approxst.m

function pdot=approxst(t,P);
global l di Pr nu rho beta Pr Pvout
ro=di/2; % pipe inside radius (inches)
a=3.14159*di*di/4; % pipe inside crosssectional area (in^2)
Pvout=8.7; % valve outlet pressure (psia)
ff=0.012; % fanning friction factor
Co=sqrt(beta/rho); % sonic velocity (in/sec)
Dn=nu*I/(Co*ro^2);
Fco=1.4;
wco=Fco*Co/l;
zco=0.001;
Av=36098169*t^9-27651150*t^8+5290046*t^7+662432*t^6-210542*t^5 ...
-41747*t^4+16928*t^3-1707*t^2+9.226*t+8.347;
if t>=0.261
    Av=0;
end
Avdot=324883521*t^8-221209200*t^7+37030322*t^6+3974592*t^5 ...
-1052710*t^4-166988*t^3+50784*t^2-3414*t+9.226;
if t>=0.261
    Avdot=0;
end

q=Av*sqrt(2*(P(2)-Pvout)/(rho*(1-(Av^2)/a^2)));
if P(2)>=Pvout
    q=q;
else
    q=-q;
end
% use S-T method
s=(1/nu)*sqrt(abs(Pr-P(2))*di^3/(l*rho));
if s<=200
    fd=2048/(s^2);
end
if s<500 & s>200
    fd=0.0425;
end
if s>=500
    fd=0.2431/(s^0.2857);
end

Pss=(q/a)^2*rho*fd*I/(2*di); % steady state pressure drop
num=rho*(1-(Av^2/a^2))^2*P(1)-2*(P(2)-Pvout)*(-2*rho*Av*Avdot)/a^2;
den=(rho*(1-(Av^2/a^2)))^2;

```

```
dirA=0.5*((2*(P(2)-Pvout))/(rho*(1-(Av^2/a^2))))^(-0.5)*num/den;
```

```
qdot=Av*dirA+sqrt(2*(P(2)-Pvout)/(rho*(1-Av^2/a^2)))*Avdot;
```

```
pdot(1)=(wco^2)*(-P(1)*2*zco/wco -P(2) -(rho*l/a)*qdot +Pr -Pss);
```

```
pdot(2)=P(1);
```

```
pdot=pdot';
```

```

% st1.m
% water hammer problem
% 1 lump tee cubed line model
% S-T method
% Specifically compare to Gerlach 1 term

function ydot=st1(u,y);
global di do length Pr Pvout nu rho beta

a=3.14159*di*di/4;           %inside cross-sectional area (in^2)
V=a*length;                %volume
C=V/beta;                  %capacitance
L=rho*length/a;           %inductance
Vo=25;                     %node volume at valve (in^3)

Av=36098169*u^9-27651150*u^8+5290046*u^7+662432*u^6 ...
-210542*u^5-41747*u^4+16928*u^3-1707*u^2+9.226*u+8.347;
if u>=0.261
    Av=0;
end
s1=(1/nu)*sqrt((abs(Pr-y(1))*di^3)/(rho*(length/2)));
if s1<=200
    fd1=2048/s1^2;
end
if s1<500 & s1>200
    fd1=.0425;
end
if s1>=500
    fd1=.2431/(s1^.2857);
end
q1=sqrt((2*abs(Pr-y(1))*di)/(rho*fd1*(length/2)))*a;
if Pr>=y(1)
    q1=q1;
else q1=-q1;
end
s2=(1/nu)*sqrt((abs(y(3)-y(4))*di^3)/(rho*(length/2)));
if s2==0
    s2=0.01;
end
if s2<=200
    fd2=2048/s2^2;
end
if s2<500 & s2>200
    fd2=.0425;
end
if s2>=500

```

```

    fd2=.2431/(s2^.2857);
end
q4=sqrt((2*abs(y(3)-y(4))*di)/(rho*fd2*(length/2)))**a;
if y(3)>=y(4)
    q4=q4;
else q4=-q4;
end
qv=Av*sqrt((2*abs(y(4)-Pvout))/(rho*abs(1-(Av^2/a^2))));
if y(4)>=Pvout
    qv=qv;
else qv=-qv;
end

ydot(1)=(3/C)*(q1-y(5));
ydot(2)=(3/C)*(y(5)-y(6));
ydot(3)=(3/C)*(y(6)-q4);
ydot(4)=(beta/Vo)*(q4-qv);
ydot(5)=(2/L)*(y(1)-y(2));
ydot(6)=(2/L)*(y(2)-y(3));
if y(1)>=y(2)
    y(5)=y(5);
else y(5)=-y(5);
end
if y(2)>=y(3)
    y(6)=y(6);
else y(6)=-y(6);
end
ydot=ydot';

```

```

%solve water hammer problem
%approxhp.m
%H-P law

function pdot=approxhp(t,P);
global l di
ro=di/2;           % pipe inside radius (inches)
a=3.14159*di*di/4; % pipe inside crosssectional area (in^2)
rho=9.574e-5;     % fluid density (lbfsec^2/in^4)
Pvout=8.7;        % valve outlet pressure (psia)
nu=0.001517;     % kinematic viscosity (in^2/sec)
mu=nu*rho;       % absolute viscosity
Beta=32e4;       % adiabatic bulk modulus (psi)
Co=sqrt(Beta/rho); % sonic velocity (in/sec)
Dn=nu*l/(Co*ro^2);
Fco=1.4;
wco=Fco*Co/l;
zco=0.001;
Av=36098169*t^9-27651150*t^8+5290046*t^7+662432*t^6-210542*t^5 ...
-41747*t^4+16928*t^3-1707*t^2+9.226*t+8.347;
if t>=0.261
    Av=0;
end
Avdot=324883521*t^8-221209200*t^7+37030322*t^6+3974592*t^5 ...
-1052710*t^4-166988*t^3+50784*t^2-3414*t+9.226;
if t>=0.261
    Avdot=0;
end

q=Av*sqrt(2*(P(2)-Pvout)/(rho*(1-(Av^2)/a^2)));
if P(2)>=Pvout
    q=q;
else
    q=-q;
end

R=128*mu*l/(3.14*di^4);
Pss=R*q; % steady state pressure drop
num=rho*(1-(Av^2/a^2))*2*P(1)-2*(P(2)-Pvout)*(-2*rho*Av*Avdot)/a^2;
den=(rho*(1-(Av^2/a^2)))^2;
dirA=0.5*((2*(P(2)-Pvout))/(rho*(1-(Av^2/a^2))))^(-0.5)*num/den;

qdot=Av*dirA+sqrt(2*(P(2)-Pvout)/(rho*(1-Av^2/a^2)))*Avdot;
pdot(1)=(wco^2)*(-P(1)*2*zco/wco -P(2) -(rho*l/a)*qdot +45 -Pss);
pdot(2)=P(1);
pdot=pdot';

```

2

## VITA

David Jon Heer

Candidate for the Degree of

Master of Science

Thesis: AN INVESTIGATION INTO THE MODELING OF A RIGID FLUID  
CONDUIT USING T<sup>3</sup> ELECTRICAL ANALOGY AND S-T METHOD

Major Field: Mechanical Engineering

Biographical:

Personal Data: Born November 25, 1968, in Woodward, Oklahoma, the son of Calvin and Bonnie Heer.

Education: Graduated from Fairview High School, Fairview, Oklahoma, in May 1987. Received the Bachelor of Science degree in May, 1992, from Oklahoma State University, with a major in Mechanical Engineering. Completed the requirements for the Master of Science degree with a major in Mechanical Engineering at Oklahoma State University in May, 1998.

Professional Experience: Employed by the School of Mechanical Engineering as a Graduate Teaching Assistant from August, 1992 to May, 1993. Employed as Laboratory Technician at FES, Inc. in Stillwater, Oklahoma from June 1991 to May 1993. Promoted to project engineer in May 1993 and remained in that position until October, 1993. Promoted to Laboratory Manager at FES, Inc. in October, 1993 and continue to serve in that position.

Professional Organizations: The author is a member of ASME.